AN ABSTRACT OF THE THESIS OF

Steven John Bares for the degree of Doctor of Philosophy in Chemistry presented on December 14, 1983

Title: Laser Excited Fluorescence and Vibrational Relaxation of Matrix Isolated Metal Oxides

Abstract approved: Redacted for Privacy

Dr. Joseph W. Nibler

The work presented in this thesis deals with the mechanisms by which a vibrationally excited diatomic molecule gives up its energy to a host monatomic lattice at low temperature. The vibrational lifetimes (v"=1) of the metal oxides BaO and AlO in their ground electronic states are studied using pulsed dual laser techniques.

Chapter 1 provides a brief overview of the theoretical and experimental details relating to the field of vibrational relaxation in matrices. In Chapter 2, laser excited fluorescence spectra are presented for BaO prepared by VUV photolysis of $Ar/Ba/O_2$ matrix samples at 18 K. Evidence was obtained for a new BaO electronic state with T_e=20,000 cm^{-1} and a radiative lifetime shorter than 15 μs. Optical-optical double-resonance studies were not successful due to the low pumping efficiency and/or rapid vibrational relaxation.

An infrared study of the aluminum oxide products formed by rapid condensation of gas phase $Ar/O_2/Al$ mixtures is presented in Chapter 3. By coupling a double-resonance infrared-visible pump/probe scheme, the

v"=0→1 transition of AlO in argon was positively identified at 974.9 cm^{-1} for $Al^{16}O$ and at 942.4 cm^{-1} for $Al^{18}O$. Laser excited fluorescence and visible absorption spectra are presented for AlO in argon at 18 K.

Vibrational relaxation studies of AlO are described in Chapter 4. The v"=1 lifetime is independent of oxygen concentration and of temperature in the region between 18 and 30 K. An upper limit of 25 ms. is measured for dilute matrices with less than one PPM AlO. At higher concentrations of Al and other oxides, this lifetime is shortened considerably by V-V transfer of vibrational energy to molecular impurities.

A quantitative study of the V-V transfer process from AlO to both polar (NH_3, ND_3, CH_2Cl_2) and non-polar (SF_6, C_2H_4, C_2H_6, CO_2, and CF_4) acceptors is the subject of Chapter 5. The transfer rate coefficients show an exponential dependence on the donor-acceptor energy gap, decreasing approximately one order of magnitude for each lattice phonon needed to take up the excess energy. A mechanism which assumes that the energy mismatch between donor and acceptor is directly transferred to the lattice is most consistent with the observed data.

Laser Excited Fluorescence and Vibrational Relaxation of Matrix Isolated Metal Oxides

by

Steven J. Bares

A THESIS

submitted to

Oregon State University

in partial fulfillment of
the requirements for the
degree of

Doctor of Philosophy

Completed December 14, 1983

Commencement June 1984

APPROVED:

Redacted for Privacy

Professor of Chemistry in charge of major

Redacted for Privacy

Chairman of the Department of Chemistry

Redacted for Privacy

Dean of Graduate School

Date thesis is presented December 14, 1983

Typed by Jackie Poppleton for Steven J. Bares

ACKNOWLEDGEMENTS

I would like to thank Dr. Joseph W. Nibler for the encouragement and direction given to me in the last four years. As an instructor, he has explained and clarified many subjects of both theoretical and experimental nature. As a researcher, he has stressed the need to be thorough and to do research of the highest possible quality. The concepts which he has taught me and the skills which he has demonstrated will be used in future work and will always be remembered.

To my friend and wife, Madge, I am sincerely indebted. Her patience over the last four years and her talents in the preparation, editing, and typing of this thesis were critical to its completion.

I am also appreciative of the time and help which were given to me by Dr. Tom Lundeen. His facility with computer programming and interfacing was extremely helpful. Mr. George Pubanz, Mr. Brian Bozlee, Ms. Margie Weir, and Mr. Glen Hopkins were also helpful, and their participation is appreciated. Lastly, I would like to express my gratitude to Mr. John Archibald, Mr. Robert Boyer, Mr. Gerald Allison, and Mr. Doyle Woodrow for their technical help.

Now reflect that it is education that brings the east and west under the authority of man; it is education that produces wonderful industries; it is education that spreads great sciences and arts; it is education that makes manifest new discoveries and institutions. If there were no educator, there would be no such things as comforts, civilization, or humanity.

'Abdu'l-Báha'

son of Baha'u'lláh

TABLE OF CONTENTS

CHAPTER 1: VIBRATIONAL RELAXATION IN MATRICES: AN OVERVIEW 1

INTRODUCTION 1

THEORY OF VIBRATIONAL RELAXATION IN MATRICES 3

Radiative Relaxation 3

Relaxation to Phonons 5

Relaxation via Rotational Modes 6

Vibration to Vibration Transfer 7

EXPERIMENTAL STUDIES OF VIBRATIONAL RELAXATION 14

SUMMARY 19

CHAPTER 2: LASER EXCITED FLUORESCENCE OF BARIUM OXIDE IN ARGON MATRICES 26

INTRODUCTION 26

EXPERIMENTAL 28

LASER INDUCED FLUORESCENCE OF BaO IN ARGON 29

VIBRATIONAL RELAXATION OF BaO IN ARGON: PRELIMINARY STUDIES 36

SUMMARY 38

CHAPTER 3: PREPARATION AND SPECTROSCOPY OF ALUMINUM OXIDE IN ARGON MATRICES 40

INTRODUCTION 40

METHODS OF AlO GENERATION 42

EXPERIMENTAL 44

SPECIES IDENTIFICATION 47

Al and Al_2 48

AlO 49

Al_2O 54

Al_2O_2 55

AlO_2 57

SPECIES IDENTIFICATION (Cont.)

Al_2O_3 58
Summary of the Ar/O_2 Reaction Products 58

ESTIMATION OF AlO AND Al CONCENTRATION 60

LASER EXCITED FLUORESCENCE OF AlO IN ARGON 65

CHAPTER 4: VIBRATIONAL RELAXATION OF AlO 72

THE INFRARED-OPTICAL DOUBLE-RESONANCE TECHNIQUE 72

Excitation of v"=1 Level and Vibrational Relaxation 77
Probing the Excited Vibrational Population 81
Analysis of the Relaxation Curves 83

VIBRATIONAL RELAXATION OF AlO IN ARGON MATRICES 84

Temperature Dependence 90
Ar/Al and O_2/Ar Dependence 90
Relaxation in $Al^{18}O$ 91

DISCUSSION 96

CHAPTER 5: V-V TRANSFER FROM AlO TO VARIOUS SPECIES IN SOLID ARGON 100

INTRODUCTION 100

EXPERIMENTAL 104

INFRARED SPECTRA OF IMPURITY SPECIES IN SOLID ARGON 107

V-V TRANSFER STUDIES 107

AlO→NH_3 (ν_2) 109
AlO→ND_3 (ν_2) 113
AlO→CH_2Cl_2 (ν_7) 113
AlO→CF_4 113
AlO→CO_2 (ν_2, Π_u) 114
AlO→SF_6 (ν_3, f_{1u}) 114

SUMMARY 116

DISCUSSION 120

The Energy Gap Law 120

Theoretical Forms of the Energy Gap Law 129

BIBLIOGRAPHY 138

APPENDICES 143

Appendix 1: Calculations of Effusion Rates of Barium and Aluminum Vapor 143

Appendix 2: Computer Controlled Vibrational Lifetime Measurements 146

LIST OF FIGURES

Figure		Page
1.	Energy level diagram showing the possible mechanisms of vibrational relaxation of matrix isolated molecule in its ground electronic state.	4
2.	Measured rates of vibrational relaxation versus J_m for molecules isolated in argon matrices.	22
3.	The optical-optical double-resonance technique of Allamandola and Nibler.[50]	24
4.	Morse potentials of barium oxide calculated from gas phase molecular parameters.[62]	27
5.	Fluorescence of BaO isolated in argon at 18 K, excited at 4727 Å.	31
6.	Comparison of observed emission intensities from Figure 5 with calculated intensities for the $A'\Sigma^+ \rightarrow X'\Sigma^+$ transition.	35
7.	Morse potentials of AlO. Calculated from gas phase molecular parameters.[62]	41
8.	Absorption spectra of AlO in argon matrices: (a) from 76, and (b) from this work (maximum absorbance = 0.1), flowrate = 6 mmol/hr, T_{Kn} = 1200°C, deposition time = 1.5 hours.	52
9.	Infrared spectrum of Al/O_2 reaction products isolated in argon matrices.	53
10.	Fluorescence of AlO in argon at 18 K excited by several Ar^+ laser lines.	66
11.	Plot of $\Delta G_{1/2}$ versus $v'' + 1$ from fluorescence data of AlO in argon.	69

12. Schematic diagram of infrared-optical double-resonance apparatus used in these experiments. 73

13. The infrared-optical double-resonance technique. Energy level diagram and schematic of possible relaxation pathways during pump and probe processes. 76

14. Fluorescence intensity from 1"→0' excitation of AlO in argon versus pump laser output. Dye laser wavelength = 4786 Å. 78

15. Calculated vibrational relaxation curves from equation (31), assuming t_D = 170 μsecs and α = 60 μsecs. 82

16. Profile of CO_2 laser pulse in time. 85

17. Typical data for AlO relaxation: a) dilute sample, and b) concentrated sample. 87

18. Plots of ln I versus time delay for files of Figure 17. 92

19. Observed rates of AlO vibrational relaxation for several Knudsen cell temperatures. Calculated Ar/Al ratios (Appendix 1), assuming an Ar flowrate = 6 mmol/hr, are also shown. 94

20. Energy level diagram showing relevant infrared active bands for V-V transfer from AlO to various matrix isolated impurities. 103

21. Infrared spectra of dopant species shown in Figure 20 in argon at 18 K. All species are 0.1% in argon. 106

22. Vibrational relaxation data for NH_3 doped matrices of AlO in argon, T_{tip} = 18 K. 110

23. Fitted B parameters from equation (36) versus mole fraction of added acceptors. 118

24. Plot of measured transfer coefficients, C_{da} versus energy gap of the acceptor. 121

25. Comparison of measured transfer coefficients with normalized transfer coefficients. 124

26. Comparison of normalized rate coefficients with donor rotation model. 134

LIST OF TABLES

Table		Page
1.	Experimental rate constants for vibrational relaxation in matrix isolated molecules.	20
2.	Vibrational relaxation rates and calculated values of J_m for molecules isolated in argon.	22
3.	Vibronic transitions and vibrational constants of BaO in argon at 18 K.	31
4.	Comparison of the gas-to-matrix shift of the O"-O' absorption of several matrix isolated metal oxides.	33
5.	Summary of the matrix infrared data for the aluminum-oxygen system.	59
6.	Vibronic transitions and vibrational constants of the $B^2\Sigma^+ \rightarrow X^2\Sigma^+$ system of AlO in argon at 18 K.	67
7.	Wavenumbers, wavelengths, and micrometer settings for the CO_2 laser 001 -- [100,020] band.	75
8.	Experimental and calculated values of O'→O" fluorescence intensity using equation (33) for Ar/O_2 = 100, T_{tip} = 18 K, T_{Kn} = 1000°C.	88
9.	Vibrational relaxation data for matrix isolated AlO as a function of Knudsen cell temperatures, Ar/O_2 ratio, and tip temperature.	93
10.	Infrared frequencies (cm^{-1}) of dopant species in argon at 18 K. All species are 0.1% in argon.	108
11.	Data obtained for all dopant species from least squares fit to equation (36).	115
12.	Calculated coefficients of V-V transfer from AlO to various polyatomic acceptors.	119

13. Calculated rotational quanta for V-V transfer. 133

14. Effusion rates of barium and aluminum from equation (A2). 145

Laser Excited Fluorescence and Vibrational Relaxation of Matrix Isolated Metal Oxides

Chapter 1

Vibrational Relaxation in Matrices An Overview

INTRODUCTION

The study of molecular energy transfer has yielded important information about the processes in the field of molecular dynamics. An understanding of the fundamental interactions which take place on a molecular scale is necessary for insight into the behavior of an entire macroscopic system. These forces determine the flow of energy on a molecular scale and, if understood, could in principle be manipulated to influence the pathway of a given chemical reaction. Experimentally, the study of the flow of energy as a function of time in a molecular system can be used to probe the mechanisms of energy transfer and, hence, elucidate the magnitude of these molecular interactions. For these reasons, the study of vibrational energy transfer, particularly in liquids and solids, has been an area of active research in recent years.

Two types of vibrational energy transfer studies in condensed media are discussed in the literature: 1) studies in the picosecond range of liquids and solids at room temperature, and 2) studies in the 100 nanosecond-to-second range of simple molecules at temperatures

below that of liquid nitrogen (77 K). These latter studies are usually investigated using matrix isolation techniques and are the subject of this thesis. In particular, this thesis is concerned with the mechanisms by which vibrational energy is lost by a model system; a simple diatomic molecule isolated in a solid inert gas host.

The solid matrix presents some distinct advantages for studying dynamic processes over those studies in other phases:

1. Except for small hydrogenated molecules, rotation is quenched and guest motion is usually limited to local librational and translational modes.
2. The matrix-to-guest ratio is high, so guest-guest interactions can usually be ignored. Matrices of nitrogen or inert gases are chosen to minimize guest-matrix interactions.
3. The temperature of the matrix is low, so population in any energy level above the ground state is negligible.

These considerations simplify the spectroscopy of the matrix isolated guest to the point where detailed studies of energy flow can be attempted. This thesis deals with such measurements on matrix isolated AlO and BaO. Before presenting the results, a survey of earlier theoretical and experimental work on vibrational lifetime measurements in matrices is given. For similar picosecond studies of pure liquids and solids, the reader is referred to several excellent reviews in the literature.[1]

THEORY OF VIBRATIONAL RELAXATION IN MATRICES

To begin the discussion of vibrational relaxation theories, we consider a diatomic molecule, vibrationally excited, and distributed randomly in a solid host matrix. Ultimately, this vibrational energy must be degraded in the form of heat and taken up by the lattice host. However, immediately after excitation, the energy has several possible decay channels open: 1) the molecules can emit light in a purely radiative process, 2) the energy can be dissipated directly into lattice phonons, 3) if the molecule is free to rotate or has lower frequency vibrations, the energy can decay into phonons via localized rotational or vibrational modes, or 4) if a suitable acceptor is near-by, the excited molecule can transfer energy by vibration-vibration transfer. All of these mechanisms are shown schematically in Figure 1 and each is discussed individually below.

Radiative Relaxation

In all the vibrational lifetime experiments to be discussed, interest centers on the non-radiative decay process. The radiative mechanism is a competitive path for vibrational relaxation, but fortunately, is relatively inefficient. In the gas phase, the radiative lifetime is related to the Einstein coefficient of emission, Amn, by the well-known expression

$$\frac{1}{\tau_{rad}} = Amn = \frac{64\pi^4}{3h} \bar{\nu}_{mn}^3 \left| \langle m|\bar{\mu}|n\rangle \right|^2 \qquad (1)$$

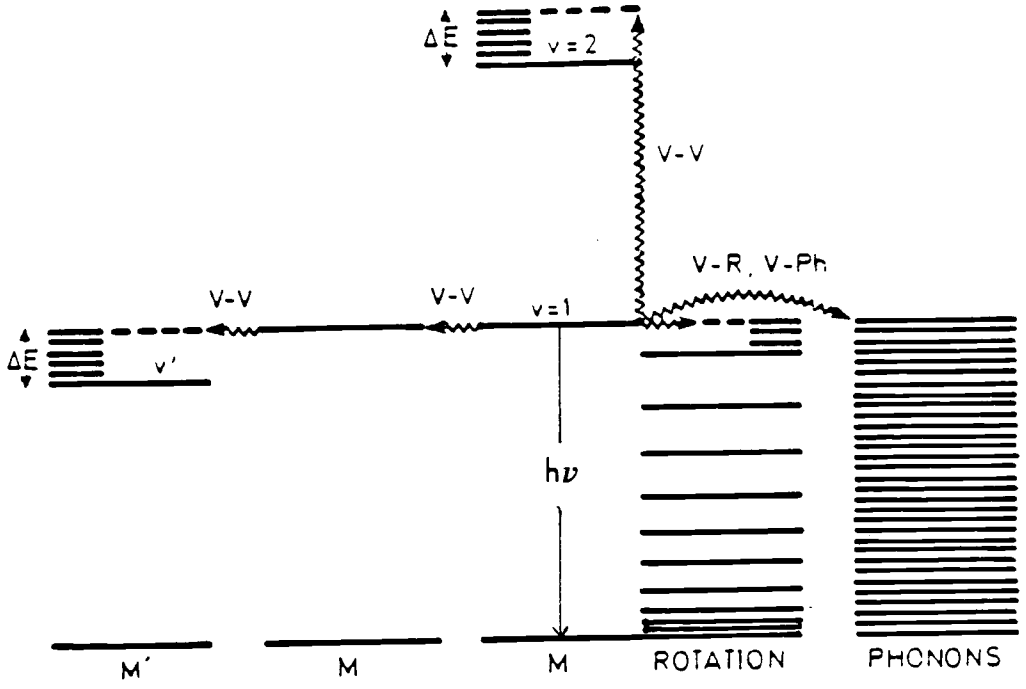

Figure 1: Energy level diagram showing the possible mechanisms of vibrational relaxation of a matrix isolated molecule in its ground electronic state. The excited molecule may decay by: 1) photon emission, 2) direct conversion to lattice phonons (V-Ph), or 3) conversion to localized rotational modes (V-R). Under conditions where the excited molecule is not isolated in the matrix, the possibility of resonant or phonon-assisted V-V transfer exists.

where $\bar{\nu}_{mn}$ is the frequency of the transition in wavenumbers and $\bar{\mu}$ is the dipole moment. Because $\bar{\nu}_{mn}$ is small, radiative lifetimes are generally long, $\sim 10^{-3}$ to 1 second.

For an estimate of the radiative lifetime in matrices, the transition moment integral, $\langle m|\mu|m\rangle$, can be assumed to be unchanged by the surrounding host. With this assumption, only the change in the local environment, due to the nearby host, must be considered. The local field at the site of the molecule is different from the vacuum field, due to the dielectric properties of the crystal. This effect leads to a decrease in the radiative lifetimes given by (2) as

$$\tau_s = \frac{9}{n(n^2+2)^2}\,\tau_g \qquad (2)$$

where τ_s and τ_g are the relaxation times in the condensed phase and gas phase, and n is the refractive index of the host medium. For argon at 20 K, the index of refraction is 1.27,[3] so that τ_s/τ_g = 0.54.

Relaxation to Phonons

The theory of multiphonon relaxation has been extensively studied by several authors.[4-7] The phonons provide a thermal bath where, except for the radiative part, the vibrational energy ultimately decays. Early theoretical work by Sun and Rice[4] and later by Nitzan[5-7] postulated a simple model for the relaxation process. In this model it is assumed that the vibrational energy is accepted directly by harmonic, delocalized lattice phonon modes which are approximated by a single frequency. Other studies by Lin[8-9] have used

more realistic Hamiltonians to take into account the non-harmonic coupling and the interactions between guest molecule and its surrounding neighbors. In all of these theories, the predicted rate is strongly dependent upon temperature and decreases exponentially with increasing value for the molecular vibrational frequency (energy gap law). The predicted temperature dependence of the lifetime takes the form

$$\frac{\tau(T)}{\tau(0)} \simeq [\exp(-h\bar{\nu}/kT)-1]^{\bar{\nu}/\bar{\nu}_D} \qquad (3)$$

where $\tau(0)$ is the lifetime at T = 0 K, $\bar{\nu}_D$ is the phonon frequency (taken to be the Debye cutoff), and $\bar{\nu}$ is the vibrational energy of the excited molecule. In 1976, Jortner[10] extended the above theory to include the case of a molecule isolated in a polyatomic host. In this situation, the host vibrations provide another path for the vibrational relaxation mechanism by reducing the amount of energy which must be converted into phonons in the first step of the relaxation.

Relaxation via Rotational Modes

To account for the relaxation behavior of small molecules such as HCl,[11] OH,[12] and NH,[13] experimenters were led to propose a different mechanism for the relaxation process. The weak temperature dependence of the relaxation rates, and the fact that the hydrides relaxed faster than the corresponding deuterides, led Brus and Bondybey[12] to propose that direct conversion to lattice phonons did not occur, but rather that the vibrational energy is lost principally by rotational excitation of the guest hydride molecule. Theoretical models which account

for the role of molecular rotation have been developed by many authors. In 1977, Freed et al.[14-15] assumed a simple two-dimensional model and showed that when the rotational mechanism is dominant, the rate varies exponentially with the square root of the vibrational frequency divided by the rotational constant, $(\omega/B)^{1/2}$, while the rate is independent of temperature at least up to 20 hB/k. A similar model was adopted by Diestler et al.[16] which was applied to the NH, OH, and HCl relaxation. Knittel and Lin[17] have extended the models by including the effect of lattice phonons explicitly. Gerber and Berkowitz[18-20] included the effect of a realistic impurity-host interaction and impurity-cage geometry. Recently, Lin et al.[21-22] have improved these models by using known impurity-host interaction potentials based on the "adiabatic" approximation. In this paper, comparison of theoretical and experimental relaxation rates of the HCl-DCl system showed good agreement.

Vibration-to-Vibration Transfer

For a polyatomic molecule isolated in a host lattice, the possibility of intramolecular vibrational mode-to-mode relaxation exists. This is currently a very active topic of research. This problem is very similar to direct vibration-to-phonon decay, except that the final state is not the ground state. From the experimental data it is clear that an energy gap law alone is insufficient to describe the relaxation process. The intermode coupling parameters, which arise from anharmonic terms in the potential energy function, are presently unknown although they must be taken into account in any quantitative theory.

For many matrices, the concentration of guest molecules cannot be considered infinitely small; therefore, the possibility of intermolecular interactions over long distances (on a molecular scale) must be considered. These long-range multipolar forces induce V-V transfer among guest molecules and are important if the intramolecular processes discussed above are inefficient compared to V-V transfer. This mechanism can be examined theoretically by considering two steps in the V-V transfer process: 1) the bimolecular microscopic process of V-V exchange between a donor and an acceptor, and 2) the collective or macroscopic evolution of the entire population of vibrationally excited molecules in time.

The microscopic process of V-V transfer in solids has been studied only in the last few years but the electronic analogue has been studied for a much longer time. The theory in this case involves the interaction between two electric dipoles (or quadrupoles), and several results can be transposed to the vibrational case without modification. The energy transfer between two molecules has been theoretically investigated by Forster[23] as early as 1948 for the case of dipole-dipole interactions. This theory was extended by Dexter[24] in 1955 to include other types of interactions. In both cases, the goal is to calculate the probability of energy transfer, P_{da}, from an excited donor molecule to an unexcited acceptor molecule. In the case of dipole-dipole coupling, assuming a random orientation of molecules, the Fermi Golden Rule applied to two oscillators in near resonance gives the transfer probability, P_{da}, as:

$$P_{da} = \frac{3\pi\hbar^7 c^6}{4n\, R_{da}^6} \frac{1}{\tau_d} \frac{1}{\tau_a} \int \frac{f_d(E) f_a(E)}{E^6} dE \qquad (4)$$

Here n is the refractive index of the medium, τ_d and τ_a are the radiative lifetimes of the donor and acceptor molecules, R_{da} is the separation distance, and $f_d(E)$ and $f_a(E)$ are the normalized lineshape functions of donor and acceptor molecules, expressed as a function of the energy, E.

According to this theory, transfer is forbidden if the overlap between the donor emission and acceptor absorption profiles is zero. However, in matrices, the transfer is assisted by way of phonon (or libration, rotation) levels which fill the energy gap between donor and acceptor. This possibility of phonon-assisted, nonresonant electronic transfer between ions in crystals was first considered by Orbach.[25] In this theory, integrated absorption coefficients of the zero phonon lines and phonon side bands are used to calculate the transfer probability. Central to the theory of Orbach is the assumption that the transition matrix elements for the donor and acceptor are reasonably close (as in the case for energy transfer between isotopes). In the more interesting case where the donor and acceptor have very different transition matrix elements, or if the phonon side bands are not observable, the method fails.

Lin et al.[26] use an approach similar to that for direct vibration-phonon relaxation in treating the case of nonresonant vibrational energy transfer between polar molecules in matrices. In this theory, cross terms between permanent and transition dipole moments are found to contribute to the overall energy transfer rate.

They obtain the following expression for the microscopic rate of V-V transfer:

$$k^{v_a \to v_a+1}_{v_d \to v_d-1} = \left[v_d(v_a+1)/3\varepsilon R^6\right] \times \left[\frac{(\mu_d^o)^2(\mu_a')^2}{2\hbar w_a^3} k_d(\Delta E) + \frac{(\mu_a^o)^2(\mu_d')^2}{2\hbar w_a^3} k_a(\Delta E)\right] \quad (5)$$

Here $\hbar w$ and $\hbar w$ are the energies of the vibrational transitions involved in the donor and acceptor, v_d and v_a are the vibrational quantum numbers of donor and acceptor, R is the intermolecular separation distance, ε is the dielectric constant of the medium, and $k_d(\Delta E)$ and $k_a(\Delta E)$ are the rates at which donor and acceptor dissipate directly into the lattice energy $\Delta E = \hbar(w_d - w_a)$.

The energy transfer rate from donor to acceptor is then related to the rates of direct multiphonon relaxation of the isolated donor and acceptor molecules. Through equation (5), a numerical value for the V-V transfer rate may be obtained if an expression for the rate dependence on the difference in energy of the donor and acceptor vibrations (energy gap) is known. Inversely, Goodman and Brus[27] used the measured V-V transfer rates from $ND(A^3\Pi)$ to CO to obtain information on the energy gap law.

Blumen et al.[28] have developed a more general first order theory for V-V transfer among diatomic molecules in matrices. The calculate the microscopic rate constant for any generalized elementary transfer process of the form:

$$M_n(v_d) + M_m(v_a) \rightleftharpoons M_n(v_d-1) + M_m(v_a+1) + \Delta E \qquad (6)$$

for the two cases of resonant and nonresonant transfer. For resonant ($\Delta E=0$) vibrational transfer, the transfer rate can be written as:

$$k_{v+1\rightarrow v}^{v\rightarrow v+1} = \frac{2}{3}\,\frac{2\pi}{\hbar\delta E}\,\frac{1}{\varepsilon^2 R^6}\left[|\mu'|^2\,\frac{(v+1)\hbar}{2w_m}\right]^2 \qquad (7)$$

Here δE (ergs) $= \pi hc\delta\bar{\nu}$: $\delta\bar{\nu}$ is the spectral linewidth in cm^{-1}, w_m ($secs^{-1}$) $= 2\pi hc\bar{\nu}$, with the vibrational frequency $\bar{\nu}$ in cm^{-1}, ε is the dielectric constant and μ' is the dipole derivative of the (assumed identical) transitions. Using the data for CO, Blumen calculated the resonance transfer rate of v"=1 excitation:

$$k_{1-0}^{0-1} = \frac{2\times 10^{15}}{\varepsilon^2[R(\text{Å})]^6} \qquad \text{(CO)} \qquad (8)$$

This value agrees with the experimental findings of Dubost and Charneau, and is close to that obtained using the Forster-Dexter theory.[29]

For phonon assisted transfer (ΔE=N phonons), the ratio of the nonresonant rate constant to the resonant rate constant is given by the expression

$$\frac{k_{1-0}^{v\rightarrow v+1}}{k_{1\rightarrow 0}^{0\rightarrow 1}} = \frac{v+1}{NN!}\,\frac{\delta E}{\hbar w_D}\left[\frac{\Delta w_{vib}}{2w_D}\left(1+\frac{1}{v+1}\right)\right]^N \times \exp\left[\frac{\Delta w_{vib}}{2w_D}\left(1-\frac{1}{v+1}\right)\right] \qquad (9)$$

where w_D is the Debye frequency of the solid host (w_D=63.9 cm^{-1} in argon), and Δw_{vib} is the gas-to-matrix shift of the donor vibrational mode.

There are several important features of this theory. The rate constants for V-V transfer depend only slightly upon temperature. More importantly, the V-V transfer rate depends strongly on the number of phonons involved in the transition. The resonant V-V processes are predicted to be several hundred times faster than the phonon assisted ones, decreasing according to (approximately) a Poisson-type law with increasing numbers of phonons. Therefore, the V-V transfer rate constants decrease faster than exponentially with energy mismatch. Lastly, V-V processes which differ by one phonon have rates which differ by only an order of magnitude.

Included in the above theories for the microscopic transfer rates is the separation distance between donor and acceptor. In the real matrices, the impurity guest molecule is surrounded by possible acceptors at many different separation distances or, in the statistical limit, by a continuous distribution of separation distances. In any reasonable theoretical description of intermolecular V-V transfer, the macroscopic behavior of a collection of donors and acceptors must be included.

Consider a system of donor molecules present in the matrix at low concentration, so the donor-donor microscopic interaction need not be considered. By assuming a random distribution and orientation of acceptors surrounding each donor, Weber,[30] following Forster,[23] has shown for multipolar interactions that the population of excited donors is given by

$$N(t) = N(t=0) \exp\left(-t/\tau_0 - \frac{4}{3}\pi\Gamma(1-3/s)Na(C_{da}t)^{3/s}\right) \qquad (10)$$

for the familiar cases of dipole-dipole (s=6), dipole-quadrupole (s=8) and quadrupole-quadrupole (s=10) coupling. In equation (10), N(t=0) is the initial population, C_{da} is the constant coefficient for the microscopic donor-acceptor probability transfer ($k_{da} = C_{da}R^{-6}$), and τ_0 is the intrinsic decay time of the donor.

The population of excited donors is given by N(t). When the donor-acceptor transfer mechanism is the rate-determining step, the population decay of donors is not a simple exponential. Initially, transfer occurs rapidly for donors having nearby acceptors and as the time progresses, transfer involves less efficient coupling to acceptors further and further away. The overall decay is characterized by an initial non-exponential portion followed by an exponential decay at a rate given by the intrinsic decay time, τ_0.

If the donor-donor interaction is not negligible and microscopic resonant transfer cannot be ignored, then diffusion within the donor system must be incorporated into the macroscopic theory. This situation has been reviewed by Weber[30] and Yokota and Tanimoto.[31] In the case where diffusion within the donor system is fast compared to the intrinsic decay time, the variations in transfer time, because of the distribution of distances, is effectively averaged out and a net exponential decay results. In the limiting case where diffusion is comparable to the donor acceptor transfer time, a non-exponential rate, similar to that when diffusion is unimportant, is obtained. However, experimentally, the diffusion limited decay rates could be discerned by the reproducible change from exponential to non-exponential in the

shape of decay curves as the acceptor concentration is increased in a system of donors known to interact.

EXPERIMENTAL STUDIES OF VIBRATIONAL RELAXATION

After the original proposal by Sun and Rice[4] that lifetimes of vibrationally excited diatomic molecules could be longer than a few picoseconds, there was much interest in the experimental verification of this phenomenon. The most striking confirmation came in 1968 with the work of Tinti and Robinson.[32] Following X-ray excitation of N_2 in rare gases, emission from the v'>0 levels in the electronically excited $A^3\Sigma_u^+$ state implied that the vibrational relaxation time in this state was slower than phosphorescence times, on the order of one second. Shirk and Bass,[33] in 1970, used a CW argon ion laser, a more selective excitation source than X-rays, to excite CuO in argon. With the observation of unrelaxed emission (v'=1), the authors concluded that vibrational relaxation in the excited state required on the order of 10^5 vibrational periods (about 10 nsecs). In 1972, Bondybey and Nibler[34] performed a similar experiment on C_2^- isolated in argon. These authors estimated a v"=1 lifetime of one second for the ground electronic state based on emission which could only result from v"=1 secondary absorption.

The development of tunable lasers covering the infrared and visible region opened up the possibility of time-resolved experiments on particular vibrational states. Direct measurements of vibrational relaxation times in both ground and excited electronic states have been reported. Bondybey, Brus and other collaborators have performed

several excellent studies using time-resolved visible fluorescence following pulsed laser excitation of several diatomic molecules (OH,[12] NH,[13] C_2^-,[35] CN,[36] NO,[37] and S_2,[38]) as well as on several polyatomic molecules (CF_2,[39] CNN,[40-41] ClCF,[42] and NCO).[43] This technique, although restricted to the study of excited vibrational states, takes advantage of the tunability of lasers and the sensitivity of detectors in the visible region.

Several very interesting results have been found in the study of OH and NH: 1) the relaxation rates of these molecules are in the 10^4 $\sim 10^5$ sec^{-1} range, several orders of magnitude larger than those for CO and N_2 (in their ground electronic states), even though the latter have smaller energy gaps, 2) the rates are faster in OH and NH than the corresponding deuterides, and 3) the rates are temperature independent. The above behavior among the hydrides led Bondybey and Brus[12-13] to propose that the vibrational energy decays into rotational energy of the trapped molecule.

For the non-hydrides, CN and C_2^-, intersystem crossing to other nearby electronic states dominates over other vibrational relaxation processes. However, the relaxation to other electronic levels was observed to obey, qualitatively, an energy gap law characteristic of a multiphonon process. For both NO and S_2, there are no nearby electronic states, and in both cases the authors suggest that the vibrational energy decays directly into the host lattice. This is supported in the case of S_2 by a tremendous change in rate with temperature (four orders of magnitude increase as the temperature increases from 9 to 28 K).

For polyatomic molecules, vibrational relaxation in the excited state is extremely fast, usually faster than the fluorescence times. Consequently, the emission from polyatomics is normally vibrationally relaxed. This fast relaxation within the excited state is a consequence of the high density of vibrational states. Even in the simple triatomics, CF_2 and CNN, relaxation only requires a few nanoseconds. In these cases, the stretching modes relax via overtones of the low frequency bending modes. In the other polyatomics, NCO and ClCF, all of the vibrational modes and their overtones play an important role in the relaxation process. These studies reflect the importance of the intermode coupling elements in understanding the relaxation process.

Most of the above vibrational relaxation studies have involved higher electronic states. Experimental studies of vibrational relaxation in the ground electronic states were first pioneered by Legay[44] in 1973. In this classic work, a frequency-doubled CO_2 laser was used to excite CO (v=1) in neon and argon matrices. The population of CO after initial excitation was then monitored by the infrared emission. It was found that the intrinsic relaxation was so inefficient that a dipole-dipole resonant transfer among the CO molecules occurred many times during its lifetime. Ultimately, the excitation migrates to a CO having a nearby impurity and it is deactivated by a V-V transfer. In the limit of high dilution in impurity-free matrices, the CO decays radiatively.

Moore and Weisenfield[11] used this same infrared fluorescence technique in a recent study of matrix-isolated HCl and DCl. Very narrow bandwidth pulses, from a Nd:YAG pumped optical-parametric oscillator (OPO), were used to excite the guest species of interest.

The rates for dilute samples of HCl and DCl were consistent with the intramolecular vibration-rotation transfer mechanism. Under concentrated conditions, the rate for HCl (v=1) decay increased dramatically. It was concluded that under these concentrated conditions, the V-V transfer to the dimers is the dominant decay channel. The relaxation time of the dimer was estimated to be less than the limit of their time resolution (0.3 μsecs) so that the dimers act as the key energy sink for the monomer vibrational energy.

Abouaf-Marquin et al.[45] have used an infrared double-resonance technique to study the relaxation of the polyatomic molecules CH_3F and CD_3F in solid krypton. In this technique, an intense CO_2 laser pulse populates the ν_3 C-F stretching mode. The transmitted power in a second, much weaker, probe laser is used to monitor the repopulation of the ground state. Again, relaxation in CD_3F takes ten times longer than relaxation in CH_3F and there is no temperature dependence. The authors conclude that rotation about the symmetry axis accepts the vibrational energy. Recently this work has been extended by Young and Moore.[46] Here, a Nd:YAG pumped OPO is used to excite the CH stretching modes of CH_3F in several rare gas solids at around 3000 cm^{-1}. The rapid, subsequent (<5 nsecs) intramolecular V-V transfer to the ν_3 C-F stretch is monitored by infrared fluorescence. The observed rates of intramolecular vibrational relaxation show a dramatic dependence on the host lattice, with an increase of two orders of magnitude in going from xenon to argon.

The infrared double-resonance technique has also been applied to the ν_2 mode of NH_3 isolated in solid N_2 and rare gas solids. It was observed that NH_3 relaxes ten times faster in rare gas solids than in

solid N_2. This was attributed to the fact that NH_3 is known to undergo almost unhindered rotation about the symmetry axis in rare gas solids, but is not free to rotate in solid N_2. A complete study of the relaxation processes in ammonia would require the measurement of the lifetime in matrix isolated ND_3. However, the ν_2 band of matrix isolated ND_3 does not overlap any of the lines of the CO_2 laser.

To investigate the homonuclear diatomic molecule C_2^-, Allamandola and Nibler[47] developed an "optical-optical double-resonance" technique for the measurement of the lifetimes. This method will be discussed in detail later in this chapter. For C_2^-, generated from VUV photolysis of acetylene, depended strongly on whether C_2H_2 or deuterated acetylene, C_2D_2 was used as the parent compound. They conclude that V-V transfer to the parent compound, of necessity present in all experiments, controls the relaxation process.

Bondybey[48] has used this same technique for the study of NH and ND in their ground $X^3\Sigma^-$ electronic states. In this study, the rates were a factor of about 200 slower in the ground electronic state than was found earlier in the excited states. Nevertheless, the absence of any temperature dependence, and the fact that the rate of the deuterated species was slower than that of the hydride, indicated that the relaxation mechanism remained the same as in the excited state. This was surprising as it was expected that the interaction with the matrix in the excited state would be considerably stronger than in the ground state.

SUMMARY

Table 1 is a summary of the known vibrational relaxation rates observed for matrix isolated molecules in their ground and excited electronic states. There are two clear features about the data in Table 1: 1) in general, the vibrational relaxation rate in an excited electronic state is several orders of magnitude higher than in the ground state, and 2) no simple energy gap law can explain the observed rates for the entire collection of molecules.

There is one other important point which could be made about the data in Table 1. For those molecules in which guest rotation accepts the vibrational energy, Legay[40] has shown that there is a simple relationship between the observed rate and the minimum number of rotational quanta necessary to match with the energy gap, J_m. For simple diatomic molecules, assuming perfect resonance with the vibrational transition, J_m is given by

$$J_m \simeq (\frac{\omega}{B})^{1/2} \qquad (11)$$

where w is the vibrational energy and B is the rotational constant.

In the case of a slight mismatch, the energy gap is assumed to be filled by one or two delocalized phonons. For the symmetric top molecules in Table 1, the situation is more complicated as there are two rotational constants, one parallel and one perpendicular to the symmetry axis. Legay give the relationship between J_m and the rotational constants as

Table 1: Experimental rate constants for vibrational relaxation in matrix isolated molecules.

Molecule	Matrix	Vibrational energy (cm^{-1})	Transition	Relaxation rate s^{-1}	Ref
CO	R.G, N_2	2140 ~ 1840	(1-0)-(11-10)	radiative	44
NO	Ar	1870 - 1700	(1→0)-(7-6)	radiative	37
N_2	N_2	2245 - 1988	(4→3)-(13-12)	4.8 - 15.6	101
CN	Ne	1964	4→3	3.6×10^2	36
C_2^-	Ar	~1770	1-0	6.8	47
	Kr	~1770	1-0	3.5	47
	Xe	1770	1-0	6.1	47
HCl	Ar	2871	1-0	8.0×10^2	11
DCl	Ar	2768	2-1	4×10^3	11
NH	Ar	3131	1-0	5.3×10^3	48
ND	Ar	2316	1-0	3.2	48
N_2 ($A\ ^3\Sigma_u^+$)	R.G.	1434 - 1347	(1-0)-(4-3)	~1	32
C_2^- ($a\ ^4\Sigma_u^+$)	Ar	926	3-2	8.4×10^7	35
CuO ($B\ ^2\Sigma$)	Ar, Kr	624	1-0	$\leq 10^8$	33
NH ($A\ ^3\Pi$)	Ar	2977	1-0	1.2×10^6	13
ND ($A\ ^3\Pi$)	Ar	2217	1-0	$\leq 2 \times 10^4$	13
CF_2 (A)	Ar	496	ν_2(1-0)	1.1×10^8	39
NH_3	Ar	974	ν_2(1-0)	$>2 \times 10^6$	44
CD_3F	Kr	987	ν_3(1-0)	9.1×10^3	45
CH_3F	Kr	1036	ν_3(1-0)	9.1×10^4	45

$$J_m \simeq \left(\frac{\omega}{\max\ (A,B)}\right)^{1/2} \qquad (12)$$

where the rotational constant (A or B) which gives the least number of rotational quanta is used. Using the gas phase values for the rotational constants, Legay was able to demonstrate a correlation between the logarithm of the rates and J_m, implying an exponential law of the form $k \alpha \exp(-aJ_m)$. Of particular interest in this work are those rates measured using argon as a matrix gas since a direct comparison of our results is then possible (Table 2, and Figure 2). From Figure 2, it is seen that the hydride data are in rough agreement with this simple V→R model but the results for C_2^- and AlO (to be discussed in this work) are not.

It is apparent from Table 1 that there is a need for data for relaxation within the ground electronic state. Moreover, all of the diatomic molecules studied so far have vibrational energies in the region above 2000 cm^{-1}. In particular, the lack of data for diatomic molecules with ω values less than 1500 cm^{-1} was instrumental in the choice of the diatomic metal oxides, BaO and AlO, as candidates for the thesis work presented here. Both species have vibrations below 1000 cm^{-1}, but still well above the lattice frequency range. Thus, direct relaxation into the lattice phonons should be inefficient. At the same time, these molecules have small values of the rotational constant (<1 cm^{-1}) so decay to localized rotational modes is not expected to be as important as it is for the hydrides.

Another very important reason for being interested in these metal oxides originates from the technique that was chosen to study these molecules. In the case of BaO, with vibrational energy of 660 cm^{-1},

Table 2: Vibrational relaxation rates and calculated values of Jm for molecules isolated in argon.

Molecule	B (cm^{-1})	ω_e (cm^{-1})	k (sec^{-1})	Jm	Size*	Ref
HCl (2-1)	8.5	2768	3.8×10^3	18	2.7	11
DCl (2-1)	4.9	2028	4.0×10^2	20	2.7	11
NH_3 (1-0) υ_2	9.9	974	$>2 \times 10^6$	10	---	45
NH	16.7	3131	5.3×10^3	14	2.2	48
ND	8.9	2316	32	16	2.2	48
C_2^-	1.75	1770	<6.3	32	3.1	47
BaO	.313	669	---	46	5.4	--
AlO	.641	975	$>4.0 \times 10^1$	39	4.0	**

* Calculated from covalent radii given in (98). These may be compared with the size of the substitutional site of argon at 18°K, given to be 3.75 A by (99).

** From Chapter 4 of this work.

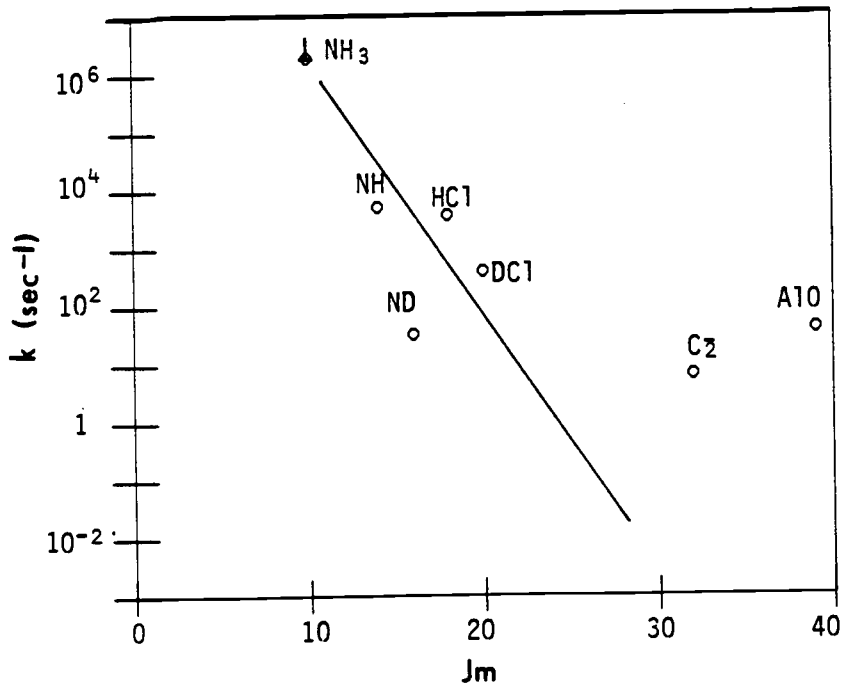

Figure 2: Measured rates of vibrational relaxation versus Jm for molecules isolated in Ar matrices.

there are no tunable infrared sources to excite the vibration. The "optical-optical double-resonance" technique (OODR), as developed by Allamandola and Nibler,[50] provides the only method of conveniently studying this molecule. In the OODR method, a short pulse from a visible laser is used to excite a particular electronic state which subsequently fluoresces, populating several of the v" levels (see Figure 3). A second probe laser, which impinges on the sample at some variable time after the pump laser, is used to monitor the v" level of interest by an absorption-fluorescence sequence. A plot of the measured fluorescence from the second probe laser versus the time delay between pump and probe serves to map out the relaxation curve of the v" level.

In principle, the OODR technique requires only allowed vibronic transitions and, therefore, can be applied to molecules without infrared allowed transitions. This is an important advantage over direct infrared fluorescence measurements and makes it possible to study molecules such as C_2^- which cannot absorb or emit in the infrared. Another important advantage lies in the fact that the detectors used in the visible region are much faster and more sensitive than those in the infrared region. Several disadvantages in this method must also be pointed out: 1) The population of any particular v" level is purely dependent upon the Franck-Condon factors, so that selective pumping into one particular v" level is not always possible. 2) If many v" levels are populated due to Franck-Condon factors, a detailed kinetic analysis, including cascading effects from upper v" levels, must be considered in extracting relaxation rates. This limits the accuracy of any particular lifetime measurement. 3) Lastly,

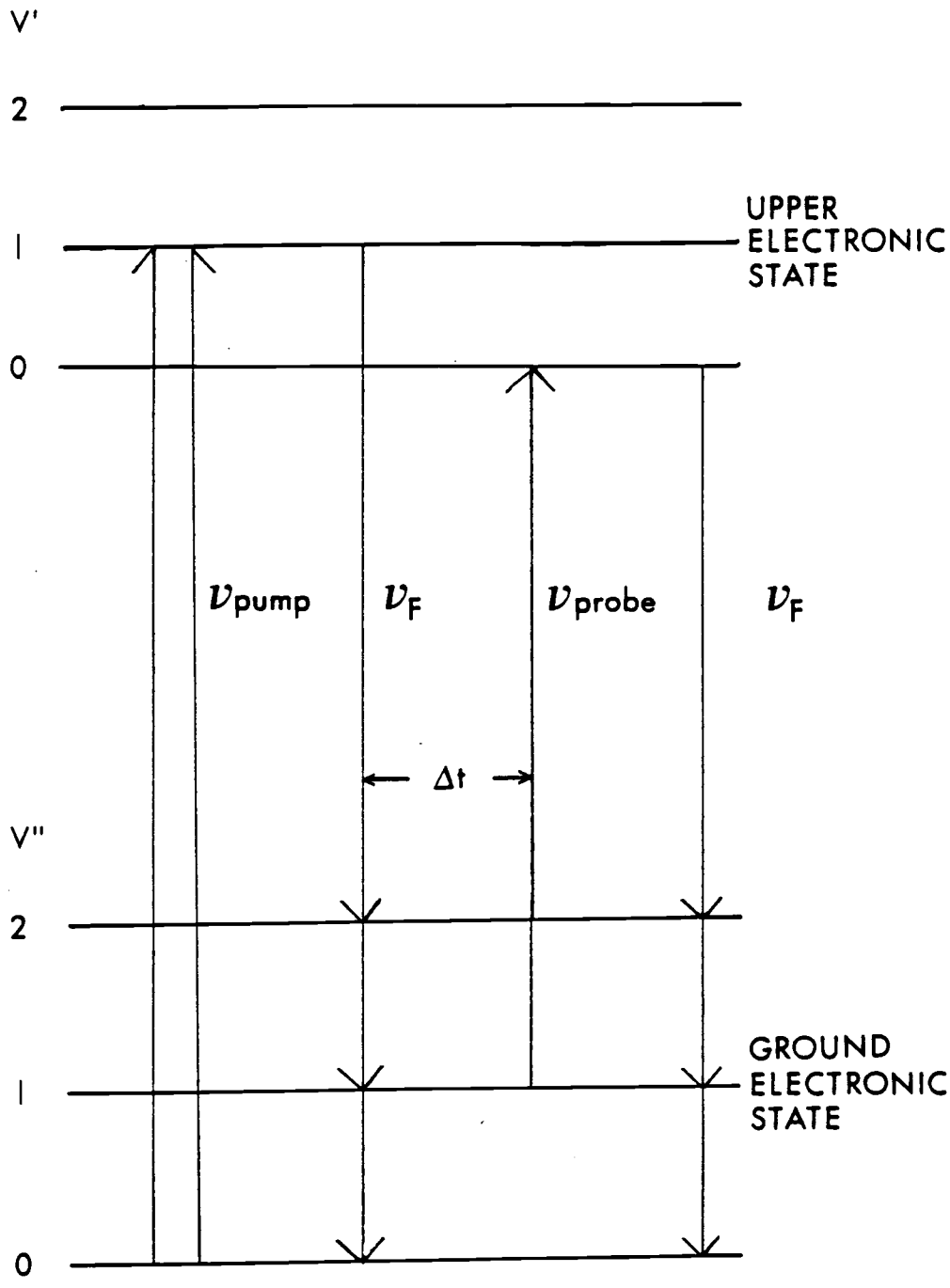

Figure 3: The optical-optical double resonance technique of Allamandola and Nibler (50).

intersystem crossing and quenching within the excited state manifolds, common among matrix isolated species, can decrease the utility of this method.

There were also important practical reasons for choosing the metal oxides for this work. In order to use the OODR technique, the molecule must absorb in regions that lasers in the laboratory can access, and it must display discrete fluorescence upon laser excitation. Since the laser-induced fluorescence of CuO had already been described as very intense and discrete,[33] we expected other metal oxides to fluoresce in a similar manner. Lastly, we intended to prepare the metal oxide by co-depositing an oxidant with metal atoms generated by Knudsen cell vaporization. Therefore, metals with low melting points, such as aluminum and barium, were chosen.

Chapter 2 presents the results, and outlines the difficulties encountered, of a preliminary study in which we apply the OODR technique to BaO in solid argon. In Chapters 4 and 5, the OODR is modified for the study of matrix isolated AlO. In the case of AlO, the v" level is populated using a CO_2 laser tuned to selectively excite the 0" to 1" transition. A visible laser is then used to probe the population of the state in the same absorption-fluorescence sequence.

Chapter 2

Laser Excited Fluorescence of Barium Oxide in Argon Matrices

INTRODUCTION

The complex optical spectrum of BaO has been studied for nearly fifty years.[62] In most of these studies, including the present one, BaO is produced by the chemiluminescent reaction of barium metal vapor with oxidants such as O_2 and N_2O.[51-52] Despite such extensive investigation, new electronic states have been identified as recently as 1979,[53] suggesting that additional states may yet be discovered. The presently known electronic states of BaO in the visible region and their approximate potential curves are shown in Figure 4.

Although the gas phase spectroscopy of BaO has been thoroughly explored,[62] very little emphasis has been placed on the study of BaO in matrices. An exception to this is the work conducted by Ault and Andrews[54] who have studied several alkaline earth oxides in the infrared. To date, no research on matrix isolated BaO in the visible region has been reported.

The following study examines the spectra of BaO prepared in argon matrices and probed by Ar^+ laser excited fluorescence. This same technique has been used to elucidate the electronic structure of matrix isolated CuO.[55] Several aspects of the emission features observed in this experiment offer evidence that a new electronic state may exist in BaO. Preliminary studies on the vibrational lifetime of BaO in the $X'\Sigma^+$ state are also discussed.

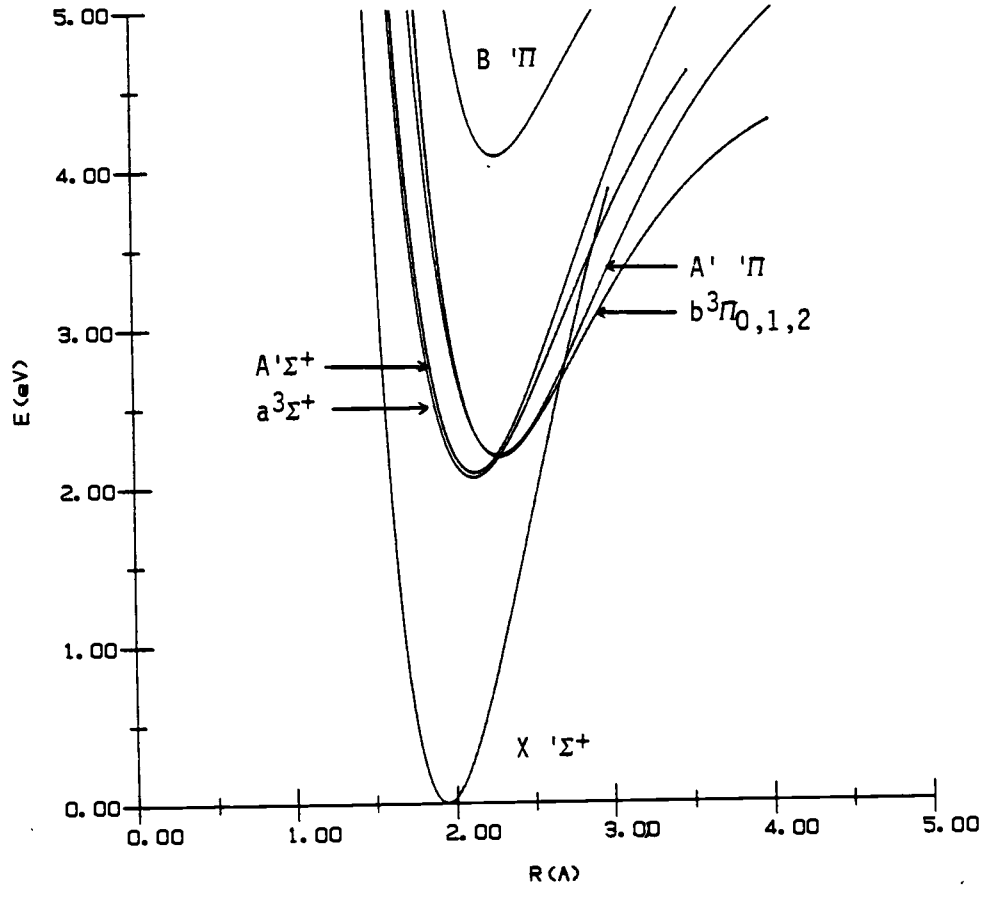

Figure 4: Morse potentials of barium oxide calculated from gas phase molecular parameters (62).

EXPERIMENTAL

Argon (Matheson, UHP 99.9995%) and O_2 (Airco, 99.99%) gas mixtures (Ar/O_2 = 100) were prepared by standard procedures. The premixed gas sample was co-deposited with barium atoms in a continuous manner onto a cooled aluminum substrate held at 18 K by an Air Products closed-cycle helium cryostat. Substrate temperatures were measured by an iron doped gold (0.07%) versus chromel thermocouple, and hydrogen vapor pressure thermometer with estimated error of ± 1 K. Flowrates of 6 mmols/hr were used for all samples.

Barium atoms were generated by electrically heating a capped tantalum tube (3/8" x 1 3/8") filled with barium metal (Alfa Inorganics 99.9%) to temperatures of 700 to 900°C (as measured by an optical pyrometer good to ± 25°C). These temperatures correspond to vapor pressures of barium of 9 mtorr to 2 torr. The barium atoms effused out of a small orifice (1 mm) onto the cooled substrate where the barium was mixed with the Ar/O_2 matrix gas. The oven assembly and geometric details of the brass shroud are explained elsewhere.[56] Barium samples were outgassed for 20 minutes prior to cool-down, at 50°C above the temperature to be used in a given experiment. The outgassing procedure removed most traces of surface oxides on the barium sample. However, the pressure in the cryostat remained at 1×10^{-5} torr during deposition, indicating that not all of the traces of oxides were removed.

Oxygen atoms for the reaction with barium were produced by VUV photolysis of the matrix sample after deposition. Photolysis was achieved with a hydrogen resonance lamp driven by a Burdick Microwave

Diathermy unit, Model Mm/200. The lamp was an air cooled glass discharge cavity with a flowing H_2/He = 3% gas sample. The output of the lamp (most intense line at 1216 A) was passed into the sample chamber through an LiF single-crystal window at 90° to the Knudsen cell oven. Following sample deposition, the cryostat was rotated for the photolysis and production of BaO. Photolysis times of 2 to 25 minutes were used.

Laser induced fluorescence of BaO was excited by a Spectra Physics 164 Ar^+ laser, capable of producing at least 100 mwatts for all laser lines. The emission was imaged onto the slits (150 um) of a Spex 1402 double monochrometer and detected with a cooled RCA 31034 photomultiplier tube. The uncertainty in the measured emission wavelengths is estimated to be 0.2 A.

Fluorescence was not observed for any of the Ar^+ laser lines until the sample had been photolyzed for at least 30 seconds. Longer photolysis times increased the intensity of fluorescence until a total photolysis time of about 2 to 3 minutes. At this point, no increase in fluoresence was observed with increased photolysis times.

LASER INDUCED FLUORESCENCE OF BaO IN ARGON

Dilute samples of BaO in argon were prepared using a Knudsen cell temperature of 800°C, followed by a two minute photolysis of the matrix sample. Using the procedure outlined in Appendix 1, a Knudsen cell temperature of 800°C and the flowrate of 6 mmols/hr corresponds to a Ar/Ba ratio of 6×10^3. Intense emission was observed from such samples with excitation from the 4880 A line of the Ar^+ laser. The emission consisted of sharp, intense (10^4 cps) features leading up to

the exciting line. With excitation by the 4727 A and 4579 A lines, the identical progression was observed, with the addition of a new feature at 4875.2 A which was no longer overlapped by the 4880 A background emission. The spectrum observed with 4727 A Ar^+, excitation is shown in Figure 5. The measured band maxima and estimated peak intensities are shown in Table 3.

Under more concentrated conditions (T_{Kn} = 900°C), the barium concentration increases by a factor of about ten. The matrix emission for all lines of the Ar^+ laser remained unchanged, except for additional sharp features shifted 20 cm^{-1} to the blue of the previously observed emission lines. The relative intensities of these new features decreased upon annealing and could not be reproduced from sample to sample. This behavior is generally consistent with the formation of an additional matrix site formed only in concentrated samples. Further discussion will center only on the samples prepared under dilute conditions (T_{Kn} = 800°C).

The spacing between successive features in the emission spectrum was 650 cm^{-1} while the gas phase 0-1 vibrational spacing is 665.7 cm^{-1}.[62] Other oxides of barium, BaO_2 and Ba_2O_2, have been studied by Ault and Andrews[54] in the infrared and vibrational transitions in these molecules appear well below 600 cm^{-1}. These authors assign an infrared transition at 612 cm^{-1} to the BaO monomer in a nitrogen matrix. Values for ω_e'' and $\omega_e x_e''$ in argon matrices were calculated with the results obtained from this work and are shown in Table 3. Clearly the fluorescing species is BaO.

There are several interesting points which confuse the assignment of the observed fluorescence. First, the emission feature is

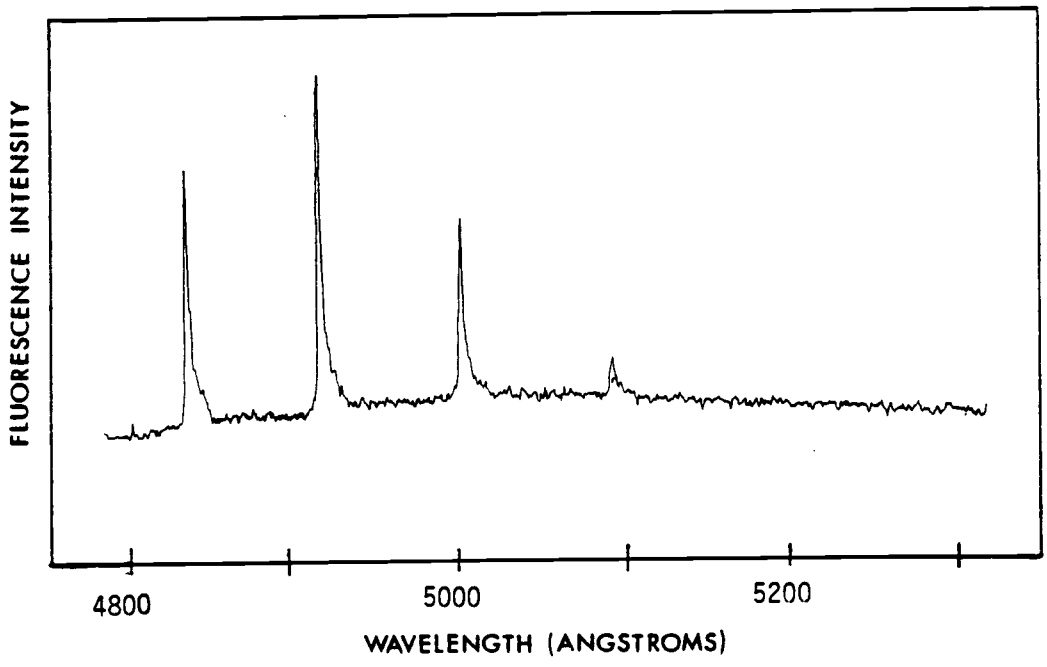

Figure 5: Fluorescence of BaO isolated in argon at 18°K, excited at 4727 A.

v'	v"	Ar Matrix (A)	Intensity	ΔG (cm^{-1})
0	0	4875.2	.30	665.6
	1	5038.8	.42	661.4
	2	5212.4	.20	653.5
	3	5396.2	.05	648.2
	4	5591.8	<.01	

Ar matrix: ω_e'' = 672.2 ± 1.0 cm^{-1} $\omega_e x_e''$ = 3.0 ± 0.5 cm^{-1}

Gas phase (62): ω_e'' = 669.76 cm^{-1} $\omega_e x_e''$ = 2.028 cm^{-1}

Table 3: Vibronic transitions and vibrational constants of BaO in argon at 18°K.

660 cm^{-1} to the red of the 4880 A line, indicating that the fluorescence is a v'→1", 2", 3", 4" sequence. With 4727 A and 4579 A excitation, the complete v"→0", 1", 2", 3" ... progression is observed. The 4727 A and 4579 A lines excite 663 cm^{-1} and 1347 cm^{-1} to higher energy than the 4880 A line. Since all of the known excited state vibrational spacings are on the order of 450 cm^{-1}, the 4727 A and 4579 A are clearly exciting different v' levels. Vibrational relaxation is occurring in the excited state from these upper v' levels to a lower final v' level from which the fluorescence occurs. The rapid vibrational relaxation within the excited state manifolds would be expected to continue from upper v' levels until the lowest v'=0 level is reached. This suggests that the observed progression should be assigned as a 0'-0", 1", 2" ... sequence from an electronic state approximately 20,000 cm^{-1} above the ground state.

There are four known excited states of BaO in the visible region with T_e values less than 17,700 cm^{-1} ($\sim$2 ev in Figure 4). In order for the observed emission to be from one of these states, the state would have to be shifted to higher energy by at least 2300 cm^{-1} for the $A^{\prime\prime}{}^1\Pi$ state and as much as 3100 cm^{-1} for the $A^1\Sigma^+$ state. This is a large matrix shift, far larger than found in other metal oxides studied in matrices. For example, in Table 4, the 0"-0' absorption of several metal oxide molecules is shown along with the gas phase value and most matrix shifts are on the order of 1000 cm^{-1} or less. This would suggest that the fluorescence observed in the matrix may originate from an electronic state that has not been previously observed in gas phase studies of BaO.

Table 4: Comparison of the gas-to-matrix shift of the 0" - 0' absorption of several matrix isolated metal oxides.

Molecule	Matrix	Transition	gas $^{0-0}_{(cm^{-1})}$	matrix	νgas - νmatrix	Ref
AlO	Ar	B $^2\Sigma^+ \rightarrow$ X $^2\Sigma^+$	20690	21858	- 1168	(73)
GaO	Ar	B $^2\Sigma^+ \rightarrow$ X $^2\Sigma^+$	25706	26323	- 617	(73)
InO	Ar	B $^2\Sigma^+ \rightarrow$ X $^2\Sigma^+$	23346	23878	- 532	(73)
ScO	Ar	B $^2\Sigma^+ \rightarrow$ X $^2\Sigma^+$	20571	20613	- 42	(100)
YO	Ne	B $^2\Sigma^+ \rightarrow$ X $^2\Sigma^+$	20742	21518	- 776	(100)
LaO	Ne	B $^2\Sigma^+ \rightarrow$ X $^2\Sigma^+$	17837	18367	- 530	(100)
CuO	Ar	B $^2\Sigma^+ \rightarrow$ X $^2\Sigma^+$	20490	20953	- 463	(33)
VO	Ne	A $^4\Sigma^- \rightarrow$ X $^4\Sigma^-$	17419	17517	- 98	(102)

There are several other observations which support this hypothesis. It is possible that the emission is phosphorescence rather than fluorescence and originates from one of the known triplet states. To examine this possibility, a measurement of the radiative lifetime of the 0'-1" emission was made. Using a short pulse (<15 usecs) at 4880 A, the time resolved fluorescence at 5039.8 A was measured. Although only a crude estimation of the lower limit of the radiative lifetime could be made with this apparatus, it was established that the radiative lifetime of the emission was less than 15 μsecs. Since most phosphorescence lifetimes are on the order of milliseconds (e.g., SnO, τ_{ph} = 0.24 msecs),[59] this short lifetime suggests that the emission is not from a triplet state, but originates from another singlet state. The intensities measured in this work, however, do not fit with the calculated Franck-Condon factors for either of the known singlet states. For example, no emission is expected from the $A^{\prime\prime}{}^{1}\Pi$ electronic state to the 0" level from any v' level possibly excited by the Ar^+ laser. For the $A'{}^{1}\Sigma^+$ state, emission to the 0" level is expected, but as shown in Figure 6, the measured intensities do not fit any of the calculated intensities of the v' < 8→v" observed transitions.

No other fluorescence features were observed with other Ar^+ laser lines. This is very surprising since it should be possible to excite the $A'{}^{1}\Sigma^+$ state with the lines to the red of the 4880 A line. However, it is also possible that these lines do not happen to match an absorption of BaO, but by using a tunable dye laser, an absorption may be found. Therefore, an Ar^+ laser pumped CW tunable dye laser (CRL 490) was used to excite fluorescence from the $A'{}^{1}\Sigma^+$ state of BaO. This

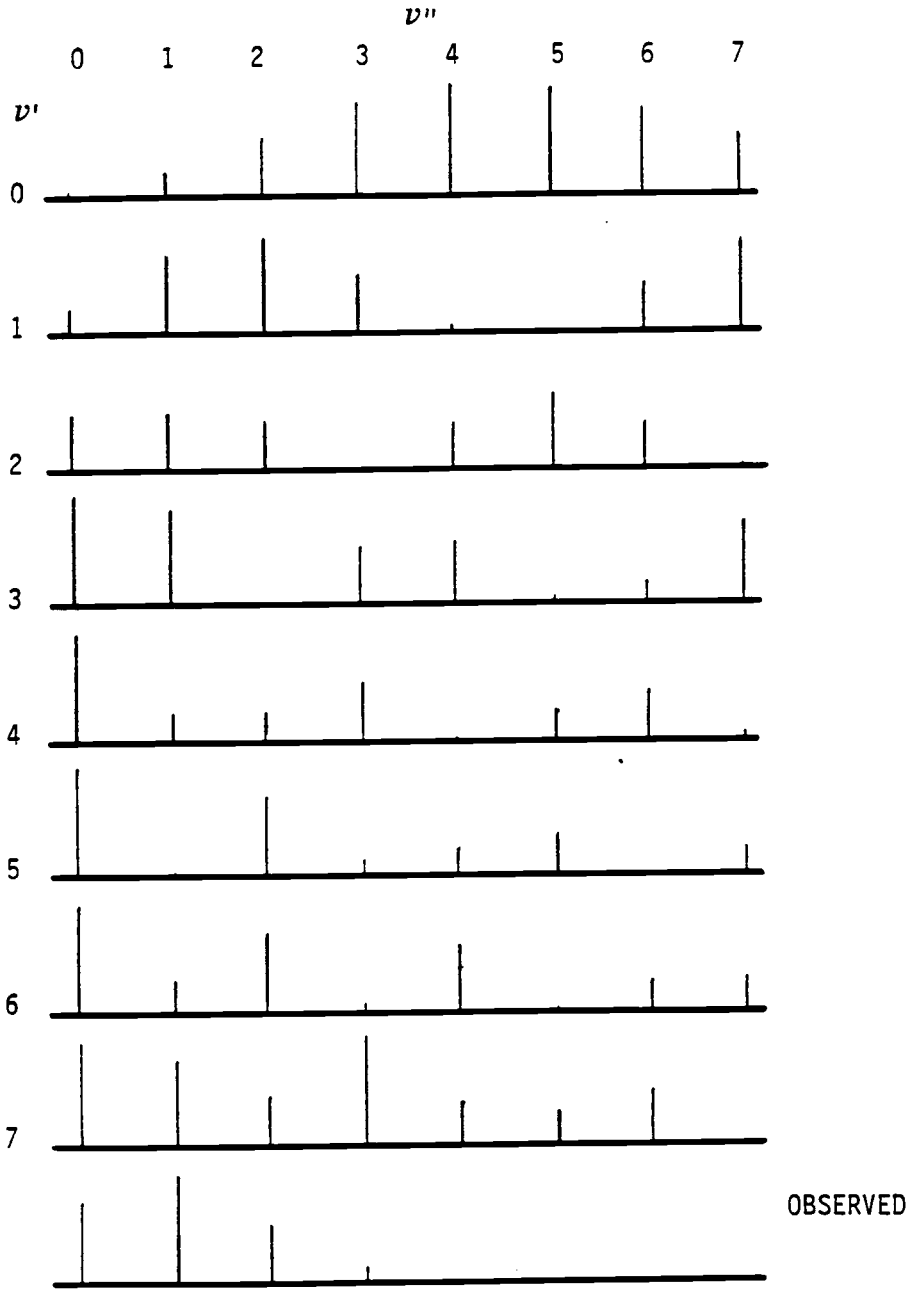

Figure 6: Comparison of observed BaO emission intensities from figure (5) with calculated intensities for the $A'\Sigma^+ - X'\Sigma^+$ transition.

laser produces approximately 200 mwatts in the region from 16,500 cm^{-1} to 17,500 cm^{-1}. However, no discrete emission from the sample was observed in this excitation region. This suggests that fluorescence from the $A'\Sigma^+$ state is completely quenched in the matrix environment. The $A'\Sigma^+$ state (and also the $A''\Pi$) is very close in energy to a lower lying triplet state (see Figure 4). Intersystem crossing in the matrix environment to the triplet state may be occurring which quenches the fluorescence.

VIBRATIONAL RELAXATION OF BaO IN ARGON

PRELIMINARY STUDIES

Originally, BaO was chosen because it was suspected that it might be a good candidate for vibrational relaxation studies using the OODR method. The application of the OODR technique, as described by Allamandola and Nibler,[50] requires the ability of not only time-resolved, but also wavelength-resolved emission. Unfortunately, wavelength resolution is not possible with BaO in argon due to the rapid vibrational relaxation within the excited state manifolds.

The measurement of the ground state vibrational lifetime of BaO using the OODR method is possible, however, if the lifetime of the v" level is much longer than the pump laser pulse. The experiment would then require two pulsed lasers to pump and probe the v" level, but in this case, the emission from each laser would be at the same wavelength. An experiment of this type was applied to the BaO case.

A short pulse from the modulated (Zenith acoustooptic modulator type M40) output of an Ar^+ laser at 4880 A (SP 164) was used to excite

fluorescence and thereby pump the v"=1 level. A Chromatix CMX-4 dye laser, tuned to excite the v"=1 level. The resulting 0"-0' emission at 4875 A was then measured. Unfortunately, no signal was detected which could be correlated to both the pump and probe lasers at any delay time. This suggested that relaxation was either very fast (<50 μsecs) or the population in the v" level was too small to measure. This problem could, perhaps, be overcome in future work by using a short pulsed (10 nsecs), high power pump laser to increase the population in the v" level and aid in the time resolution.

SUMMARY

In this chapter we have shown that BaO fluoresces in the matrix environment. The interpretation of the observed fluorescence spectrum is complicated by the complex electronic structure of BaO in the visible region. Indirect evidence was obtained which suggests that there is another electronic state for BaO with T_e = 20,000 cm^{-1}, previously unobserved in gas phase studies. A direct absorption measurement of this new state would be necessary to determine the important molecular parameters that characterize the state. Sensitive absorption measurements in the matrix are extremely difficult, due to the scattering nature of the matrix sample, the low concentration of the guest molecules, and the short pathlength inherent in the matrix isolation technique. In the last several years, Patel and Tam[58] have pioneered piezoelectric-crystal detection of very weak absorptions at low temperatures. This very sensitive technique may be useful in sorting out the absorption spectrum of BaO in the argon matrix, and perhaps, observation of this new electronic state.

We have also encountered in this chapter, problems in the application of the OODR method to the measurement of the ground state vibrational lifetime of BaO. The very sensitive nature of the photomultiplier tube could not be exploited because pump and probe lasers produced emission at the same wavelength and could not be discriminated. Conceivably, if a larger number of molecules were in the excited vibrational state, the emission from the probe laser could be distinguished from that of the pump laser. This is a manifestation of a problem common with the measurement of vibrational lifetimes

within the ground electronic state, that is, how do we selectively obtain reasonable concentrations of vibrationally excited molecules?

In the Legay type infrared fluorescence experiments, large populations of vibrationally excited molecules are produced by direct infrared absorption. Although this is very selective in the excitation process, the insensitivity of infrared detectors, particularly below 1000 cm^{-1}, makes the subsequent decay difficult to monitor. In the OODR technique, the population in the excited vibrational level is easily monitored due to the sensitivity of photomultiplier tubes. Unfortunately, the selective excitation of the vibrational level is not always possible. In the following chapter, a new method for the measurement of vibrational lifetimes in matrices is introduced which will be referred to as the Infrared-Optical Double-Resonance technique (IODR). In this method, direct infrared absorption of the guest molecule is used to selectively excite a particular vibration. However, the population in the excited vibrational level is then monitored by a visible laser absorption-fluorescence sequence. This new method combines the advantages of both the infrared fluorescence and OODR techniques.

This technique is not applicable to a molecule such as BaO since there are no tunable infrared lasers to excite the v" level at 660 cm^{-1}. However, a molecule which absorbs in the region covered by the CO_2 laser lines, such as AlO, is an excellent candidate for this method. In the following chapters, the IODR technique is applied to AlO isolated in argon matrices and is discussed in detail.

Chapter 3

Preparation and Spectroscopy of Aluminum Oxide in Argon Matrices

INTRODUCTION

In this chapter, some of the basic considerations regarding the synthesis and spectroscopy of matrix isolated AlO, necessary for the vibrational lifetime study in the following chapter, are considered. In the gas phase, AlO has been well studied and has had a long history of experimental investigation. Since its first observation in 1927,[61] there have been extensive studies of its optical spectra, both experimentally and theoretically.[62] The presently known electronic states and their approximate potential curves are diagrammed in Figure 7.

Of particular interest in this work are the two lowest lying electronic states, $A^2\Pi$ and $B^2\Sigma^+$, since for these excitation is possible with our experimental apparatus. The $A^2\Pi$ level was originally thought to exist due to perturbations which were observed on the well-known B state.[63] Theoretical considerations also suggested that a new state, lower in energy than the B state, might exist. Emission to this state was finally observed in 1969 by McDonald and Innes.[64] Since then, several experimental observations involving this state have been reported in the literature.[65-66]

In contrast to the A level, the $B^2\Sigma^+$ state has been documented many times in the literature.[62] The characteristic blue-green emission from the $B^2\Sigma^+ - X^2\Sigma^+$ system of AlO has been extensively studied due to its astrophysical and geophysical importance. Emission

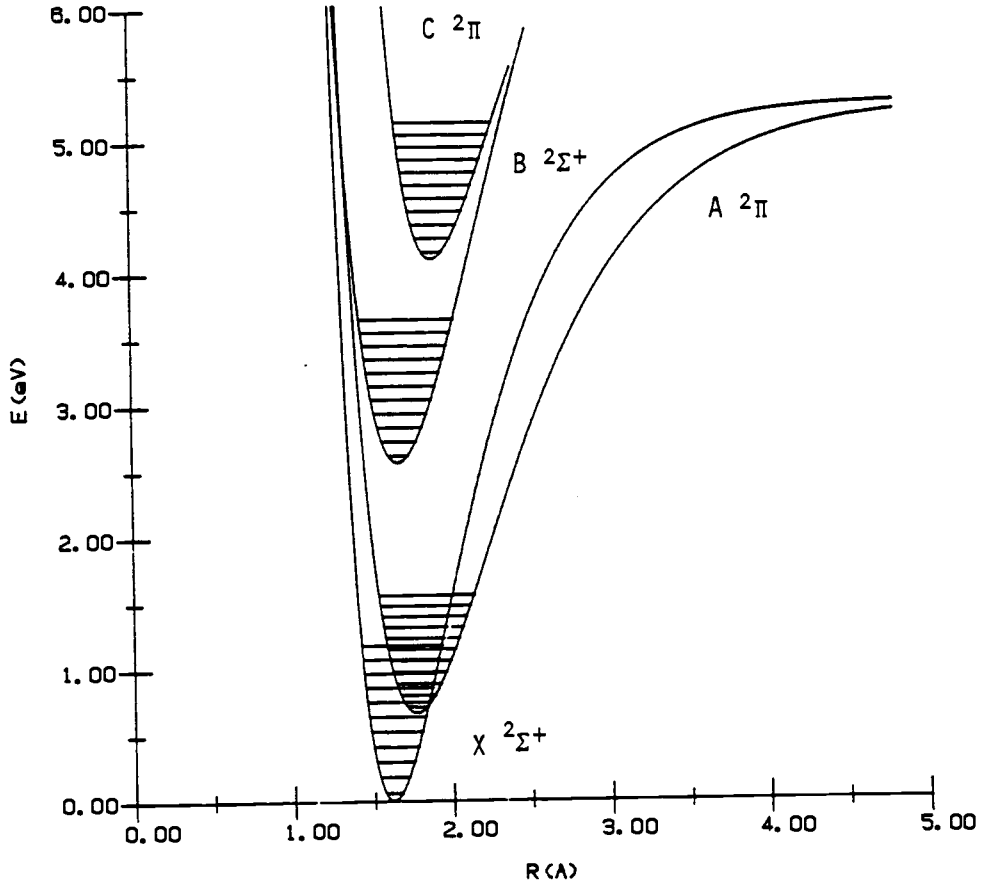

Figure 7: Morse potentials of AlO. Calculated from gas phase molecular parameters (62).

from this system has been observed from M-type stars,[67] and has also been used as a diagnostic tool in the measurement of temperature in the upper atmosphere.[68]

Laser induced fluorescence (LIF) studies of the $B^2\Sigma^+ - X^2\Sigma^+$ system have been used to examine the kinetics of the gas phase oxidation of the aluminum atoms:

$$Al + O_2 \rightarrow AlO + O \qquad (13)$$

Several studies using LIF to probe this reaction have been reported which gave the product state distribution of AlO molecules as a function of the Al atom velocity[69] and the O_2 partial pressure.[70] The radiative lifetime of this system has been measured to be 127 ± 4 nsecs.[71]

METHODS OF AlO GENERATION

For this present work, a convenient source of AlO was needed. Most of the previous work has centered around the high temperature vaporization of alumina, Al_2O_3. The vapor species over molten alumina have been investigated by mass spectrometry[72] and found to consist mainly of atomic Al and oxygen. Under reducing conditions (Al + Al_2O_3), tungsten and rhenium cells at 2500 K contain mainly Al, AlO, and Al_2O as the dominant vapor species with Al_2O_2, the dimer of AlO, present at lower concentrations. Unfortunately, at the lower temperatures accessible with our Knudsen apparatus, around 1200 to 1500 K, the vapor is composed of aluminum atoms and aluminum suboxide, Al_2O.

Another method that has been used to generate AlO is the gas phase reaction of aluminum atoms with an oxidant such as N_2O or O_2. Low concentrations of these gases in argon can be easily prepared and reacted with a beam of metal atoms, as in the barium oxide experiment. The reaction with N_2O has been used to prepare several of the group IIIA oxides in argon matrices.[73] In a kinetic study of the reaction of Al and O_2 by Fontijn, Felder and Houghton,[74] a very high rate coefficient for this reaction [$k = (3 \pm 2) \times 10^{-11}$ cm^3 $molecule^{-1}$ sec^{-1}] was found. More importantly, this rate coefficient showed no appreciable dependence on temperature over the range from 1000 to 1700 K. This implies that the reaction of Al and O_2 has no activation energy, in contrast to most metal combustion reactions. From the measured value for the rate constant, the authors conclude that a reaction between Al and O_2 occurs for one collision in ten.

Both N_2O and O_2 would be suitable oxidants for forming AlO but N_2O has the disadvantage that a low frequency bending mode of unreacted N_2O, at 588 cm^{-1}, might provide a significant path for relaxation of the excited AlO. Unreacted O_2, with a vibrational frequency of 1550 cm^{-1}, would not be expected to effect the lifetime experiments. Therefore, it was chosen to prepare the AlO in argon by co-depositing mixtures of argon and oxygen with atomic aluminum generated by Knudsen cell vaporization.

EXPERIMENTAL

In all experiments, matrices were prepared by continuous deposition of premixed gas samples onto a cooled 1" x 1" x 2" aluminum substrate. The tip was held at 18-20 K by an Air Products "Displex" closed cycle helium cryostat. Flowrates of 2 to 8 mmols/hr, as measured by a calibrated flowmeter, were used. Temperatures were measured with an iron-doped gold (0.07% Au) versus Chromel thermocouple and a hydrogen vapor pressure thermometer. Uncertainties in the temperatures are estimated to be 1 K. For annealing studies in the infrared, temperatures above 18 K were maintained by carefully controlling the helium bypass on the compressor, thus reducing the cooling capacity of the cryostat. For the fluorescence work, the temperature could be raised in a more controlled manner by passing AC current through a resistive heater at the cooled tip.

Argon/oxygen mixtures were prepared on an oil diffusion pumped vacuum system, capable of producing a final pressure of better than 1×10^{-4} torr. Oxygen, Airco (99.9%), was initially added to an empty bulb which was subsequently filled to a final pressure, greater than atmospheric, with argon (Matheson UHP 99.9995%). Concentrations in the range between 0.1 to 1% oxygen in argon were prepared. Pressure measurements were made using a calibrated Granville-Phillips "Pirani" type gauge (series 275) and/or a 0 to 1000 torr Validyne pressure transducer (Model AP10-42). Concentrations are estimated to have an error of no more than 5% in their nominal value. Samples containing $^{18}O_2$ were prepared from isotopically enriched oxygen (95% Stohler, Inc.) and were diluted with argon in the same manner.

Some difficulty was encountered in finding a stable source for the aluminum atoms. Liquid aluminum, as well as its vapor, is extremely caustic to most materials, so obtaining an appropriate container for these species is a problem. Graphite is porous to liquid aluminum, and tantalum and molybdenum both form stable amalgams. In the preliminary experiments, aluminum was placed directly into the same Knudsen cells used for the barium oxide study. Upon heating to the point where a reasonable concentration of aluminum would reach the matrix tip (1000°C), the liquid aluminum would leak through the tantalum and wet the outside surface of the Knudsen cell. Hence, control of the Knudsen cell temperature, and therefore, control of the aluminum concentration could not be maintained.

This problem was solved by using a boron nitride crucible to contain the aluminum sample. Boron nitride is a white, chalky material which is not chemically attacked at the operating temperatures of the Knudsen cell (<1500 K). The boron nitride (Carborundum Co. HP low oxygen grade) could be machined easily into 3/8" x 1 1/8" crucibles. A BN removable cap was fit onto the crucible to prevent the liquid or vapor sample from touching the surrounding tantalum heating jacket. A 1 mm orifice was drilled in the side of the crucible so that the hole matched the orifice on the existing tantalum cells. After enlarging the existing hole in the tantalum cell, the BN assembly was then inserted into the tantalum cell and assembled as before.[56]

Two different sources of aluminum were used: 1) 20 mesh powdered aluminum (Fischer Scientific Co., A-547, 99.9%), and 2) aluminum rod (Alfa assayed rod, 99.995%). No change in any of the relaxation rates

or any of the spectral features were observed with the different sources.

Infrared spectra were recorded on a Perkin-Elmer grating spectrometer (Model PE-180) with a resolution between 1 to 3 cm^{-1}. Uncertainties in the measurement of the bands is estimated to be 0.5 cm^{-1} in the region from 500 to 1050 cm^{-1}. In other regions, the errors are specified in the text. Samples were deposited on a polished aluminum substrate for approximately 1 hour. A reflection apparatus (shown in Reference 56), mounted in the sample compartment of the PE-180 instrument, was used to increase sensitivity. A polished CsI window capable of transmission down to 200 cm^{-1} was used. At 90° from the CsI window was a cleaved LiF single crystal used for photolysis studies. Dilute samples were made with a Knudsen cell temperature of 1000°C and concentrated samples above 1150°C. After 1200°C, the Knudsen cell would sometimes condense aluminum on the orifice, thus liquifying on the tantalum surface near the orifice, and destroying the tantalum cell. Most runs were kept below this value to maximize the lifetime of the Knudsen cell.

Optical spectra were obtained using the same apparatus as above, except that the aluminum substrate was replaced by a sapphire window. Quartz transmission windows on either side of the cold tip permitted scans from 700 nm to 190 nm, the limits of the Cary-15 visible spectrophotometer. Uncertainties in the measured wavelength values are estimated to be on the order of 1 nm.

Fluorescence spectra were excited by a Spectra-Physics 164 argon ion laser. Samples were deposited on an aluminum substrate similar to that in the infrared apparatus. The emission was collected and imaged

onto the 150 μm slits of a Spex 1402 monochromator equipped with a cooled RCA 31034 photomultiplier tube. The monochromator and photomultiplier signals were completely controlled by a PDP 11/10 laboratory computer. The uncertainties of the measured wavelength values are estimated to be less than 0.2 A. Errors in the actual peak measurements are due to the broad nature of the fluorescence features, or about 0.5 A.

SPECIES IDENTIFICATION

The ultimate goal of this work was to measure the vibrational lifetime of AlO in a known matrix environment. In the best case, only the molecular species of interest would be isolated in the matrix host. This can actually be accomplished in the study of stable molecular species, such as HCl or CO, since very pure and accurate gas mixtures of these species can be prepared.

The study of unstable species such as AlO, requires more care since accurate concentrations of radicals are difficult to make. The synthesis of these radicals may also generate other molecular species which can require attention in the analysis of the lifetime measurement. In the best situation, these impurities may be present, but have a negligible effect on the observed lifetimes. In any case, the identification of these species is a necessary requirement prior to the lifetime analysis.

The types of species which might be observed in the matrix may not be limited to those species in equilibrium in the Knudsen cell vapor. The process of condensation may trap molecules and ions not

normally seen under equilibrium conditions. Reactions and aggregations at the surface of the matrix may complicate the situation further.

Identification of the possible Al_mO_n species which may be observed, was aided in part by those studies on this system already done in the literature. For many of the species, spectral assignments are still under active discussion, thus making conclusions difficult. Several of the spectral features that were initially observed in this work have not been reported in the literature. Because of these points, a brief study, including isotopic substitution, was undertaken to clarify the assignments of the matrix isolated species. Each of the aluminum oxide species thus far described in the literature and determined by this work, is discussed in the following.

Al and Al_2

Conclusive studies on the spectra of matrix isolated aluminum atoms have been recently reported by Abe and Kolb.[75] In their work, a resistively heated tungsten Knudsen cell was used to produce aluminum atoms which were co-deposited with inert gas samples. These authors report a triplet at 291 nm, 287 nm, and 285 nm, as well as a single peak at 338 nm. These are attributed to the 3p-4d and 3p-4s transitions, respectively.

In our work, broad bands at 338 nm and 289 nm were observed in all matrices, independent of the Knudsen cell temperature. The assignment to the above aluminum atom transitions seems reasonable. The resolution of our Cary-15 instrument in this region was not sufficient to resolve of the triplet structure of the 3p-3d transition.

When the Knudsen cell temperature was raised to 1300°C, new bands at 406 nm, and 416 nm were observed. Matrices prepared in this fashion had a distinctive gold tint. Abe and Kolb observed four bands around 399 nm which were attributed to transitions in Al_2. Although the peaks observed in this work are slightly different in wavelength, it would seem logical, based on the Knudsen cell temperature behavior, to assign the above transitions to Al_2. Over time, these peaks disappeared in the spectrum while the peaks for AlO and Al remained unchanged. The Al_2 peaks also completely disappeared after seven minutes of Hg lamp photolysis. This bleaching behavior is very interesting as the Al_2 molecules are not disassociating into Al atoms or reacting with unreacted O_2 to make more AlO. The light appears to induce further aggregation, but the products do not absorb in the visible region.

AlO

The gas phase constants for the three lowest lying electronic states of AlO are well known.[62] The $B^2\Sigma^+ - X^2\Sigma^+$ transitions in argon matrices have been reported by Knight and Weltner[65] and other authors.[73,76] The values for the transitions are independent of the method for AlO generation and occur at 21859 cm^{-1}, 22726 cm^{-1}, and 23556 cm^{-1} in an argon matrix.[76] These bands are assigned to the (0,0), (1,0), and (2,0) transitions of the $B^2\Sigma^+ - X^2\Sigma^+$ system of AlO, and, as is typical for ionic molecules in matrices, are relatively broad (FWHM 300 cm^{-1}).

From infrared studies, Knight and Weltner[65] have assigned the Al-O stretch to a strong peak at 917 cm^{-1}. This implies a large

matrix shift from the gas phase value of 979.2 cm^{-1}.[77] Two other bands at 974 cm^{-1} and 944 cm^{-1} were unassigned. Using a hollow cathode sputtering apparatus to generate AlO, Finn et. al.[76] did not observe a peak at 974 cm^{-1} or 917 cm^{-1} when strong AlO visible absorptions were observed in argon matrices. These authors assign the Al-^{16}O stretch to a strong peak at 946.5 cm^{-1} and the Al-^{18}O stretch at 901 cm^{-1}. The experimental ratio (ν_{16}/ν_{18}) is 1.305, compared to a theoretical value of 1.0368 assuming no anharmonicity.

In our work, the well-documented visible absorption spectrum of AlO was also observed. Optical absorptions at 456.9 nm (21880 cm^{-1}), and 439.7 nm (22740 cm^{-1}) were seen and assigned to the (0,0) and (1,0) $B^2\Sigma^+ - X^2\Sigma^+$ transitions. The (2,0) transition was hidden because of the strong Al_2 absorptions. It was difficult to detect the AlO transitions when the Knudsen cell temperature was below 1150°C, but they were easily seen for temperatures above 1200°C. The visible spectrum recorded in this work and the spectrum reported by Finn et al. are shown in Figure 8.

Of particular importance in the relaxation experiments is the presence of species which absorb in the infrared region below 1000 cm^{-1}, near the AlO stretch. A spectrum of this region for a sample prepared in the same manner as in the visible experiments (T_{kn} = 1150°C) is shown in Figure 9. Under these conditions of high Al concentrations, several peaks in this region are observed, with the strongest occurring at 992.8 cm^{-1} and 912.0 cm^{-1}. Weaker peaks at 975.0 cm^{-1}, 965 cm^{-1}, 944 cm^{-1}, and 886 cm^{-1} were also observed. With a lower Knudsen cell temperature, only the peaks at 992.8 cm^{-1} and 912.0 cm^{-1} were left in the spectrum.

Under ^{18}O substitution, new absorptions appear at 949.5 cm^{-1}, 900.0 cm^{-1}, 878 cm^{-1}, and the strongest at 888.0 cm^{-1}. This spectrum is shown in Figure 9. Due to the presence of the strong ^{16}O impurity peaks, it can be assumed that some of the bands do not represent pure ^{18}O species, but contain ^{16}O as well.

It is apparent from the number of studies of the AlO molecule that a conclusive identification ofthe Al-O stretch in an argon matrix has been difficult. Using infrared data alone, there are so many peaks in the region that sorting out the identity of a particular peak has not been possible. It has been tacitly assumed in the literature that the Al-O band should be intense in the infrared when the corresponding electronic transitions are seen in the visible. This may not be the case, based on a recent paper by Lengsfield and Liu.[78]

In this paper, ab-initio calculations of the dipole moment function in the $X^2\Sigma^+$ state have been reported. Their results indicate that the dipole moment function is relatively constant during vibration, due to a gradual transition from Al^+O^- to $Al^{++}O^=$ as the bond length decreases. The authors calculate a vibrational band oscillator strength of $f = (4.0 \pm 3.0) \times 10^{-7}$ for the infrared active vibration. This extremely small value indicates that the infrared Al-O stretch is very weak (compared to CO: $f = 2 \times 10^{-5}$).

Making a conclusive identification of this very weak transition is a difficult problem. In this work, the Al-O absorption was conclusively found only by a double-resonance experiment involving simultaneous infrared and visible excitation of fluorescence. The work is described in detail in later sections, but the results indicate that

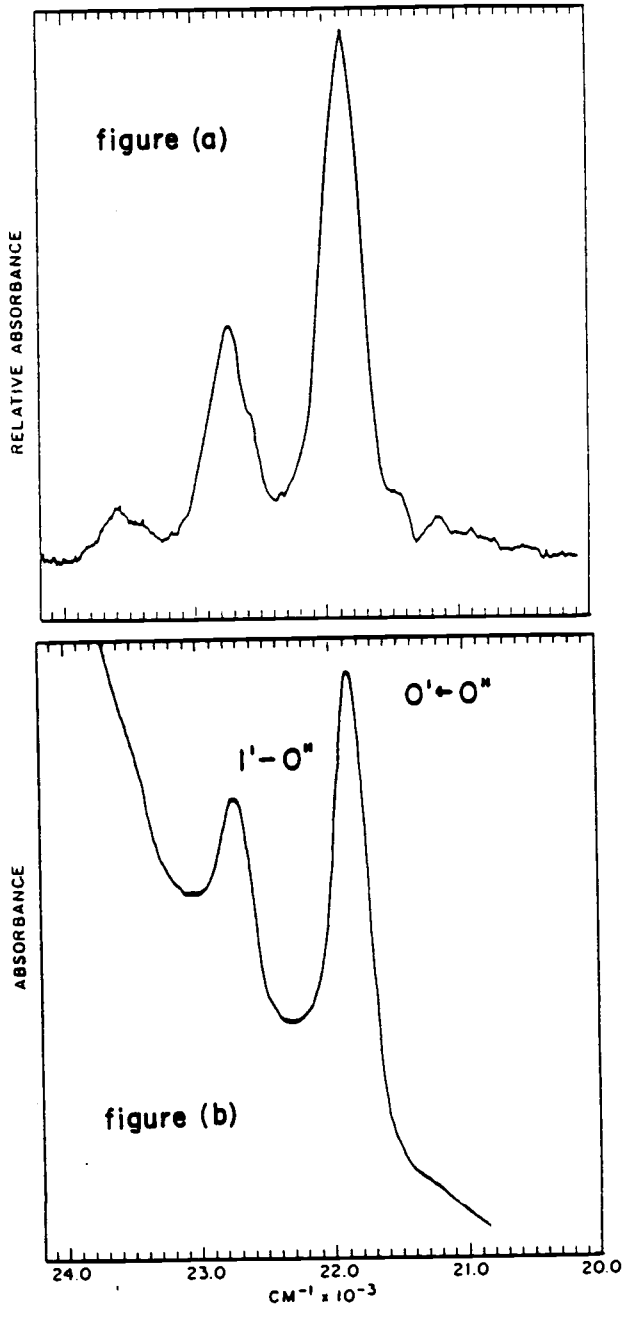

Figure 8: Absorption spectra of AlO in argon matrices: (a) from (76) and (b) from this work (maximum absorbance = 0.1), flowrate = 6 mmol/hr, T_{Kn} = 1200 C, deposition time = 1.5 hr.

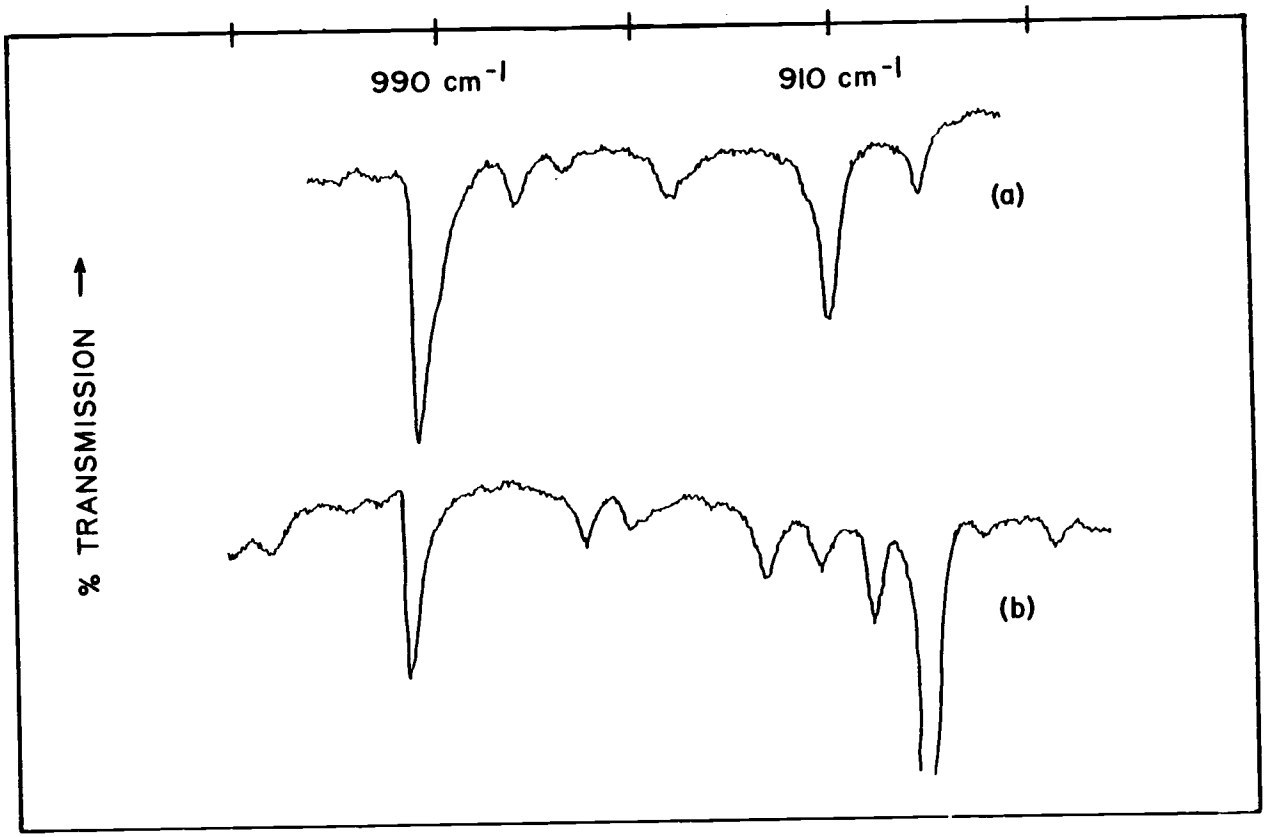

Figure 9: Infrared spectrum of Al/O_2 reaction products isolated in argon matrices. (a) 1% $^{16}O_2/Ar$, (b) 1% $^{18}O_2/Ar$. For both spectra, T_{kn} = 1150°C, flow-rate = 6 mmol/hr, T_{tip} = 18°K, and deposition time = 1.5 hr.

the $Al^{16}O$ and $Al^{18}O$ bands are close to the CO_2 laser lines at 974.9 cm^{-1}, [R(18)], and 942.4 cm^{-1} [P(22)]. This would give an experimental value for the isotopic ratio of 1.034, compared to the theoretical value of 1.0305. This agreement is certainly reasonable since the CO_2 laser lines do not necessarily excite right at the band maxima.

The infrared spectrum (of $Al/^{16}O_2$ products) shown in Figure 9 has a peak at 975 cm^{-1}, which is therefore assigned to the $Al-^{16}O$ stretch. The $Al-^{18}O$ band appears to be too weak to detect. The 975 cm^{-1} value corresponds to a small shift from the gas phase value of ω_e = 979.2 cm^{-1}. This in turn implies that the ground state of AlO is not perturbed greatly by the matrix environment. However, the absorption bands in the visible, and as we shall see, the emission features are quite broad. This would suggest that the excited electronic state is more strongly couples to the lattice.

<u>Al_2O</u>

Matrix isolated aluminum suboxide, Al_2O, has been studied more than any of the aluminum oxide species.[79-83] For this molecule, only one of the vibrations, the ν_3 antisymmetric stretch, has been conclusively assigned, at 994 cm^{-1} for $Al_2{}^{16}O$ and 951 cm^{-1} for $Al_2{}^{18}O$. The ν_1 symmetric stretch has been reported by Linevsky[79] and Mackowiecki[80] at 715 cm^{-1}. However, this assignment has been questioned due to the different behavior that this and the 994 cm^{-1} vand have upon annealing.[65,83] Mackowiecki[80] has assigned the bending mode to an absorption 503 cm^{-1}, but this has been questioned as well.[80,82,83] The ν_2 band is likely to be below 250 cm^{-1}.[65,79,80]

In our work, the strong ν_3 absorption at 992.8 cm^{-1} was observed in all cases even when no AlO band at 975 cm^{-1} was present. Under concentrated conditions, a peak at 715 cm^{-1} was present, but as observed by others,[83] was not always in the same intensity ratio to the 992.8 cm^{-1} band.

On ^{18}O substitution, a weak counterpart to ν_3 was observed at 949.5 cm^{-1}. It is odd that the $Al_2{}^{18}O$ band was not considerably stronger since the stated ^{18}O content of the sample was 95%. This observation would lead one to suspect that either very little ^{18}O was present in our isotopic sample due to a vacuum leak, or that the original isotopic assignment[76] is wrong. The appearance of strong peaks in the ^{18}O sample could result in either case so that a resolution of this inconsistency will require more careful study of the isotopic species.

Al_2O has also been studied in the UV by Abe and Kolb.[75] These authors report a strong Al_2O absorption at 268 nm which we see at 267 nm in our studies. The fact that the Al_2O band was always present in the UV is consistent with its constant appearance observed in the infrared spectra.

$\underline{Al_2O_2}$

Most of the previous matrix experiments on Al_2O involved co-depositing argon with the effluent from Knudsen cells containing Al and Al_2O_3. Marino and White[82] investigated the behavior of this system when small amounts of oxygen impurity were added to the argon. When 5% $^{16}O_2$ was added to the argon, a new band at 496 cm^{-1} appeared. This band shifted to 481 cm^{-1} when 5% $^{18}O_2$ was used instead. For a 5%

$^{18}O_2$:$^{16}O_2$ mixture, three closely spaced peaks were observed at 496 cm^{-1}, 489 cm^{-1}, and 481 cm^{-1}. These authors attribute these bands to the B_{2u} mode of rhombic (D_{2h}) form of Al_2O_2. Finn et al.[76] observed the same peaks in their experiments using hollow cathode sputtering techniques, along with a new band 490.5 cm^{-1}. This new peak, weaker than the B_{2u} mode of Al_2O_2, was assigned as the corresponding mode in a C_{2v} structure.

Neither of these two studies identified the other two infrared active modes of rhombic Al_2O_2. These B_{1u} and B_{3u} modes have been found for other metal oxide dimers such as Si_2O_2,[84] Li_2O_2,[85] and Sn_2O_2.[86] In all cases, the B_{1u} and B_{3u} modes are observed well below the B_{2u} mode in the infrared spectrum. By comparison, it is reasonable to assume that the B_{1u} and B_{3u} modes are lower in energy than the B_{2u} mode for the Al_2O_2 molecule, far below 400 cm^{-1}.

In our work, only two peaks at 535 cm^{-1} and 510 cm^{-1} were observed in the 500 cm^{-1} region. The strong peak at 510 cm^{-1} was present in all matrices, independent of the intensity of the monomer peak. When the concentration of oxygen was reduced from 1% to 0.2%, both bands decreased proportionately. Upon VUV photolysis, the 535 cm^{-1} band disappeared while the 510 cm^{-1} peak did not change. Isotopic substitution studies yielded only one new feature, at 480 cm^{-1}.

Interpretation of the above infrared data was hindered by the strong water vapor absorptions in this region which may have overshadowed weaker peaks in the spectrum. It seems reasonable to make a tentative assignment of the 510 cm^{-1} peak to the B_{2u} mode of $Al_2{}^{16}O_2$, somewhat shifted from the 496 cm^{-1} absorption observed by Marino and White.[32] The 480 cm^{-1} band is assigned to the same mode in the

isotopically substituted molecule.

This Al_2O_2 band was observed in all of the matrices. There are several possible mechanisms for the production of the dimer, such as: 2 AlO - Al_2O_2; $Al_2O + O - Al_2O_2$; $Al_2 + O_2 - Al_2O_2$. Because of the number of possible reactions leading to Al_2O_2, it is not surprising that it should be so permanent a feature in the spectrum.

$\underline{AlO_2}$

The existence of several metal dioxygen species such as LiO_2,[85] KO_2,[87] and NiO_2[88] have been reported. In general, the structure of these molecules is believed to be C_{2v}, with sideways bonding of the oxygen molecule to the metal. Spectroscopic evidence for AlO_2 has been reported by Finn et al.[76] and has also been observed in mass spectroscopic studies.[89]

Based on an elaborate annealing study, Finn et al. assigns two bands at 1177 cm^{-1} and 1168 cm^{-1} to the ν_1 mode of AlO_2. The two peaks are from two different matrix sites. These bands shift to 1143 cm^{-1} and 1137 cm^{-1} on ^{18}O substitution. The ν_2 and ν_3 bands were tentatively assigned to weak peaks at 717 cm^{-1} and 525 cm^{-1} (693 cm^{-1} and 510 cm^{-1} for the isotopically substituted compound). This data represents the only spectroscopic observation of AlO_2.

In this work, relatively weak bands were observed in all spectra at 1173 cm^{-1} and 1165 cm^{-1}. These bands shifted to 1140 cm^{-1} and 1133 cm^{-1} upon isotopic substitution. A band observed at 715 cm^{-1} did not maintain a constant intensity ratio with these peaks. Also, no peak in the region of 525 cm^{-1} could be attributed to the AlO_2 molecule. We conclude that the two peaks at 1173 cm^{-1} and 1165 cm^{-1} are

assigned to the ν_1 mode of AlO_2 but the tentative assignment made by Finn et al. regarding the other two peaks must be incorrect.

Al_2O_3

In all of the experiments, the Al_2O feature at 992.8 cm^{-1} was the most prominent band in the spectrum. With sufficient concentrations of O_2, a reaction between these two species to form Al_2O_3, seems likely. However, no previous assignment of this molecule to an infrared bands of the matrix have been reported in the literature.

In this work, the very strong feature at 912.0 cm^{-1} was observed consistently, and is tentatively assigned to the Al_2O_3 molecule. When 0.2% O_2/Ar samples were used, this peak decreased in intensity by a factor of five, in accord with this assignment. The band shifted to 888 cm^{-1} upon ^{18}O substitution. In the work by Knight and Weltner,[65] both the Al_2O band at 994 cm^{-1} and a band at 917 cm^{-1} were observed. In this study, however, the aluminum oxides were generated using 2500 K vaporization from cells containing alumina and molten aluminum. Under these extreme conditions, small amounts of oxygen impurity might explain the appearance of the Al_2O_3 band. It is surprising that no other strong features which could be attributed to the Al_2O_3 species was observed in the infrared spectrum.

Summary of the Ar/O_2 Reaction Products

A summary of the infrared bands observed in the reaction of aluminum atoms and oxygen molecules is given in Table 5. Also shown in Table 5 are the assignments of the various peaks to the aluminum oxide species observed in this work. As can be seen from this table,

Table 5: Summary of the matrix infrared data for the aluminum-oxygen system. All transitions are in cm^{-1}.

Species	Symmetry	$^{16}O_2$: Ar	$^{18}O_2$: Ar	Assignment
AlO	$C_{\infty v}$	974.9	942.4*	Al - O
Al_2O	$D_{\infty h}$ or C_{2v}	992.8	949.5	ν_3
Al_2O_2	D_{2h}	510	480	
AlO_2	C_{2v}	1173	1140	ν_1
		1165	1133	ν_1
Al_2O_3 ?		912	888	

Unassigned Peaks

$^{16}O_2$: Ar	$^{18}O_2$: Ar
1932	1111
1142	1096
1126	900
958	865
944	
921	
886	
715	
690	
535	

* From IODR method described in the following chapter

a number of the observed peaks are unassigned. Some of these might be expected to arise from possible impurities in this study.

Even with the greatest of care, all traces of water and air (in particular N_2 and CO_2) cannot be removed from the matrix apparatus. Therefore, it is possible that some of the unassigned peaks correspond to aluminum oxide species which have reacted with these impurities. The protonated aluminum oxide species might well occur since adsorbed moisture in the apparatus is difficult to remove.

Other species such as negative or positive ions could be present due to the electropositive character of aluminum. It is not possible to discern ionic species from neutral species on the basis of infrared data alone. Several aluminum containing ionic molecules have been observed by mass spectrometric methods on sputtering products from aluminum targets.[76]

ESTIMATION OF AlO AND Al CONCENTRATION

It would be useful in all of the relaxation studies to be able to determine the concentration of AlO molecules in the argon matrix. Obtaining quantitative concentrations would require the knowledge of oscillator strengths or the transition moments of some observed spectral feature. In this experiment, the optical bands of AlO are a characteristic feature of the AlO molecule and may be used for this determination.

Oscillator strength determinations in matrices are possible,[76] but such data is not available for the AlO molecular species. Nonetheless, an estimate of the concentration of AlO can be had by using gas phase oscillator strengths or radiative lifetimes. These values

can be related to the absorption coefficient in the matrix. This, with the measured absorption spectrum and a path length estimate, is in turn, sufficient to deduce the concentration.

The visible absorption spectrum of AlO is shown in Figure 8. This spectrum represents a relatively concentrated sample of AlO, far more concentrated than most of the samples used in the relaxation experiments and comparable to the infrared spectra shown in Figure 9.

To begin the calculation of the AlO concentration, the radiative lifetime of the observed $B^2\Sigma^+ \rightarrow X^2\Sigma^+$ transition is needed. In the gas phase, this value is reported to be 127 nsecs.[66] In an argon matrix, this value is smaller under the assumptions described in Chapter 1 by a factor of 0.54. A value of τ_{rad} = 69 nsecs results which is related to the Einstein coefficient of absorption, B_{00} by:

$$B_{00} = \frac{A_{00}}{8\pi h\bar{\nu}^3} = \frac{1}{\tau_{rad}\, 8\pi h\bar{\nu}^3} \qquad (14)$$

Wilson, Decius, and Cross[90] give a relationship between B_{00} and the absorption coefficient which upon integration yields

$$\int \alpha(\lambda)d\lambda = \frac{h}{c\bar{\nu}} B_{00}(N_0'' - N_0') \qquad (15)$$

where N_0'' and N_0' are the lower and upper state number densities.

In a real experiment, the absorbance of a sample, A, is measured as a function of wavelength, λ. The absorbance at any wavelength value is defined by the equation:

$$\ell\alpha = \ln \frac{Io}{I} \quad 2.303 \log \frac{Io}{I} = 2.303\ A \tag{16}$$

For a molecular transition, this equation must be integrated over the entire band. Equation (16) then becomes:

$$\ell \int \alpha(\lambda) d\lambda = 2.303 \int A(\lambda) d\lambda \tag{17}$$

Equation (17) may be combined with equation (15) to yield the desired relationship between the calculated number density and the measured parameters. If the number density in the upper state is considered negligible, this relation is given by:

$$\ell\ N_0'' = \frac{2.303\ c\bar{\nu}}{h\ B_{00}} \int A(\lambda) d\lambda \tag{18}$$

Using the measured band maximum (21859 cm^{-1}), the radiative lifetime and the appropriate constants, this equation may be evaluated to yield:

$$\ell\ N_0'' = 3.9 \times 10^{22}\ cm^{-3} \int A(\lambda) d\lambda \tag{19}$$

The integration over the entire absorption band may be approximated assuming a triangular type function such that $\int A d\lambda = A_{max}\ \Delta\lambda\frac{1}{2}$, where A_{max} is the maximum observed absorbance and $\Delta\lambda\frac{1}{2}$ is half of the base width in cm^{-1}. For the spectrum shown in Figure 8, $A_{max} = 0.08$ and $\Delta\lambda\frac{1}{2} = 75$ Angstroms. With these values, equation (19) becomes:

$$\ell\ N_0'' = 2.3 \times 10^{15}\ cm^{-2} \tag{20}$$

The film thickness, ℓ, could be measured using the laser fringe method. Alternatively, the thickness may be estimated from the measured

deposition rate, deposition time and area of the cooled substrate surface. It is this calculation that will be done here:

The thickness, ℓ, of the sample is given by:

$$\ell = \frac{(\text{deposition rate})\ (\text{deposition time})}{(\text{area})\ (\text{density})} \tag{21}$$

For the spectrum of AlO shown in Figure 8, the deposition rate = 6 mmole/hr, deposition time = 1.5 hr and the substrate was a 1" diameter sapphire disc. Using these values and the density of argon at 20 K, $\rho = 1.762\ \text{gm/cm}^3$,[91] the thickness of the sample is calculated to be:

$$\ell \simeq 400\ \mu\text{m} = 0.04\ \text{cm} \tag{22}$$

With this value of ℓ, the number density of molecules in the sample, N_o'', is calculated to be:

$$N_o'' = 6 \times 10^{16}\ \text{cm}^{-3} \tag{23}$$

Using the density of argon at 20 K, the number density of argon is $2.65 \times 10^{22}\ \text{cm}^{-3}$. The mole ratio (M/R), defined as the number of host species to the number of guest molecules, is then 5×10^5.

It would be interesting to perform this same calculation using the data for a comparable infrared sample. However, the radiative lifetime of the vibrationally excited molecule is not known in the gas phase or matrix. The radiative lifetime may be calculated using the theoretical oscillator strength of Lengsfield and Liu[78] of 4×10^{-7}. This calculation is described in a later section. If this is done and the same calculation is performed on the infrared band at 975 cm^{-1}, a mole ratio of 10^5 is obtained. It is satisfying that the two methods yield approximately the same result.

For the matrices used in the lifetime studies, the AlO concentration was much lower. Thus, even if these calculations are off by a factor of 10, the results still indicate that the guest concentration is quite low. This is an important consideration since we assume in the lifetime studies that the guest-guest interactions can be ignored.

In principle, concentration calculations can be done for all impurities in the matrix. Unfortunately, the radiative lifetimes for the molecular impurities have not been measured. Finn et al.[76] have reported an estimate of the oscillator strength of 0.107 for the 3p-4s transition of aluminum atoms in an argon matrix. With this value and the observed spectrum, an estimate of the Al atom concentration can be obtained. More importantly, since the absorption spectrum was recorded in the same sample as the AlO, an estimate of the ratio of Al atoms to AlO molecules can be obtained.

For the AlO spectrum shown in Figure 8, the aluminum atom 3s-4p transition occurs at 338 nm. For this band, $A_{max} = 0.37$, $\Delta\lambda_{\frac{1}{2}} = 150$ A. The calculated aluminum atom density is:

$$N_0'' = 3 \times 10^{17} \text{ cm}^{-3} \tag{24}$$

or five times the AlO concentration. This is a surprisingly large number of unreacted aluminum atoms considering the reactivity of atomic aluminum. In the matrix, a large percentage of unreacted O_2 would be expected. The presence of unreacted aluminum atoms would indicate that the aluminum probably does not have much freedom in the lattice to react with any nearby O_2. This would suggest that most of the Al/O_2 chemical reactions occur in the gas phase or at the surface of the matrix.

Now that a measure of the concentration of both the Al and AlO species has been made for the spectrum in Figure 8, it would be interesting to calculate the total amount of aluminum which was deposited. From this estimate, the amount of other aluminum containing impurities can be estimated. The details of this Knudsen effusion calculation are described in Appendix 1. For the spectrum in Figure 8, the Knudsen cell temperature = 1200°C and the Ar/O_2 flowrate = 6 mmoles/hr. Under these conditions, the calculated deposition rate of aluminum is 8×10^{-4} mmol/hr. The ratio of argon to the initially deposited aluminum is then ∿750/1. This can be compared to the calculated ratio of argon to Al of 9×10^4. This indicates that most of the aluminum aggregates or forms compounds in the concentrated samples.

LASER EXCITED FLUORESCENCE OF AlO IN ARGON

When matrix samples prepared by co-depositing aluminum atoms with Ar/O_2 mixtures were irradiated with the 4579 A line of the Ar^+ laser, a strong fluorescence was observed. The emission consisted of four intense, broad features close to the exciting line. Excitation with the 4545 A and 4658 A lines yielded a similar fluorescence spectrum. The fluorescence spectra from these excitation lines is shown in Figure 10. Listed in Table 6 are the observed emission bands along with the measured peak areas.

The intensity of fluorescence was strongly dependent on the excitation wavelength. For dilute samples, T_{Kn} <1100°C, the maximum fluorescence intensity from the 4545 A line was about a factor of ten less than the emission from the 4579 A line (10^4 cps). The emission

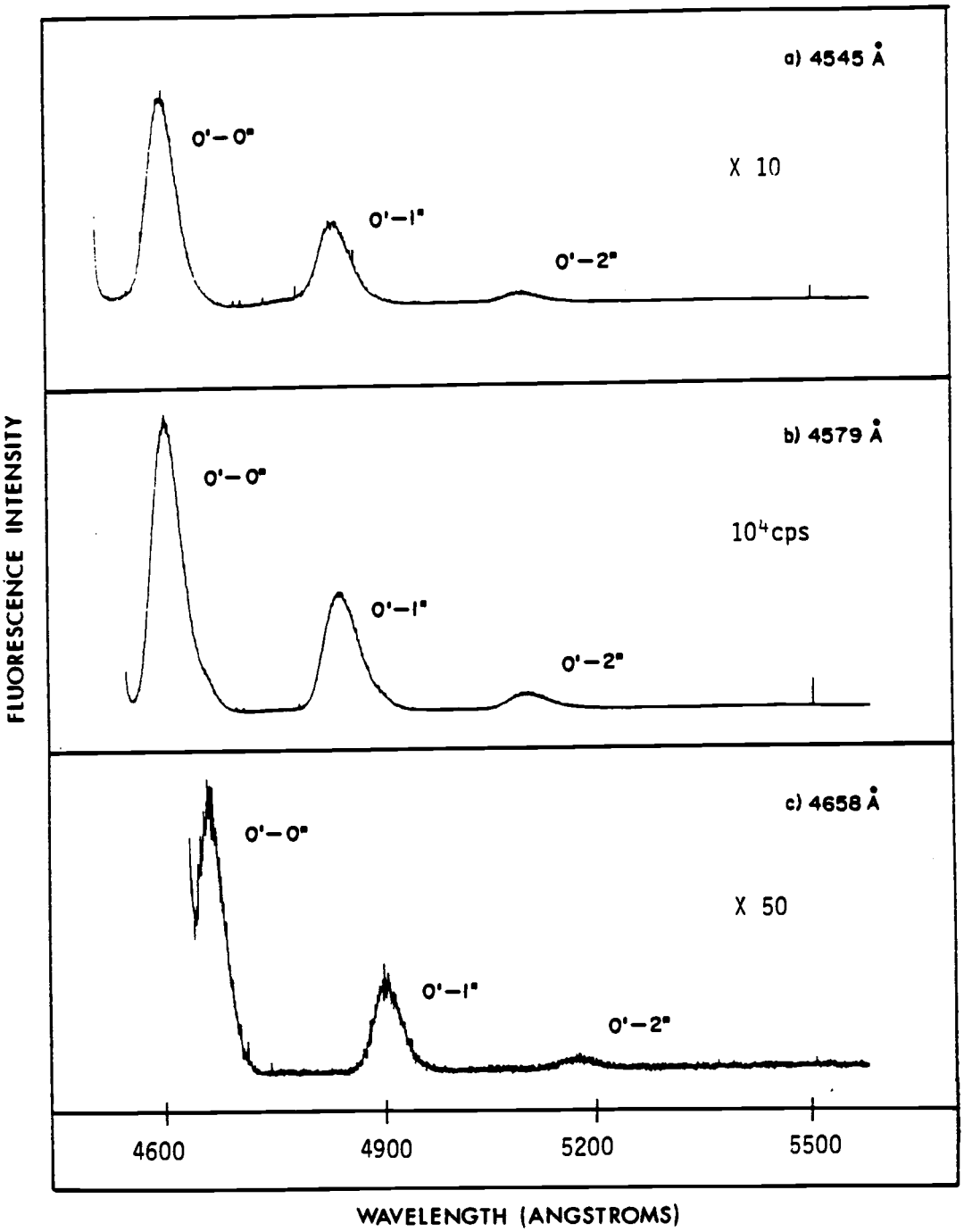

Figure 10: Fluorescence of AlO in argon at 18 K excited by several Ar^+ laser lines.

Table 6: Vibronic transitions and vibrational constants of B $^2\Sigma^+$ — X $^2\Sigma^+$ system of AlO in argon at 18°K.

FLUORESCENCE

Excitation wavelength (Å)	Assignment v'	Assignment v"	Observed emission	Intensity	ΔG (cm^{-1})
4658	0	0	4686	0.64	961
		1	4907	0.27	946
		2	5146	0.08	
4579	0	0	4633	.63	965
		1	4850	.30	949
		2	5084	.05	939
		3	5339	.01	
4545	0	0	4605	.63	965
		1	4819	.30	953
		2	5051	.07	

ABSORPTION

Assignment v'	Assignment v"	Argon Matrix (Å)	Gas Phase (Å)	Frank-Condon factors (92)
0	0	4569	4846.1	0.73
1	0	4397	4651.2	0.22
2	0	--	4454.3	0.04

	w_e'' (cm^{-1})	$w_e x_e''$ (cm^{-1})
Argon Matrix	976 ± 2	6 ± 1
Gas Phase	979.23	6.97

from the 4658 A line was about fifty times weaker than that from the 4579 A line.

With all exciting lines, the first emission feature was shifted by a small amount from the exciting line. The shift was 128 cm^{-1}, 255 cm^{-1}, and 286 cm^{-1} for 4658 A, 4579 A, and 4545 A excitation. This difference in energy is far less than the excited state vibrational frequency (850 cm^{-1}) and indicates that the emission is from the same v' level. These shifts in emission frequency can arise if the absorption-emission process involves the phonon side bands of the molecular transitions and perhaps, an inhomogeneous transition as well.

As can be seen in Figure 8, all laser lines are exciting the 0'-0" transition $B^2\Sigma^+ \leftarrow X^2\Sigma^+$ systems of AlO. The maximum of this transition is at 4569 A, very close to the 4579 A line. The 4545 A line excites well to the blue of the maximum and the 4658 A line excites far to the red of the maximum. The emission is a progression of lines originating from the 0' level to the 0", 1", 2", and 3" levels. The calculated Franck-Condon factors[92] for these transitions, along with their assignments are shown in Table 6.

Since each emission spectrum consists of three to four lines, approximate values for ω_e" and $\omega_e x_e$" can be obtained by plotting the $\Delta G_{1/2}$ values versus v" + 1 from all of the emission spectra. This has been done and is shown in Figure 11. The data can be fit to a straight line and the resultant values for ω_e" and $\omega_e x_e$" are shown in Table 6 along with the gas phase values.

It is apparent that the ground state parameters of AlO, calculated for the matrix, do not differ greatly from the gas phase values. This might suggest that the ground state is not strongly interacting with

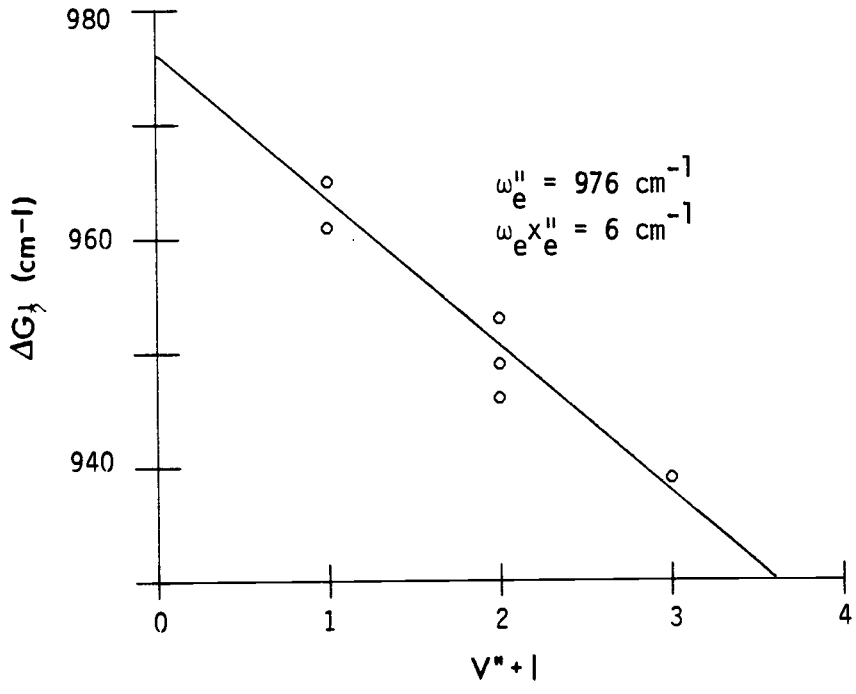

Figure 11: Plot of $\Delta G_{\frac{1}{2}}$ vs. v" + 1 from fluorescence data of AlO in argon. The straight line is from a least-squares fit to this data.

the matrix environment. However, the absorption and emission spectra show broad features, far broader than the gas phase. This would indicate that the excited state of AlO is strongly perturbed by the matrix.

The emission spectra of most AlO samples were not very sensitive to the aluminum concentration. As the Knudsen cell temperature was increased, only small increases in fluorescence intensity was observed. Often, when the Knudsen cell temperature was increased past about 1250°C, the aluminum would wet the outer surface of the Knudsen cell, allowing far larger quantities of aluminum to be deposited. During deposition, a bright blue chemiluminescence could be observed just above the matrix tip. Matrices prepared under these conditions, although of poor quality, were extremely concentrated. The fluorescence intensity exceeded 10^5 counts for the 4579 A line. These spectra were very similar to those already observed, but exhibited a shoulder, 250 cm^{-1} to the red of each fluorescence feature. It is important to point out that this shoulder cannot be attributed to unrelaxed emission. This energy difference is far larger than the difference between excited state and ground state vibrational energies (100 cm^{-1}) as would be expected if the shoulders originated from unrelaxed emission.[62] These additional features probably represent a new matrix site, which is formed only in extremely concentrated matrices.

In these concentrated matrices, fluorescence, around 6000 A, was observed in addition to the AlO features. This emission consisted of a sequence of broad lines spaced by about 210 cm^{-1}, and was independent of the exciting line used. None of the species discussed so far have visible absorptions except Al_2. The ground state vibrational spacing

of Al_2 is approximately 350 cm^{-1},[62] far larger than the observed spacing. It may be that the emission consists of two Al_2 interleaved sequences arising from two matrix sites. It is also possible that this emission originates from higher aggregates of aluminum which are so far uncharacterized.

Lastly, several experiments varying only the Ar/O_2 ratio were done. Only a slight intensity decrease in the fluorescence features was observed as the ratio of oxygen to argon was varied from 1% to 0.1%. Upon VUV photolysis, a very small increase in intensity (1-10%) was observed for the dilute matrices but no change was seen for the concentrated matrices.

Chapter 4

Vibrational Relaxation of AlO

THE INFRARED-OPTICAL DOUBLE-RESONANCE TECHNIQUE

In this chapter we discuss the measurement of the vibrational lifetime of matrix isolated AlO with the goal of learning more about the mechanisms for vibrational energy transfer in the cold matrix environment.

We begin by considering some of the basic experimental features of the infrared-optical double-resonance technique, as it is applied to AlO. The experimental apparatus is diagrammed in Figure 12. For this work, a polished NaCl window is used as a sample window to allow both infrared pumping and a visible probing of the matrix sample.

An Apollo XAT CO_2 laser was modified for tunability with the addition of a 75 line/mm grating and was used to excite AlO molecules from the v"=0 level to the v"=1 level. The grating, blazed at 10 μm in first order, was rotated about a pivot point in the center of the CO_2 laser axis, thus tuning it to a particular line in the [001]-[100,020] bands. The CO_2 laser requires a flowing gas sample made up of 6% CO_2, 18% N_2, and 74% He (Matheson) mixture.

The output of the CO_2 laser consists of 125 μsec FWHM pulses centered approximately 170 usecs after a sync out reference pulse. The repetition rate may be varied continuously from 10 hz to 120 hz. The output pulse is approximately Gaussian in time, with an average peak power of around 20 watts. For the weaker lines at the ends of the gain curve, the output power is approximately 500 mwatts. The

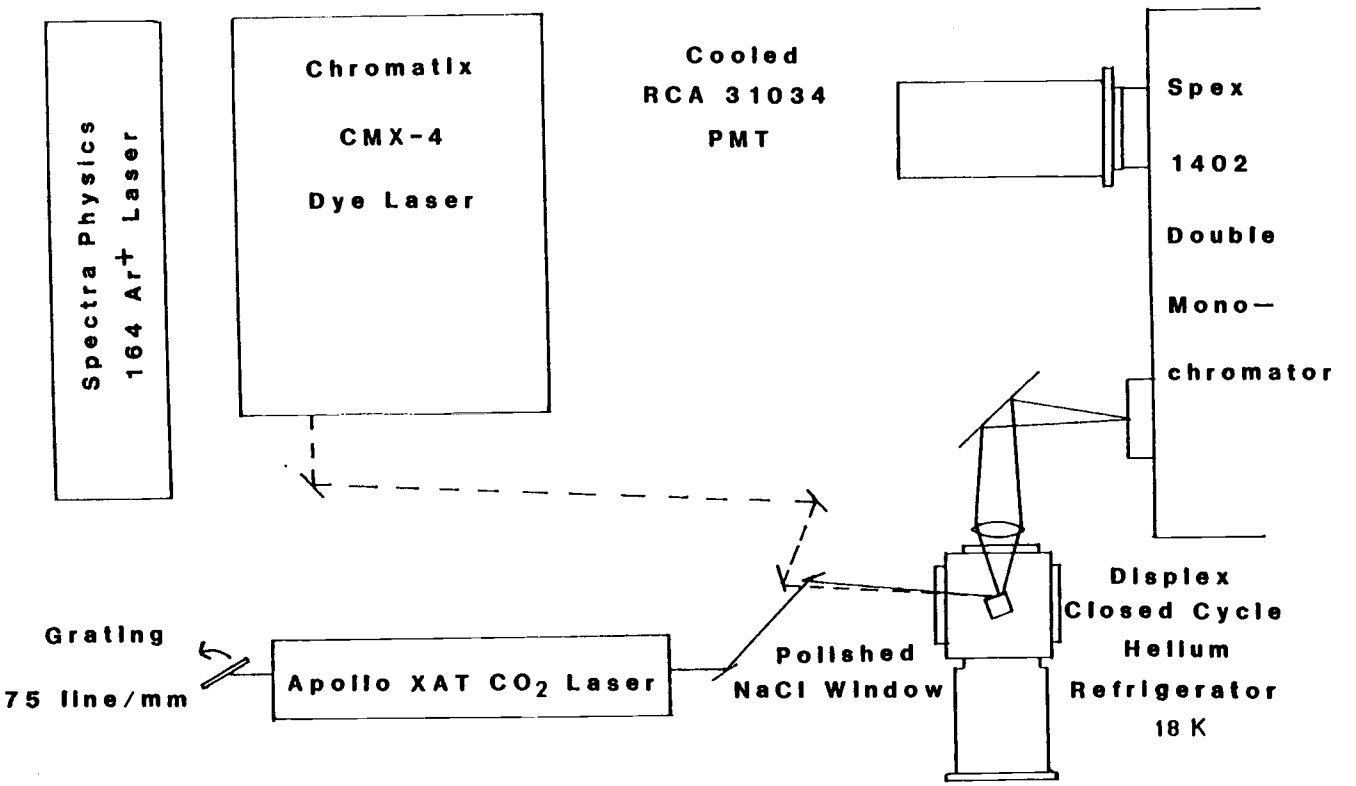

Figure 12: Schematic diagram of infrared-optical double resonance apparatus used in these experiments. An argon-ion laser (SP-164) was used for all cw laser excited fluorescence experiments.

repetition rate of the CO_2 laser may be adjusted to be in sync with the PE-180 chopper motors. The frequency of the output may then be measured by scattering radiation from the laser into the blocked sample beam. The micrometer on the CO_2 laser grating was calibrated as a function of wavelength. The Apollo XAT laser was not intended to be a tunable laser, therefore, the short cavity length and 50% reflecting front mirror prevented oscillation on the weaker lines. Consequently, only the [R(6)-R(30)] and [P(6)-P(30)] lines were available. Table 7 displays the observed laser lines for the 10.6 μm CO_2 laser line and the micrometer settings for a few of these lines.

To probe the v"=1 level of AlO, a Chromatix CMX-4 dye-laser was used. This laser produces 1 usec FWHM Gaussian pulses which may be fired by an external trigger. The laser, using Exciton Coumarin 480 dye, was tuned to excite the 1"-0" absorption at 4786 A (see Figure 13). The maximum output of the Coumarin 480 dye occurs at 5000 A, but a stable output at 4786 A was achieved with some care.

The fluorescence from the 0' level was imaged onto a Spex 1402 monochromator equipped with a cooled RCA 31034 photomultiplier tube. The signal from the photomultiplier tube is processed and then sampled. The monochromator was set to the 0"-0' fluorescence maximum at 4633 A. Since the emission was to the blue of the exciting wavelength, only the desired emission from the coupled 0"-1"-0'-0" sequence was measured, other than the small amount of background fluorescence from the dye laser. The monochromator slits were opened until this fluorescence was observed, around 250 μm.

Before starting the relaxation experiments, the CO_2 laser had to be tuned to the 0"-1" transition of AlO. To do this, the CMX-4 dye

Table 7: Wavenumbers, wavelengths and micrometer settings for the CO_2 laser 00 1 - (10°0,02°0) band.

Line	Microns air (um)	Wavenumber air (cm^{-1})	Micrometer setting
P(32)	10.72	932.8	---
P(30)	10.69	935.5	152
P(28)	10.67	937.2	---
P(26)	10.65	939.0	---
P(24)	10.63	940.7	154
P(22)	10.61	942.5	156
P(20)	10.59	944.3	---
P(18)	10.57	946.1	158
P(16)	10.55	947.9	---
P(14)	10.53	949.7	---
P(12)	10.51	951.5	160
P(10)	10.49	953.3	---
P(8)	10.47	955.1	---
R(8)	10.33	968.1	---
R(10)	10.31	969.9	170
R(12)	10.30	970.9	172
R(14)	10.19	971.8	---
R(16)	10.27	973.7	---
R(18)	10.26	974.9	178
R(20)	10.24	976.6	---
R(22)	10.23	977.5	---
R(24)	10.22	978.5	184
R(26)	10.20	980.4	186
R(28)	10.19	981.4	---
R(30)	10.18	982.3	---

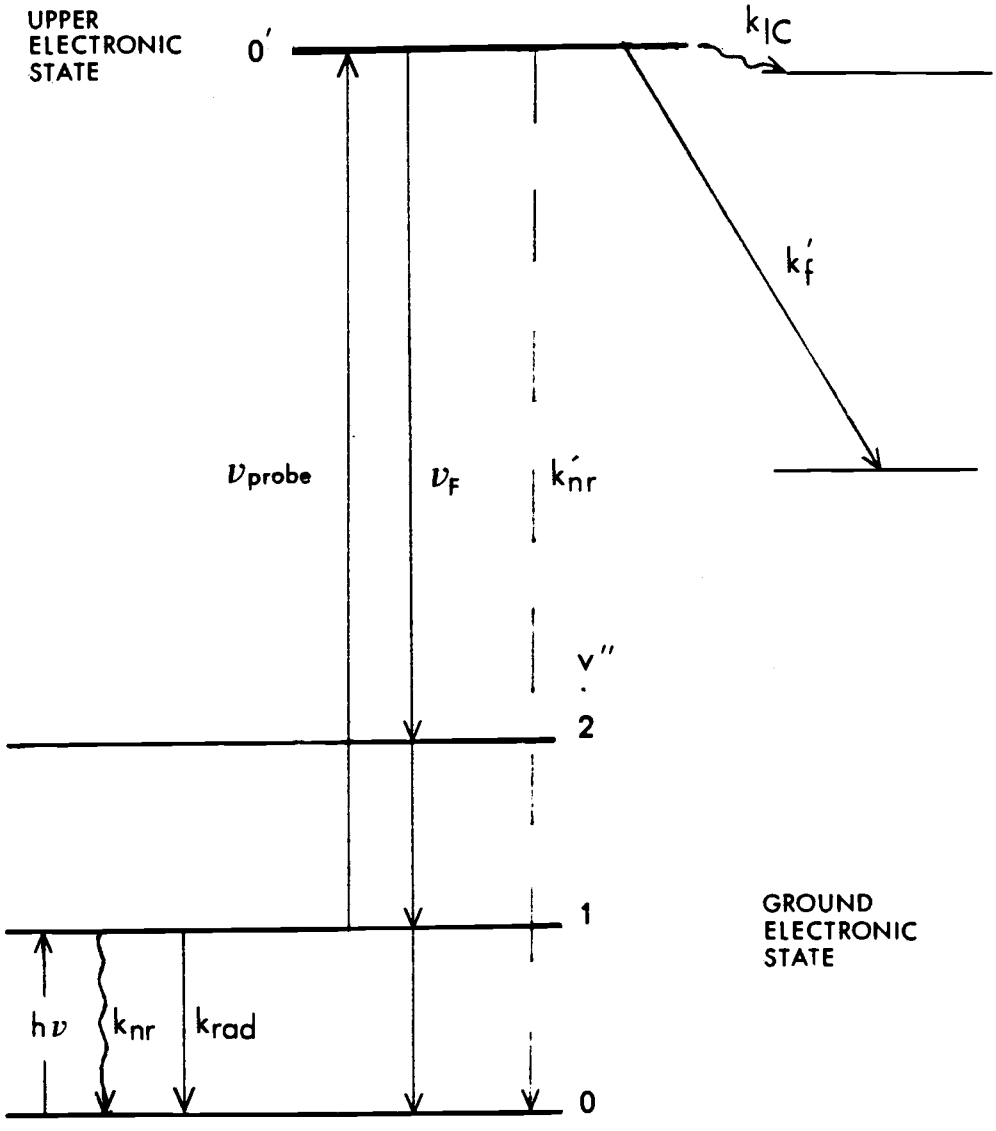

Figure 13: The infrared optical double resonance technique. Energy level diagram and schematic of possible relaxation pathways during pump and probe process.

laser was timed so as to fire at the CO_2 laser maximum, 170 μsec after the t=0 sync out pulse. The resulting fluorescence was then measured as a function of wavelength. The result for $Al^{16}O$ is shown in Figure 14. When equimolar samples of $^{18}O_2$ and $^{16}O_2$ were used, the resulting plot shown in Figure 14 was obtained.

The maximum signal for the $Al^{16}O$ molecule was observed at the R(18) line of the CO_2 laser at 974.9 cm^{-1}. The corresponding maximum for the $Al^{18}O$ molecule occurs at the P(22) line at 942.4 cm^{-1}. The small shoulders in Figure 14 are attributed to the fact that the laser may oscillate on two different lines. This may be a result of the lack of resolving power in the 75 line/mm grating or mode-hopping to non-TEM_{00} modes.

To measure the lifetimes of the AlO molecule, the sync-out timing pulse provides the t=0 origin. All delay times are measured with respect to this point. Before proceeding, the kinetics of the IODR method need to be examined to verify that a plot of the measured intensity of fluorescence versus time delay from the t=0 pulse is sufficient to map out the relaxation curve. The IODR technique consists of three main steps: 1) excitation of the v"=1 vibrational level and vibrational relaxation, 2) monitoring the population as it decays, and 3) analysis of the observed relaxation curve for rate information. In the following discussion, each of these areas will be examined; first in a general sense, and then as it applies to the AlO example.

Excitation of v"-1 Level and Vibrational Relaxation

Let us consider an idealized diatomic molecule isolated in the matrix, such that only intramolecular decay channels need to be

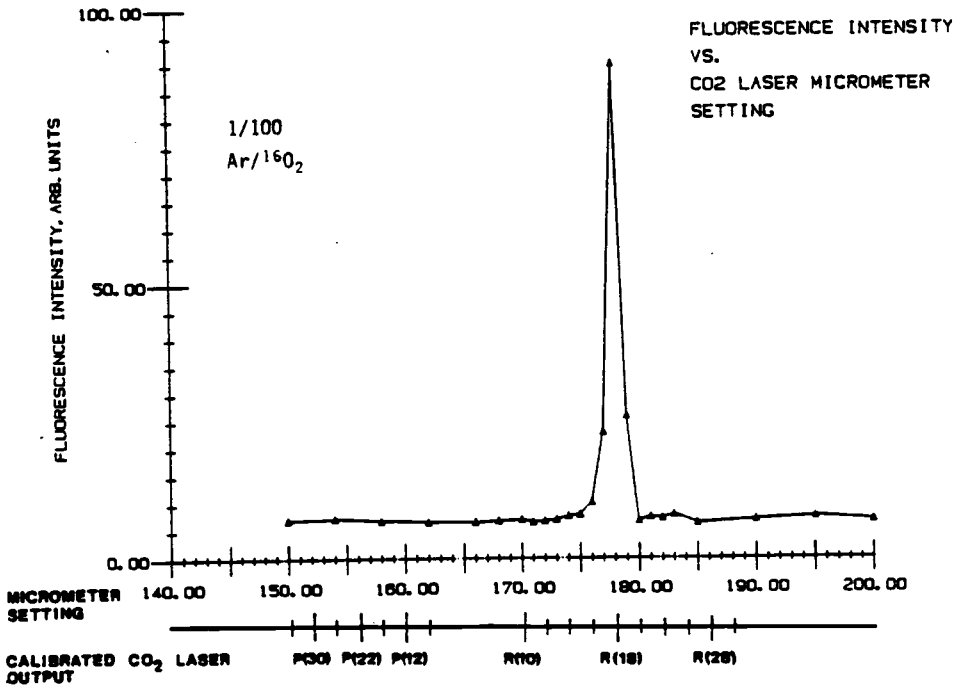

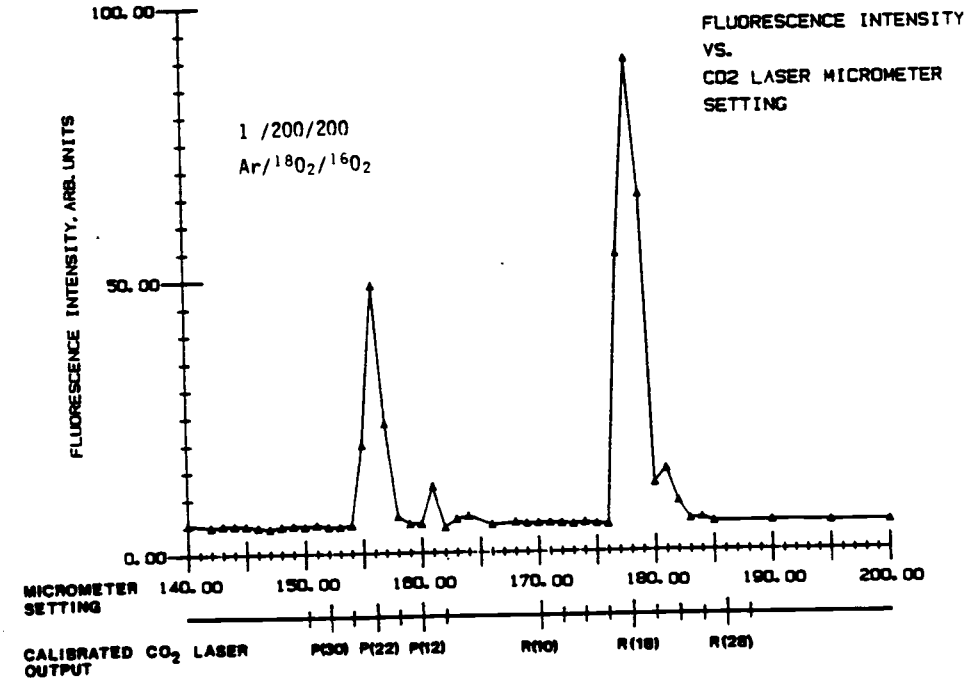

Figure 14: Fluorescence intensity from 1" — 0' excitation of AlO in argon vs. pump laser output. Dye laser wavelength = 4786 A.

considered. The diatomic molecule has a relatively simple electronic structure so only the ground state and first excited state of the same multiplicity are within experimental access. Lastly, the rotational constant of the guest molecule is small compared to the vibrational frequency (<0.1%) so that deactivation via localized rotational modes is relatively inefficient. Under these assumptions, the vibrational energy will decay via a purely first order path into delocalized lattice phonons. At time t=0, the fraction of molecules in excited vibrational levels is given by a Boltzmann distribution, and at the temperature of the matrix, <25 K, can be considered negligible, N* (t=0)=0. At time t_0, an infrared pulse excites a fraction of the guest molecules (equation 25). Once excited, the molecules may decay via two possible channels (see Figure 13): 1) radiatively, with first order rate constant, k_{rad}, and 2) non-radiatively, with first order rate constant, k_{nR}. These paths are described in equations 26 and 27.

$$N \xrightarrow{I_{ext}(t)} N^* \tag{25}$$

$$N^* \xrightarrow{k_{nR}} N \tag{26}$$

$$N^* \xrightarrow{k_{rad}} N \tag{27}$$

In equations 25 to 27, we are interested in the time rate of change of the excited vibrational level, dN*/dt. From these equations, the rate of change, dN*/dt is given by:

$$\text{before pump} \qquad N^* = \frac{dN^*}{dt} = 0 \tag{28}$$

$$\text{after pump} \qquad \frac{dN^*}{dt} = I_{ext}(t)\, N - (k_{nR} + k_{rad})\, N^* \tag{29}$$

One would normally expect the radiative lifetime to be much larger than the non-radiative lifetime. If we assume that $k_{rad} << k_{nR}$, and assume that the pump pulse only excites a small fraction of the ground state population, then equation (29) is readily solved to yield:

$$N(t) = N(0)e^{-k_{nR}} \int_0^t e^{k_{nR}t'} I_{ext}(t')dt' \qquad (30)$$

Equation (30) can be solved if the temporal profile of the pump laser is known. If the pump pulse is assumed to be a Gaussian centered at $t=t_D$, $I_{ext}(t) = \exp(-\alpha(t'-t_D)^2$, then equation (30) can be solved analytically. Under this assumption, the number of vibrationally excited molecules as a function of time is given by:

$$N^*(t) = N(0)\, e^{-k_{nR}t} \int_C^{\sqrt{\alpha}t-C} e^{-t'^2} dt' \qquad (31)$$

where $C = \sqrt{\alpha}\,[t_D + k_{nR}/2\alpha]$.

In this work, we can approximate the CO_2 laser pulse by a Gaussian centered at t_D = 170 μsecs. Equation (31) is plotted in Figure 15 for several values of k_{nR}.

Implicit in this analysis is the assumption that the radiative rate of decay is far smaller than the non-radiative rate. The radiative lifetime of the v'=1 level of AlO has not been measured but it can be estimated from the theoretical oscillator strength, calculated by Lengsfield and Lui[78] [$f=(4.0 \pm 3.0) \times 10^{-7}$]. Steinfeld[93] gives a simple relationship between the radiative lifetime and the oscillator

strength, calculated by Lengsfield and Lui[78] [f=4.0 ± 3.0) x 10^{-7}]. Steinfeld[93] gives a simple relationship between the radiative lifetime and the oscillator strength: $\tau_{rad} = 1.51/f\bar{\nu}^2$. For the AlO transition at $\bar{\nu}$ = 975 cm^{-1}, the calculated radiative lifetime is about four seconds. This value can be compared with an experimental measurement for CO in an argon matrix of 16 msecs.[49]

If one assumes that the transition moment integrals are approximately equal for these two diatomics, the AlO radiative lifetime is given by (from equation (1)):

$$\tau_{AlO} = \frac{\bar{\nu}_{CO}^3}{\bar{\nu}_{AlO}^3} \tau_{CO} \qquad (32)$$

The radiative lifetime of AlO, using $\bar{\nu}_{CO}$ = 2100 cm^{-1}, is then about 190 msecs. Since the transition moment integral of CO is probably far greater than for AlO, this calculation gives a lower limit for the radiative lifetime of AlO. For this reason, in the following we will take the approximation $k_{rad} < k_{nR}$ as a valid approximation.

Probing the Excited Vibrational Population

Once a fraction of the guest molecules are in the excited vibrational state, the population may be monitored by an absorption-fluorescence process. In the best situation, the Franck-Condon factors would be such that only two or three transitions between the excited vibrational state and the upper electronic state would be allowed. This would maximize the percentage of molecules which could be promoted to the electronically excited state without sacrificing emission

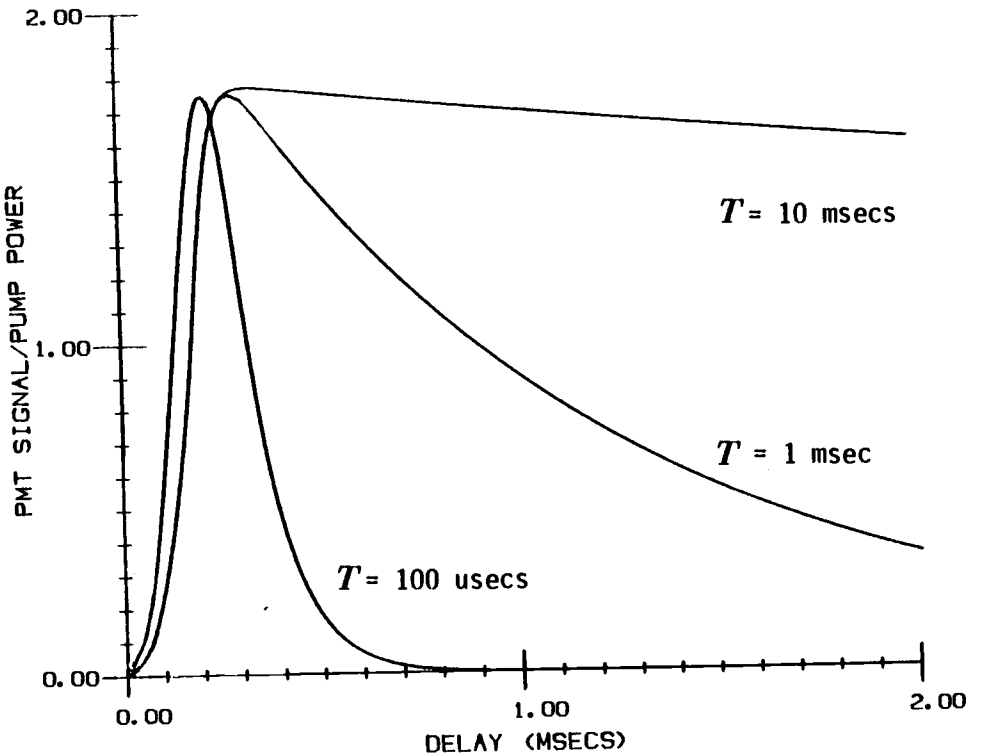

Figure 15: Calculated vibrational relaxation curve from equation (31), assuming t_D = 170 usecs and α = 60 usecs.

intensity. The maximum sensitivity would be in the case where the probe laser pumps the 1"-0' transition and the 0'-0" emission is collected. In this situation, the laser is not of sufficient energy to pump the competing 1"-1' transition.

The visible probe laser excites some fraction of the vibrationally excited molecules into the excited electronic state, where (as in Figure 13) they can return to the ground state via several possible paths: 1) the molecules may relax directly into the ground state by a radiative or non-radiative path, k'_{rad} and k'_{nR}, 2) if there is a lower lying electronic state, the molecule may fluoresce to that state k'_f, and 3) the molecule may non-radiatively cross into another electronic state, k'_{IC}. All of these processes serve to reduce the intensity of the measuved fluorescence. There is no reason to suspect that these processes might have a different rate with each laser pulse. Consequently, the intensity of fluorescence is proportional to the v"=1 population.

Analysis of the Relaxation Curves

From the previous discussion, there are two possible methods for the data analysis. First, the data can be fit by convoluting over the measured fluorescence intensity in a point by point fashion. This method would require an accurate knowledge of the functional behavior of I (t) at all points, plus an accurate knowledge of the statistical behavior at each point. Such a method would be mathmatically very complicated, but have the virtue that very fast relaxation rates could be calculated.

The second possible method would include only those points in the

data analysis after the intensity of the pump pulse is zero. As this is the most simple method, requiring the fewest mathematical manipulations, it was applied to the following AlO relaxation analysis. The temporal behavior of the pump pulse is shown in Figure 16. From this diagram, it is clear that the intensity of the pump pulse is zero after a 380 μsec delay. Therefore, in all the data analysis, only data points after 400 μsec are included.

To obtain accurate lifetimes from any experiment measuring data of intensity versus time, the intensity should be measured from its initial value to the baseline where intensity = 0. If the baseline is known to be zero or constant, then one or two decade changes in the initial value of intensity are often considered adequate.[12] However, if the baseline is non-zero and variable, it must be included as a parameter in the lifetime calculation. This is the case with the present work on AlO. The background fluorescence of the dye laser provides a small, fluctuating (<3% of the initial value), but non-negligible background. To fit the data, a model function which includes this baseline must be used (see equation (33), page 107).

VIBRATIONAL RELAXATION OF AlO IN ARGON MATRICES

The collection of all vibrational lifetimes were done using a PDP 11/10 microcomputer with 10 bit analogue-to-digital converters. The main program labeled "Vibtm" was used for all subsequent data files. The FORTRAN and assembly Language routines used in this program, as well as the important documentation, are listed in Appendix 2.

The most important points regarding the collection of relaxation curves in this experiment are listed below:

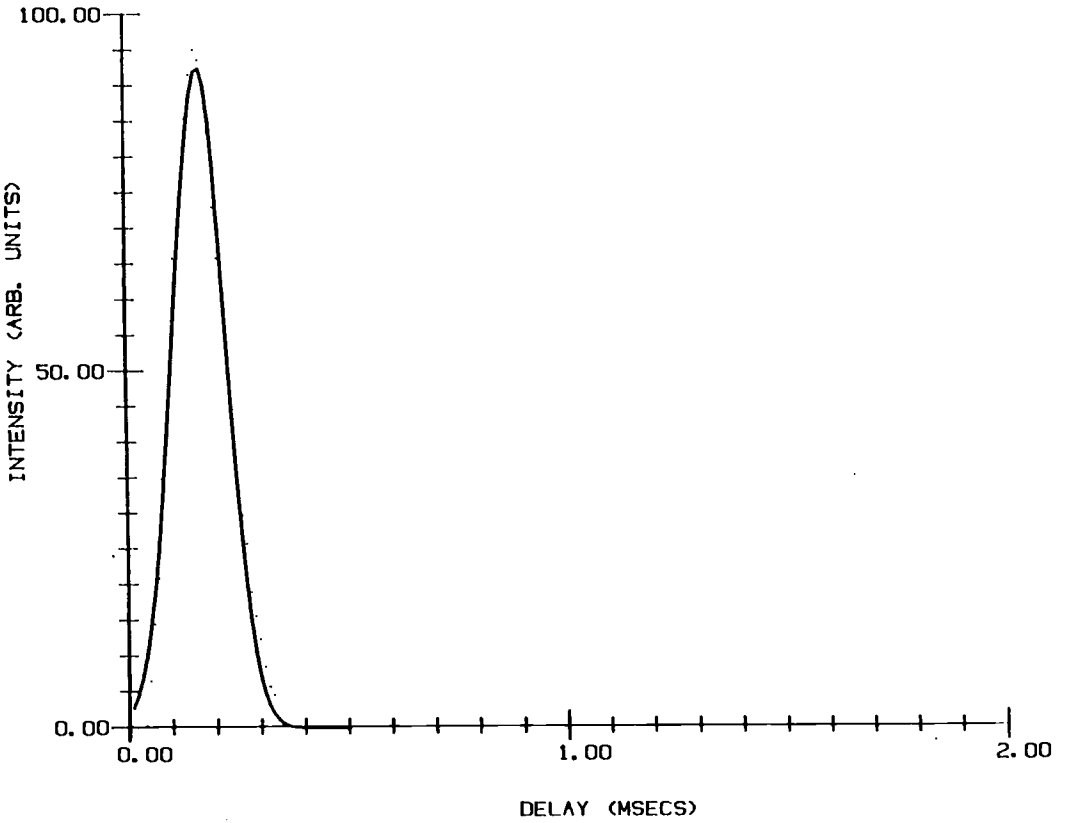

Figure 16: Profile of CO_2 laser pulse in time. Each laser pulse occurs 170 usecs after a reference t=0 trigger, and is 120 usecs (FWHM) in duration.

1. At each delay time, an average of 5-25 shots were taken. The average of these shots and the standard deviation in the average were calculated and recorded.
2. A maximum delay time of 2 msecs, 10 msecs, 20 msecs, and 100 msecs could be chosen, depending on the observed lifetime.
3. For all sample files, there are 100 points in each curve, spaced equally in time.
4. Each curve took approximately 2-4 minutes to record, the average, stability time of the CO_2 laser.
5. Between 3 and 9 different recordings of each relaxation curve were collected and stored. An average value of the fitted parameters could then be calculated.
6. For each CO_2 laser and dye laser shot, the dye laser power, CO_2 laser power, and fluorescence intensity were measured. A ratio of the fluorescence to the dye laser was calculated and stored.

The purpose of this present study is to examine the rate of vibrational decay dependence on a number of important parameters, such as temperature, Al concentration, and O_2 concentration. To establish the relaxation time as a function of these parameters, over 75 different samples were prepared. A relaxation curve of a typical dilute sample is contrasted to that for a very concentrated sample also shown in Figure 17.

The data from the upper trace in Figure 17 and analyzed functional values are shown in Table 8. The delay times and experimental 0'-0"

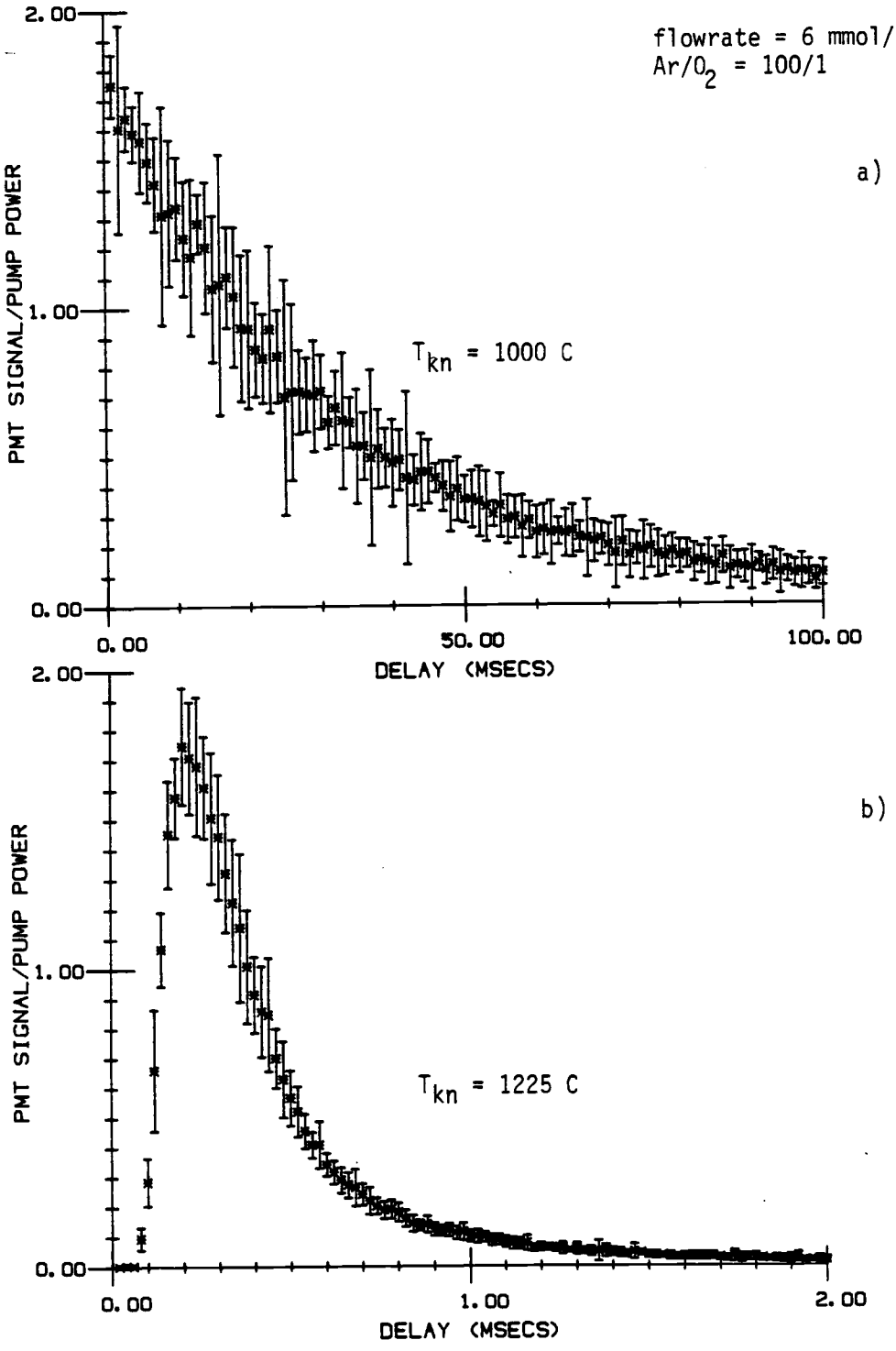

Figure 17: Typical data for AlO relaxation: a) dilute sample and b) concentrated sample.

Table 8: Experimental and calculated values of $0' \rightarrow 0''$ fluorescence intensity using equation (33) for $Ar/O_2 = 100$, $T_{tip} = 18$ K, $T_{kn} = 1000$ C.

Point number	t(msec)	Intensity experimental	Intensity calculated	Absolute differences
1	1.00	95.00000	95.71326	-0.71326
2	1.00	95.00000	95.71326	-0.71326
3	2.00	87.08079	92.56818	-5.48740
4	3.00	89.03390	89.52905	-0.49515
5	4.00	86.21105	86.59230	-0.38125
6	5.00	84.73097	83.75450	0.97647
7	6.00	80.99261	81.01229	-0.01968
8	7.00	76.99486	78.36247	-1.36761
9	8.00	71.25763	75.80193	-4.54430
10	9.00	71.73064	73.32764	-1.59699
11	10.00	72.58513	70.93673	1.64840
12	11.00	67.07677	68.62634	-1.54957
13	12.00	63.67411	66.39378	-2.71967
14	13.00	69.76229	64.23648	5.52581
15	14.00	65.42885	62.15182	3.27702
16	15.00	57.92162	60.13740	-2.21578
17	16.00	58.62352	58.19086	0.43266
18	17.00	59.99679	56.30986	3.68693
19	18.00	56.44154	54.49226	1.94927
20	19.00	50.71957	52.73589	-2.01632
21	20.00	50.52120	51.03869	-0.51749
22	21.00	46.79810	49.39866	-2.60056
23	22.00	45.19595	47.81388	-2.61794
24	23.00	50.50594	46.28250	4.22344
25	24.00	45.57742	44.80271	0.77470
26	25.00	38.07019	43.37277	-5.30258
27	26.00	39.04674	41.99100	-2.94426
28	27.00	39.07726	40.65580	-1.57854
29	28.00	38.58898	39.36556	-0.77658
30	29.00	38.36010	38.11879	0.24131
31	30.00	39.12304	36.91404	2.20899
32	31.00	33.50787	35.74987	-2.24200
33	32.00	36.14761	34.62490	1.52271
34	33.00	33.82830	33.53786	0.29044
35	34.00	33.44684	32.48743	0.95941
36	35.00	29.12865	31.47238	-2.34373
37	36.00	29.18969	30.49154	-1.30186
38	37.00	27.06874	29.54373	-2.47499
39	38.00	28.60986	28.62786	-0.01800
40	39.00	27.02297	27.74284	-0.71987
41	40.00	26.07693	26.88764	-0.81070
42	41.00	26.61099	26.06125	0.54973
43	42.00	23.31513	25.26270	-1.94757
44	43.00	22.93366	24.49105	-1.55739
45	44.00	24.38323	23.74541	0.63783
46	45.00	24.45952	23.02487	1.43465
47	46.00	23.28461	22.32862	0.95599
48	47.00	21.85031	21.65582	0.19448
49	48.00	19.86669	21.00569	-1.13900
50	49.00	21.23996	20.37746	0.86250
51	50.00	19.37841	19.77040	-0.39198
52	51.00	19.39367	19.18378	0.20989
53	52.00	18.93591	18.61693	0.31899
54	53.00	18.05092	18.06917	-0.01826
55	54.00	16.67764	17.53987	-0.86223

Table 8: Continued

Point number	t(msec)	Intensity experimental	Intensity calculated	Absolute differences
56	55.00	18.24928	17.02840	1.22087
57	56.00	15.65532	16.53417	-0.87885
58	57.00	16.03678	16.05658	-0.01980
59	58.00	14.38885	15.59508	-1.20623
60	59.00	15.47221	15.14913	0.32308
61	60.00	13.29023	14.71821	-1.42798
62	61.00	13.79377	14.30180	-0.50803
63	62.00	13.18342	13.89942	-0.71600
64	63.00	13.42756	13.51060	-0.08303
65	64.00	13.10713	13.13487	-0.02774
66	65.00	13.50386	12.77180	0.73205
67	66.00	12.35946	12.42097	-0.06151
68	67.00	12.13058	12.08195	0.04863
69	68.00	11.61179	11.75436	-0.14257
70	69.00	12.08481	11.43780	0.64701
71	70.00	10.84886	11.13191	-0.28305
72	71.00	9.39929	10.83632	-1.43703
73	72.00	11.45920	10.55069	0.90851
74	73.00	9.09412	10.27468	-1.18056
75	74.00	10.22326	10.00797	0.21528
76	75.00	9.82653	9.75025	0.07628
77	76.00	10.46739	9.50121	0.96619
78	77.00	9.20093	9.26056	-0.05963
79	78.00	8.71266	9.02802	-0.31536
80	79.00	9.71972	8.80331	0.91642
81	80.00	8.69740	8.58617	0.11123
82	81.00	9.13990	8.37634	0.76355
83	82.00	7.62930	8.17359	-0.54429
84	83.00	8.07180	7.97767	0.09413
85	84.00	7.59878	7.78834	-0.18956
86	85.00	6.98844	7.60540	-0.61696
87	86.00	8.77369	7.42862	1.34508
88	87.00	6.45439	7.25779	-0.80340
89	88.00	7.01895	7.09272	-0.07377
90	89.00	6.69852	6.93321	-0.23469
91	90.00	6.53068	6.77907	-0.24839
92	91.00	7.47671	6.63013	0.84658
93	92.00	5.98137	6.48620	-0.50483
94	93.00	7.11050	6.34713	0.76338
95	94.00	5.69146	6.21274	-0.52128
96	95.00	6.24076	6.08287	0.15789
97	96.00	5.56939	5.95738	-0.38800
98	97.00	5.90508	5.83612	0.06895
99	98.00	5.70671	5.71894	-0.01223
100	99.00	4.53180	5.60572	-1.07392
101	100.00	5.56939	5.49630	0.07308

Dependent variables:	I(0)	k	I(t=∞)
Initial values:	100.0	0.05	0.0
Final values:	96.7 (7.6)	0.034 (0.002)	2.4 (2.5)

fluorescence intensities are given in Columns 2 and 3. The fitted values using a three parameter model function (equation (33)): a two parameter exponential and a baseline parameter, are shown in Column 4. These functional values were calxulated using a non-linear-least-squares-curve-fit program based on the method of Marquardt as outlined by Bevington.[94] In Figure 18, a plot of the logarithm of the experimental values and the computer-fitted value versus time delay is shown for two aluminum concentrations. Table 9 summarizes the results from all experiments to date and serves as the basis for the following discussion.

Temperature Dependence

No discernable temperature effect on the rate of vibrational decay for any sample, over the range 18 K-30 K, was observed. Although this is a small temperature range, it is clear that a pronounced temperature dependence does not exist. This is in contradiction to all theoretical models involving direct vibrational relaxation to lattice phonons, and implies that few phonons are involved in the relaxation process.

Al/Ar and O_2Ar Dependence

Several experiments were designed to examine the dependence of the vibrational decay on the reactant/argon ratios. To see the effect of the Ar/Al ratio, the rate of decay was measured as a function of the Knudsen cell temperature, keeping flowrate = 6 mmols/hr and Ar/O_2 = 100. At low Knudsen cell temperatures, the observed rate was relatively independent of the cell temperature. Below T_{Kn} = 950°C, however, no fluorescence signal could be detected. As the temperature

was raised past 1100°C, the characteristic blue emission from AlO could be seen just above the matrix surface, however, no change in the rate was observed until the temperature was approximately 1150°C. After 1200°C, the aluminum would wet the outer surface of the Knudsen cell and the rate would increase dramatically due to the uncontrolled increase in the Al atom vaporization.

A plot of the rate of vibrational relaxation versus the Knudsen cell temperature is shown in Figure 19. Using the method outlined in Appendix 1, the calculated Ar/Al ratios are also indicated. For Ar/Al ratios greater than 5000/1, the relaxation rate was independent of the aluminum concentration. For ratios below this value, the rate of relaxation increased by about seven for every 50 degree change in temperature.

Contrary to the strong Al concentration dependence, changes in O_2 concentration had no effect on the observed rates. To examine the dependence on Ar/O_2 ratios, the rate of decay was measured as a function of the Ar/O_2 ratio, keeping the flowrate constant at 6 mmol/hr and T_{Kn} constant. A change in the Ar/O_2 ratio from 100/1 to 1000/1 produced no change in rate for T_{Kn} = 1100°C.

Relaxation in $Al^{18}O$

When an equimolar mixture of 200/200/1 of $^{18}O_2/^{16}O_2$/Ar was used, the rate of decay of both the AlO isotopic species could be measured. As the fluorescence features are broad, the visible laser excited the 1"-0' transition in both the isotopic species. However, by tuning the CO_2 laser, the population in either of these species could be selectively excited. In the mixed sample, the observed rate of decay of the

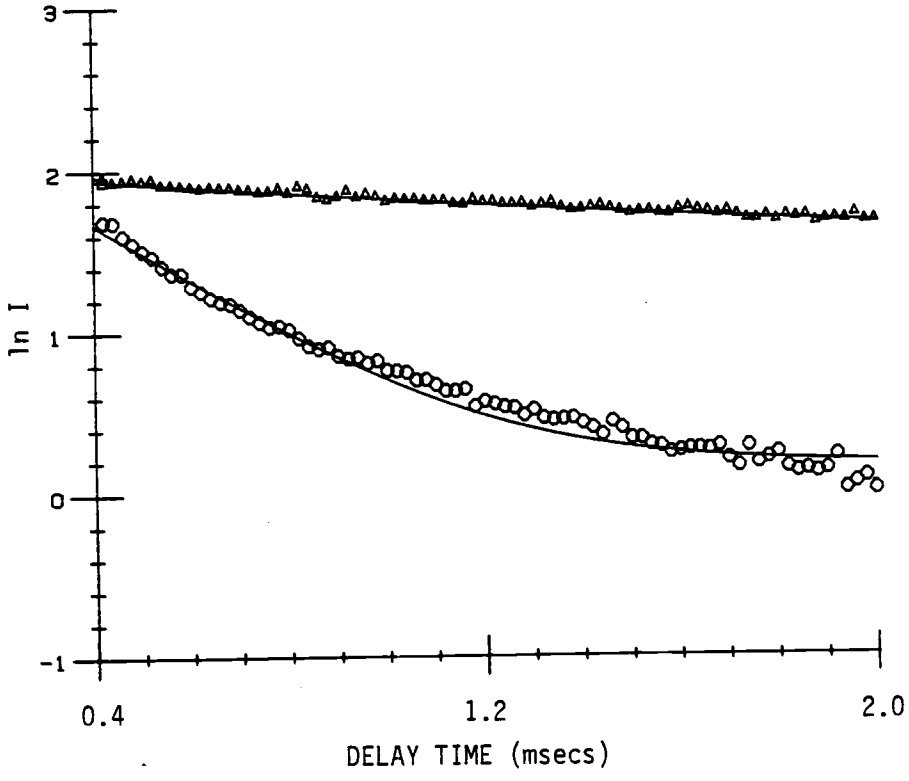

Figure 18: Plots of ln I vs. time delay for files of figure (17). Solid lines are the results of a least-squares fit of data to equation (33).

Table 9: Vibrational relaxation data for matrix isolated AlO as a function of Knudsen cell temperature, Ar/O_2 ratio, and tip temperature. In all samples flowrate = 6 mmol/hr.

Ar/O_2	T_{kn} (C)	T_{tip} (K)	Rate, ($msecs^{-1}$)
100/1	1000	18	0.034 ± 0.001
100/1	1050	18	0.045 ± 0.005
100/1	1150	18	0.153 ± 0.012 *
100/1	1175	18	0.84 ± 0.31
100/1	1200	18	1.59 ± 0.24
100/1	1225	18	4.2 ± 1.0 **
1000/1	1200	18	1.41 ± 0.12
100/1	1100	18	0.088 ± 0.041
100/1	1100	>30	0.092 ± 0.040
100/1 $Ar/^{18}O_2$	1150	18	0.306 ± 0.018 *
200/1/1 $Ar/^{18}O_2/^{16}O_2$	1150	18	0.143 ± 0.013 †
			0.212 ± 0.014 ††

*The rates of relaxation in these samples may be directly compared, as they were deposited under completely identical conditions with the same Knudsen cell.

**Aluminum wet outer surface of Knudsen cell.

†CO_2 laser tuned to excite $Al^{16}O$

††CO_2 laser tuned to excite $Al^{18}O$

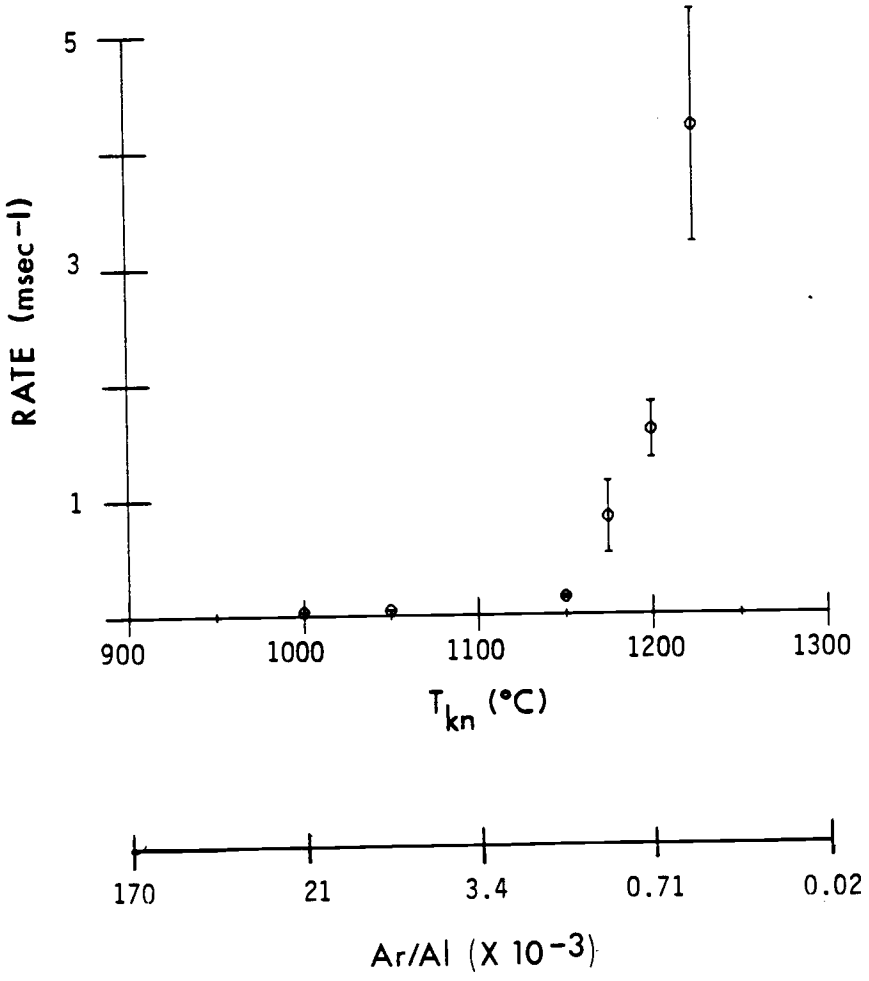

Figure 19: Observed rates of AlO vibrational relaxation for several Knudsen cell temperatures. Calculated Ar/Al ratios (Appendix 1), assuming an Ar flowrate = 6 mmol/hr, are also shown.

$Al^{18}O$ species was faster than the $Al^{16}O$ species, the experimental ratio of the two rates being, $k(Al^{18}O)/k(Al^{16}O) = 1.5$.

Since the absorptions in the matrix isolated AlO molecules are broad, there is no way of discriminating the 0'-0" emission from the two isotopic species. Unfortunately, this would imply that the v"-1 populations of both species were being probed with each shot of the visible laser in the mixed sample. If transfer of vibrational energy from the excited $Al^{16}O$ species to the $Al^{18}O$ species takes place, then the observed $Al^{16}O$ rate is a sum of the real $Al^{16}O$ rate, plus the percentage of energy which is transferred to the $Al^{18}O$ molecules. However, as the energy of the $Al^{16}O$ species is 30 cm^{-1} higher than the $Al^{18}O$ molecule, there is insufficient energy in the lattice to effect the reverse process.

To examine the effect of isotopic substitution, two different gas samples containing 100/1 $Ar/^{18}O_2$ and 100/1 $Ar/^{16}O_2$ were used to prepare two separate AlO samples. The measured rates for the $Al^{18}O$ species were again faster than the $Al^{16}O$ molecule, the experimental ratio being $k(Al^{18}O)/k(Al^{16}O) = 2$. Within the experimental error in the rates, this ratio is very close to the mixed sample, and indicates that V-V transfer among the isotopic species is unimportant.

DISCUSSION

It is apparent from the lack of temperature dependence, that few phonons are involved in the relaxation process. This would imply that either intramolecular transfer to local rotational or intermolecular V-V transfer are the dominant mechanisms of energy relaxation.

For the AlO molecule, direct infrared evidence for rotation in the matrix cannot be obtained, since the rotational constant is smaller than the resolution of the infrared instrument. From Table 2, the AlO molecule is somewhat larger than the argon substitutional site but hindered molecular rotation might be possible. Indirect evidence of rotational freedom resulted from polarization experiments. The rate of vibrational decay was examined when the dye laser was polarized parallel and perpendicular to the CO_2 laser output. Surprisingly, no change in fluorescence intensity or relaxation rate was observed. This indicates that the molecule reorients after CO_2 laser excitation. This is possible only if the molecule has orientational freedom.

All present theories of intramolecular vibration to rotation transfer predict that the rate is linear in $(\omega/B)^{1/2}$. For the measured rates of decay in AlO, the $Al^{18}O$ molecule relaxed faster than $Al^{16}O$, a contradiction to this theory. This observation would indicate that, although the AlO molecule may rotate in the lattice, the number of rotational quanta needed to match the vibrational energy is too large, and the intramolecular relaxation process is inefficient.

An alternative explanation to this mechanism is the intermolecular V-V transfer among impurity Al_mO_n species. In this

mechanism, the vibrational energy of AlO would be taken up by an impurity vibrational mode, which acts as an energy sink. The plausibility of this mechanism is born out by the observed aluminum concentration dependence. Under concentrated conditions, the identification of the acceptor vibrational mode would be difficult due to the number of unidentified aluminum and non-aluminum containing impurities in the sample. Each of these impurities would have a different energy gap from the AlO stretch and therefore, a different transfer probability. The dependence of the transfer probability on this energy gap is expected to be very sensitive, but the exact behavior is unknown.[27]

Under dilute conditions, T_{Kn} <1100°C, there are impurities in the sample which could be the possible acceptor. Since dipole-dipole transfer is considered to be much more efficient than other types of transfer,[49] the vibrational mode of the responsible acceptor would be expected to appear in the infrared. For these conditions, only bands corresponding to Al_2O, AlO_2, Al_2O_2, and Al_2O_3 were observed in the infrared. In the following, the possible role of each of these species in the vibrational relaxation process will be considered.

One of the likely acceptors in this experiment is the dimer species Al_2O_2. The band at 510 cm^{-1} assigned to the B_{2u} mode of Al_2O_2 was observed at low Knudsen cell temperatures. The other modes, although unobserved, are expected to be even lower in energy. The difference in energy between the AlO band at 975 cm^{-1} and the B_{2u} mode of Al_2O_2 is 465 cm^{-1}. For a transfer to this mode, 465 cm^{-1} has to be taken up by the argon lattice in a multiphonon process. This amount of energy is very large, and the transfer probability would be

expected to be small. Due to the large number of phonons required in the transfer, a reasonable temperature dependence would be expected as well. This energy difference could be minimized if transfer was to a higher overtone or combination band of infrared activity, however, no band in the region between 1000 cm^{-1} and 900 cm^{-1} has been assigned for Al_2O_2. These considerations suggest that Al_2O_2 is not the likely acceptor.

The ν_1 mode of AlO_2 was observed at 1170 cm^{-1}. Transfer to this mode would require 200 cm^{-1} from the lattice. At 18 K, kT is around 13 cm^{-1}, far less than what is needed for transfer. The other modes of AlO_2 remain unassigned but these are expected to be below 750 cm^{-1},[76] and are probably very weak. The fact that these modes are weak in the infrared implies that the dipole-dipole transfer probability is small.

The strongest features in the infrared spectrum were distributed to Al_2O and Al_2O_3. For transfer to the ν_3 mode of Al_2O at 993 cm^{-1}, 18 cm^{-1} has to come from the lattice. Again, kT is 13 cm^{-1}, and transfer is not likely. At 25 K, kT should be sufficient for transfer. However, no temperature effect was observed up to 30 K. Thus, Al_2O is not the likely acceptor.

The other feature in the infrared spectrum at 912 cm^{-1} was tentatively attributed to Al_2O_3. The difference in energy of this band and the AlO stretch is 63 cm^{-1}, very close to the Debye cutoff for Argon at 64 cm^{-1}. For this "one phonon" process, very little temperature dependence would be expected, in agreement with the observed data.

The Al_2O_3 band, shifted to 888 cm^{-1} with isotopic substitution, is only 54 cm^{-1} from the $Al^{18}O$ stretch. This difference is 9 cm^{-1} less than this same difference in $Al_2{}^{18}O_3$, and would imply a more efficient transfer. This again is in agreement with the experimental data and suggests that Al_2O_3 is the acceptor species.

The possibility that this small difference of 9 cm^{-1} in the energy gap might produce such a dramatic difference in the rates, implies that the transfer is extremely sensitive to the energy gap.

Theoretically, Blumen et al.[28] and Lin et al.[26] have examined the V-V transfer efficiency as a function of the energy gap, but no experiments have adequately examined the energy gap law. In the following chapter, this subject is explored in detail.

Chapter 5

V-V Transfer from AlO to Various Species in Solid Argon

INTRODUCTION

The vibrational energy relaxation times of diatomic molecules in condensed inert gases can be quite long.[42-48] In the previous chapter, for example, the lifetime of AlO in argon exceeded 25 msecs, limited only by a V-V transfer to matrix impurities. This V-V transfer mechanism has been used to understand the relaxation rates in such matrix isolated systems as CO in argon,[45] concentrated samples of HCl in argon,[11] and C_2^- in argon.[47] However, the quantitative rate dependence on the donor-acceptor separation and the donor-acceptor vibrational energy mismatch was not obtained in these studies.

Goodman and Brus[27] have semi-quantitatively studied the V-V transfer from ND and NH ($A^3\Pi$) to CO and N_2 in solid argon. In their work, the rates of vibrational decay of both electronically and vibrationally excited NH and ND were examined as a function of the concentration and vibrational energy of the impurity acceptor molecule. However, the disadvantages of working with electronically excited donors, i.e., the short experimental time scale (10^{-6} sec) and correspondingly high acceptor concentrations, prevented measurements of vibrational lifetimes at low concentrations. Their results suggest a strong energy gap (transfer exothermicity) law of the form: $k \alpha \exp(-\Delta E/28\ cm^{-1})$. Unfortunately, the small amount of data prevented a complete analysis of the energy gap dependence.

In this chapter, the vibrational relaxation of AlO by V-V transfer to several different impurities will be examined. The AlO/Ar system, as described in the previous chapter, provides an excellent medium for the study of the V-V transfer mechanism. The $v''=1$ vibrational level may be selectively excited by an infrared laser so that relatively large populations of excited molecules may be obtained. The subsequent vibrational decay may then be monitored using tunable dye lasers and sensitive photomultiplier tubes. The high sensitivity of detection means that dilute mixtures of AlO in argon (1×10^6) may be studied and, therefore, resonant energy transfer among the donor system may be ignored. There are disadvantages in working with a radical such as AlO. Obtaining a known concentration of the AlO species in argon is not possible. Other impurities are known to exist in matrices containing AlO and the concentrations of these species are difficult to specify.[76] These disadvantages may be overcome by working under dilute conditions, where small changes in reaction conditions (T_{Kn} and the Ar/O_2 ratio) have no effect on the rate of decay. Therefore, the resultant relaxation rate is independent of the concentration of these intrinsic impurities.

The goal of the present work is to examine the V-V transfer rate dependence on the donor-acceptor difference in vibrational energy (energy gap). The acceptor molecules chosen for this experiment provide a variety of different energy gaps, as shown in Figure 20. These acceptors are inert, stable polyatomic molecules with at least one infrared fundamental absorption below the AlO stretch at 975 cm^{-1}. A stable mixture of these molecules in argon of known concentration can be prepared. At the temperature of the matrix experiment, 19 K, kT is

approximately 14 cm^{-1} and, consequently, only processes that are exothermic within 14 cm^{-1} should occur. Therefore, only the acceptor vibrational modes which lie below 990 cm^{-1} are important in the V-V relaxation process.

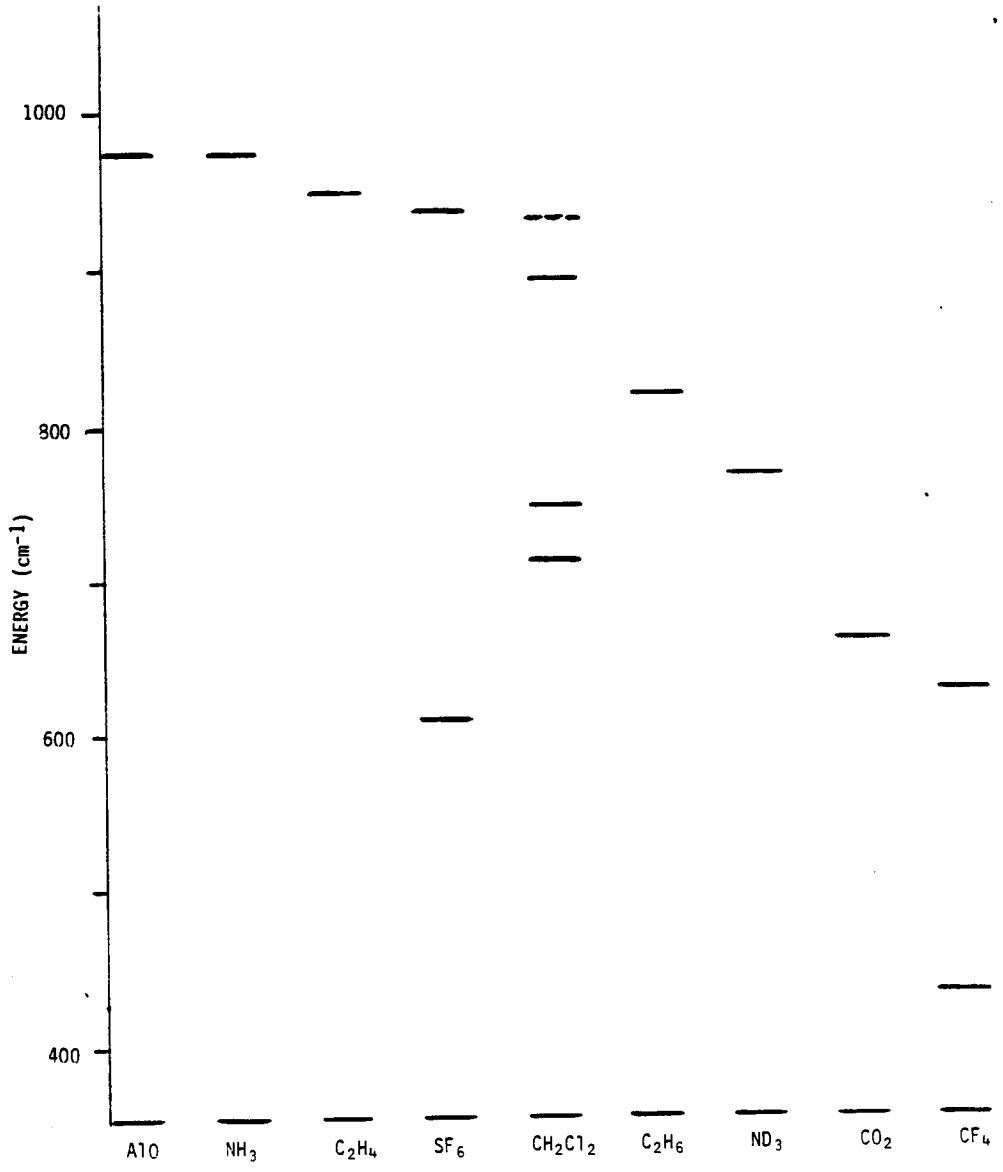

Figure 20: Energy level diagram showing relevant infrared active bands for V-V transfer from AlO to various matrix-isolated impurities. Solid lines denote fundamental infrared absorptions. Broken lines indicate infrared active combination band or overtone.

EXPERIMENTAL

The cryostat, aluminum source, visible laser, CO_2 laser, and collection routines are the same as described in the previous chapter. All samples of impurity doped AlO/Ar matrices were prepared using a low Knudsen cell temperature, T_{Kn} = 1025 ± 25°C, as measured by an optical pyrometer. The cold-tip temperature was maintained at 18 to 19 K during deposition and for all subsequent relaxation measurements.

Matrices of Ar, O_2, and various dopants were made by successive dilutions of a concentrated sample prepared on a greaseless, glass vacuum line, using standard monometric techniques. The Ar/O_2 ratio in all matrix samples was 100/1, independent of the dopant concentration. The various gases, source, and purity used in the experiment are listed below. Unless specified, samples were used directly from the cylinder without further purification. All gas samples were co-deposited onto the cooled substrate with aluminum atoms at a constant flowrate of 6 mmols/hr.

Ar	Matheson	99.9995% UHP
O_2	Airco	99.9%
SF_6	Matheson	99.8%
CF_4	Matheson	99.7%
C_2H_4	Matheson	99.0%
C_2H_6	Matheson	98.0%
NH_3	Matheson	99.9% anhydrous vacuum distilled
CO_2	Airco	99.8%
CH_2Cl_2	Baker	99.999% spectral grade
ND_3	Merck	99.5% D

Prior to the ND_3 experiments, all portions of the gas handling apparatus were in contact with D_2O for 8 hours. After this time, the apparatus and sample bulbs were flushed with 5 torr D_2O and then pumped out three times, consecutively. Sample bulbs containing various concentrations of ND_3 were then prepared. The experimental apparatus which comes in contact with the gas sample was subjected to the same D_2O flushing procedure prior to installation of the sample.

To determine frequencies and relative absorption intensities of the acceptors in argon, infrared spectra in the region from 1050 cm^{-1} to 500 cm^{-1} were obtained. The wavenumber error in each reported band is estimated to be ± 0.5 cm^{-1}. Samples containing several dopant species were deposited at 6 mmols/hr for approximately 30 minutes to 1 hour. In all mixtures, the Ar/dopant ratios were 1000/1. In the determination of relative absorbances, CF_4(1/1000) was used in all samples. The absolute areas in each sample were then measured with respect to the ν_4 bend of CF_4 at 630.2 cm^{-1}. With this internal standard, the relative absorbances shown in Table 10 could be measured without the accurate determination of pathlength.

Two to three measurements of the relaxation curve were made for each matrix sample. At each time delay, the intensity of fluorescence and the dye laser power was measured and ratioed. The result of 10 shots at each delay time was used to calculate an average value and standard deviation which was subsequently stored for later data analysis. The monochromator slits were adjusted to minimize the background fluorescence from the dye laser (250 μm). This dye laser fluorescence provided a small fluctuating non-zero background which was minimized to less than 3% of the maximum intensity.

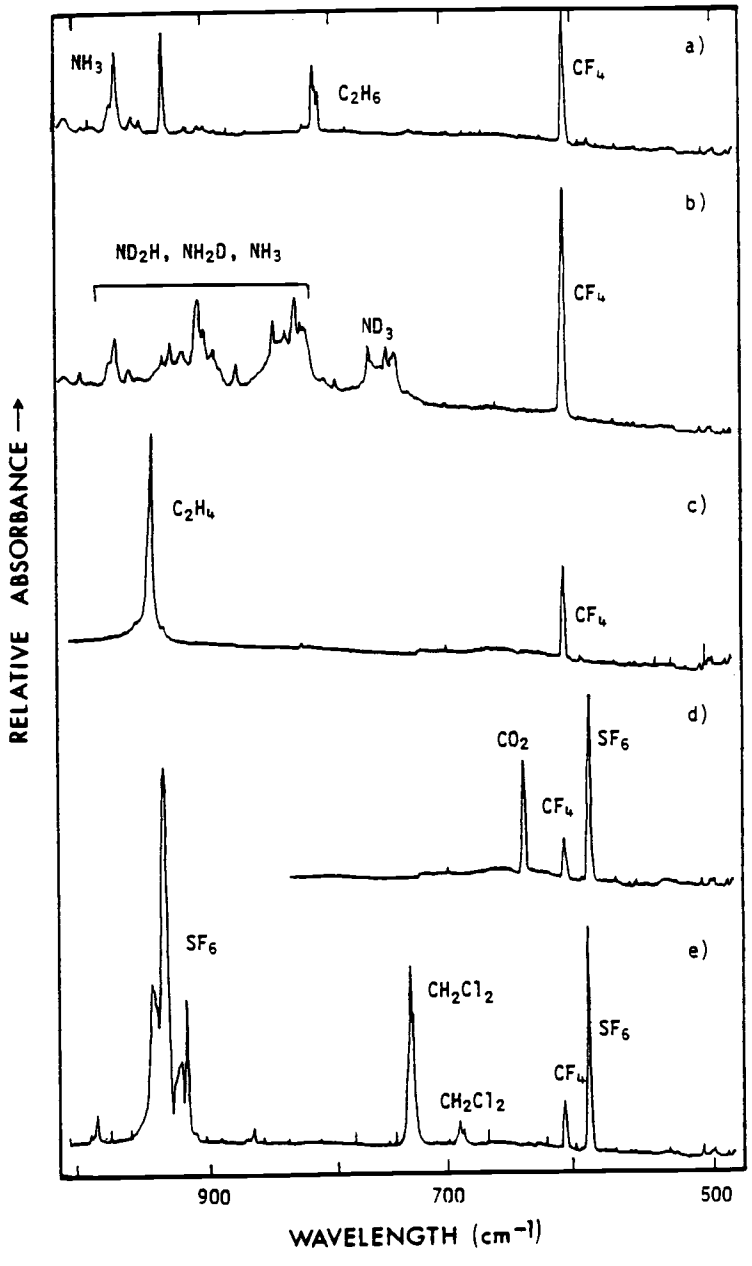

Figure 21: Infrared spectra of dopant species shown in figure (20) in argon at 18°K. All species are 0.1% in argon.

INFRARED SPECTRA OF IMPURITY SPECIES IN SOLID ARGON

Infrared spectra of all dopant species in argon are shown in Figure 21. Listed in Table 10 are the assignments of each peak, along with the gas phase values from the literature.[96] The absorbance of each peak relative to the ν_3 (f_{1u}) peak of SF_6 at 940 cm^{-1} are also shown in Table 10.

V-V TRANSFER STUDIES

In the previous chapter, the relaxation dynamics of dilute samples of AlO/Ar were established. The vibrational spacing of AlO in argon matrices is $E(v=1) - E(v=0) = \Delta G_{1/2} = 975$ cm^{-1}. The relaxation rates of vibrationally excited (v"=1) AlO in argon was found to be constant with Knudsen cell temperatures less than 1050°C. The lifetime of AlO was determined to be limited by a V-V transfer mechanism to aluminum containing impurities generated along with the AlO. The relaxation rate was also found to be insensitive to the Ar/O_2 ratio. This is consistent with a V-V transfer mechanism, as transfer from AlO to O_2 is endothermic by 600 cm^{-1} and not expected to occur.

For this work, the relaxation rates for samples prepared with a Knudsen cell temperature of 1025°C and $Ar/O_2 = 100$ were measured several times. The data were fit to the three parameter function of equation (33) using the non-linear least-squares analysis of Marquardt, given in reference 94.

$$I(t) = I(0)\ e^{-k_0 t} + I(t=\infty) \qquad (33)$$

Table 10: Infrared frequencies (cm^{-1}) of dopant species in argon at 18°K. All species are 0.1% in argon.

Molecule	Wavelength (cm^{-1})	Assignment	Wavelength (cm^{-1}) from lit. (96)	ΔE (cm^{-1})*	Relative Absorbance
NH_3	974	ν_2 (a_1)**	968	0	0.064
SF_6	940 (m)	ν_3 (f_{1u})	965	35	1.0
	611.8	ν_4 (f_{1u})	617	363	0.13
C_2H_4	946.8	ν_7 (b_{1u})	949	28	0.20
ND_3	770 (m)	ν_2 (a_1)	749	205	0.034
CH_2Cl_2	710.9	ν_3 (a_1)	704	264	0.025
	748.4	ν_9 (b_2)	737	227	0.21
	894	ν_7 (b_1)	899	81	0.0049
	--	$\nu_3 + \nu_4$ (a_1)	935	40	--
C_2H_6	821 (t)	ν_9 (e)	820.8	154	0.023
CF_4	630.2	ν_4 (f_2)	630	344	0.038
	430	ν_2 (e)	437	545	--
CO_2	662.2	ν_2 (Π_u)	668	312	0.086

t = triplet, m = multiplet

*ΔE represents the difference in energy of the matrix isolated band from the AlO stretch at 975 cm^{-1}.

**The strong feature is assigned to the R (0), $1^+ \rightarrow 0^-$, branch of the ν_2 bend in argon.

The third parameter in equation (33), $I(t=\infty)$, represents the small background fluorescence from the dye laser present at $t=\infty$. The standard deviation in the measured intensity at each delay time was dependent on the fluctuations in this term. At small delay times, this term was small, relative to the measured intensity and fluctuations made little difference. At large delay times, fluctuations in the background were large compared to the measured intensity. Therefore, the standard deviation, relative to the magnitude of the measured intensity, was far larger. To emphasize the data points with small errors in the fitting procedure, each data point was weighted as the inverse square of the measured error ($1/sigma^2$). The average value of the vibrational relaxation rate constant of AlO with no added impurities, hereafter labeled k_0, was determined to be:

$$k_0 = (0.0404 \pm 0.0017) \times 10^{-3} \text{ sec}^{-1}$$

V-V Transfer, AlO→$NH_3(\nu_2)$

The AlO v'=1 lifetime was extremely sensitive to the concentration of NH_3. When small amounts of NH_3, Ar/NH_3 = 50,000, were added to the Ar/O_2 mixture, a dramatic increase in the rate of vibrational decay was observed. As higher concentrations of NH_3 were used, the rate increased until it was too fast to measure accurately, at Ar/NH_3 > 7500. For the more concentrated samples, the relaxation curves are slightly non-exponential, primarily at small delay times. The data collected for several Ar/NH_3 ratios is shown in Figure 22.

The R(0) line of the ν_2 bend in NH_3 was observed at 974 cm^{-1} in argon, consistent with other studies of matrix isolated NH_3.[97] The transfer from AlO at 975 cm^{-1} to this vibration is essentially a

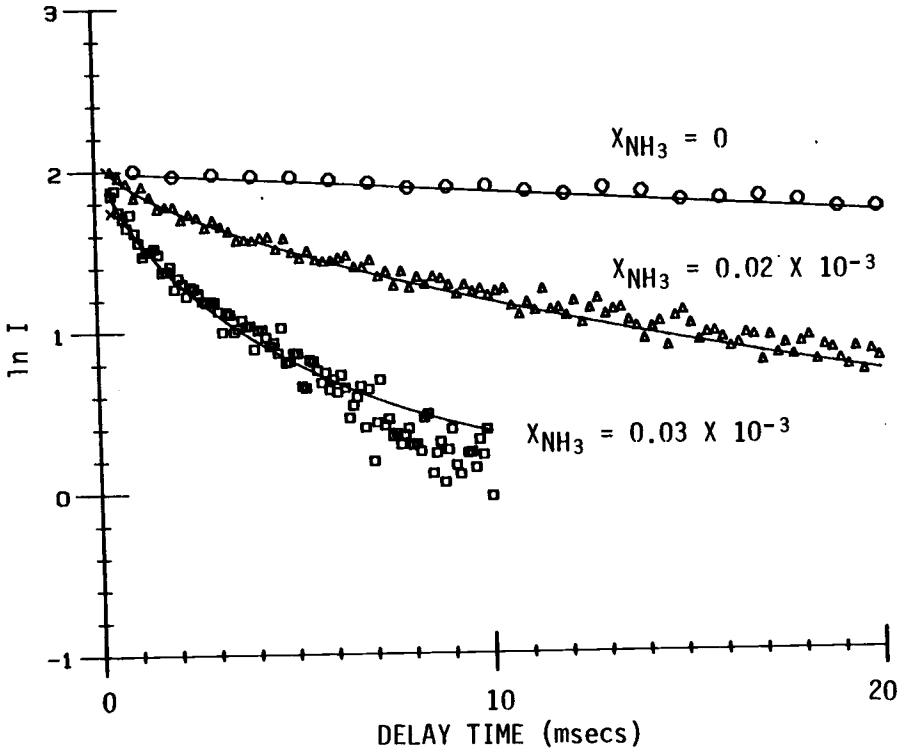

Figure 22: Vibrational relaxation data for NH_3 doped matrices of AlO in argon, T_{tip} = 18 K. Solid lines are theoretical fits to the data, equation (36).

resonant process ($\Delta E=0$). The efficiency of this process, when compared to other possible relaxation mechanisms, is reflected in the dramatic effect which small concentrations of NH_3 have on the rate. For Ar/NH_3 = 50,000, the most probable AlO-NH_3 separation distance is $\sim$100 Å.[47] Yet the effect on the vibrational lifetime is still quite pronounced. The dipole-dipole interaction, as originally considered by Forster,[23] is the principle coupling between polar molecules such as AlO and NH_3.

Forster considered the long-range dipole-dipole transfer of electronic energy between dyes in solution. This theory may be used in the present case where the transfer of vibrational energy involving vibrational transition dipoles is of interest. The microscopic transfer rate, k_{da}, between a donor and acceptor falls off as R^{-6} such that:

$$k_{da} = C_{da}R^{-6} \tag{34}$$

where C_{da} is a constant coefficient containing all of the interactions between donor and acceptor, and R is the separation distance. For a collection of non-interacting donors, each surrounded by a random distribution of possible acceptors, the evolution of the excited population in time is given by equation (10) after setting s=6 as:

$$N(t) = N(0)\exp(-k_0t - \frac{4}{3}\pi^{3/2}x_a(C_{da}t)^{1/2}) \tag{35}$$

where x_a is the mole fraction of the added acceptors relative to the host species and k_0 is the rate of relaxation with no added acceptors.

For the present work, equation (35) was used to fit the measured data of the AlO vibrational relaxation. Equation (35) may be re-written in a form more convenient for least-squares fitting as in equation (36).

$$I(t) = I(0)\ \exp(-k_0 t - B\ t^{1/2}) + I(t=\infty) \qquad (36)$$

where I(t) represents the measured fluorescence intensity at time t, and B contains all of other constants in equation (35). The last term in equation (36), $I(t=\infty)$, represents the background fluorescence of the dye laser.

When the four parameter function of equation (36) was used in matching the experimental NH_3 doped AlO relaxation curves, an excellent fit was obtained. However, the fitted value of k_0 ranged from -0.5 to 0.90 and did not converge to the measured value of k_0 = 0.0404. This difficulty is primarily due to a large correlation among parameters, common when multi-exponentials are used as model functions.

To circumvent this problem, the value of k_0 in equation (36) was fixed to the measured value of k_0 = 0.0404 and the resulting three parameter function was used to fit the NH_3 data. Again, each data point was weighted as $1/\text{sigma}^2$ to emphasize the points with smaller relative errors. For each sample, the relaxation curve was recorded between two to three times and stored on separate data files. Each file was subjected to the least-squares fitting procedure and the average value of the parameter B was calculated for each acceptor concentration. The results obtained for the NH_3 doped AlO matrices are

shown in Table 11. In the following, this same procedure was used to obtain the value of B for all of the acceptors.

AlO→ND_3 (ν_2)

The ND_3 molecule, like the NH_3 analogue, undergoes complete rotation in the matrix.[97] However, the rotational branches are not as easily resolved in the matrix infrared spectrum. The center of the band is at 768 cm^{-1}, 207 cm^{-1} from the AlO stretch at 975 cm^{-1}. As expected, the relaxation rate was much smaller with added ND_3 than with the corresponding concentrations of added NH_3. The measured values of the relaxation rate for each ND_3 concentration is shown in Table 11. The dramatic decrease in the rate in going from NH_3 to ND_3 clearly establishes the V-V transfer mechanism as the primary mode of vibrational relaxation.

AlO→C_2H_4 (ν_7)

The $\nu_7(b_{1u})$ mode of C_2H_4 occurs at 947 cm^{-1} in the argon matrix. No other bands are expected in the infrared spectrum below the AlO stretch at 975 cm^{-1}. The off resonance (ΔE=28 cm^{-1}) transfer to this mode is expected to be less efficient than transfer to NH_3. However, it should be far faster than the ND_3 experimental values as far less energy has to be taken up by the lattice. The measured values of B obtained for C_2H_4 doped matrices are shown in Table 11.

AlO→CF_4

There are three modes of CF_4 below 1000 cm^{-1}. The $\nu_2(e)$ mode and $\nu_4(f_1)$ mode are infrared active, and occur at 437 cm^{-1} and 630 cm^{-1}, respectively. The $\nu_1(a_1)$ mode is only Raman active and occurs

at 904 cm^{-1} in the liquid.[96] In the argon matrix, the ν_4 and ν_2 bands are found at 630 cm^{-1} and 430 cm^{-1}, with the ν_2 band being very weak. The measured rates for CF_4 doped AlO/Ar matrices are shown in Table 11. By comparison to the rates for ethane, the transfer cannot be solely to the Raman mode, only 75 cm^{-1} away; but has to be mainly to the 630 cm^{-1} band, 345 cm^{-1} lower in energy than the AlO stretch. This clearly indicates that transfer to Raman active modes are much less efficient than the dipole-dipole V-V relaxation process.

AlO→CO_2 (ν_2, Πu)

Only one mode of CO_2 occurs in the region below 975 cm^{-1}. The ν_2 (Πu) band, which occurs at 667 cm^{-1} in the gas phase, shifts to 662 cm^{-1} in the argon matrix. This mode is shifted by 313 cm^{-1} from the AlO stretch. The rates for CO_2 doped matrices are shown in Table 11.

AlO→SF_6 (ν_3, f_{1u})

The $\nu_3(f_{1u})$ mode at 965 cm^{-1} and the $\nu_4(f_{1u})$ mode at 617 cm^{-1} are very intense features in the gas phase infrared spectrum of SF_6. The ν_3 mode is one of the strongest bands known in the infrared spectrum. The ν_3 band is substantially shifted in the matrix to a broad feature with a maximum at 940 cm^{-1}. Under more dilute conditions (<0.05% SF_6) the ν_3 band consists of six sharp features centered around 940 cm^{-1}.[98] The ν_4 band is a sharp feature at 612 cm^{-1}. The observed rates for several different SF_6 doped AlO/Ar matrices are shown in Table 11.

Table 11: Data obtained for all dopant species from the least squares fit to equation (36). All values are in ($msecs^{-\frac{1}{2}}$).

X_a (X 1000)	NH_3	SF_6	C_2H_4	ND_3	CH_2Cl_2	C_2H_6	CF_4	CO_2
0.020	.597 (0.091)							
0.025	1.37 (0.12)	0.99 (0.13)	0.407 (0.087)					
0.033	1.51 (0.15)							
0.050	1.67 (0.26)	2.01 (0.41)	0.95 (0.16)	0.119 (0.072)	0.140 (0.035)	0.075 (0.050)		
0.10	4.31 (0.50)	4.12 (0.49)	2.10 (0.53)	0.232 (0.089)	0.215 (0.067)	0.156 (0.051)		
0.13	6.43 (0.42)							
0.20			4.05 (0.62)	0.44 (0.14)	0.42 (0.11)	0.291 (0.057)	0.107 (0.042)	
0.40					0.832 (0.088)	0.409 (0.062)	0.113 (0.011)	
0.50				1.08 (0.14)				
1.0				1.86 (0.31)	1.74 (0.34)	0.755 (0.075)	0.332 (0.074)	0.123 (0.050)
2.0						1.51 (0.16)	0.48 (0.13)	0.262 (0.089)
10.0								0.93 (0.13)
Slopes from figure (23)	47.7 (2.3)	41.07 (0.44)	20.22 (0.46)	1.949 (0.074)	1.867 (0.082)	0.759 (0.031)	0.265 (0.021)	0.0931 (0.0052)

SUMMARY

Shown in Table 11 are the values of the parameter B from equation (36) obtained for all dopant species, as well as the uncertainties in the fitted value of B. The large uncertainties in the values of B indicate that there is a strong correlation among the three parameters used in the double exponential fit of equation (36). This correlation introduces about a 10% error in the fitted parameters when the relaxation occurs on a time scale much faster than the intrinsic relaxation rate, $k_0 = 0.0404$. When the relaxation rate is much slower, closer to k_0, the correlation produces a much larger error in the fitted parameters. This large correlation is reflected in the 50% error observed in some of the values of B as shown in Table 11.

It is clear from the wide range of values in Table 11 that the efficeincy of V-V transfer from AlO strongly depends on the identity of the acceptor species. On a microscopic level, the rate of transfer from AlO to an acceptor is given by equation (34). The coefficient, C_{da}, in this equation is a measure of the microscopic strength of interaction and contains all the molecular parameters of interest. The microscopic rate coefficient may be obtained by use of the macroscopic equation shown in equation (35).

For a given acceptor, the measured values of B should be linear in the added acceptor concentration with a slope equal to $\frac{4}{3}\pi^{3/2}C_{da}{}^{1/2}$. For the values measured in this work, plots of this type are shown in Figure 23. For each dopant species, the data was subjected to a one-parameter linear regression by forcing the

intercept to equal zero. Each data point was weighted as the inverse square of the error to emphasize the points at higher values of B. The slopes obtained for each different species, and the calculated values of C_{da} from these slopes are shown in Table 12. These coefficients form the basis of the following discussion.

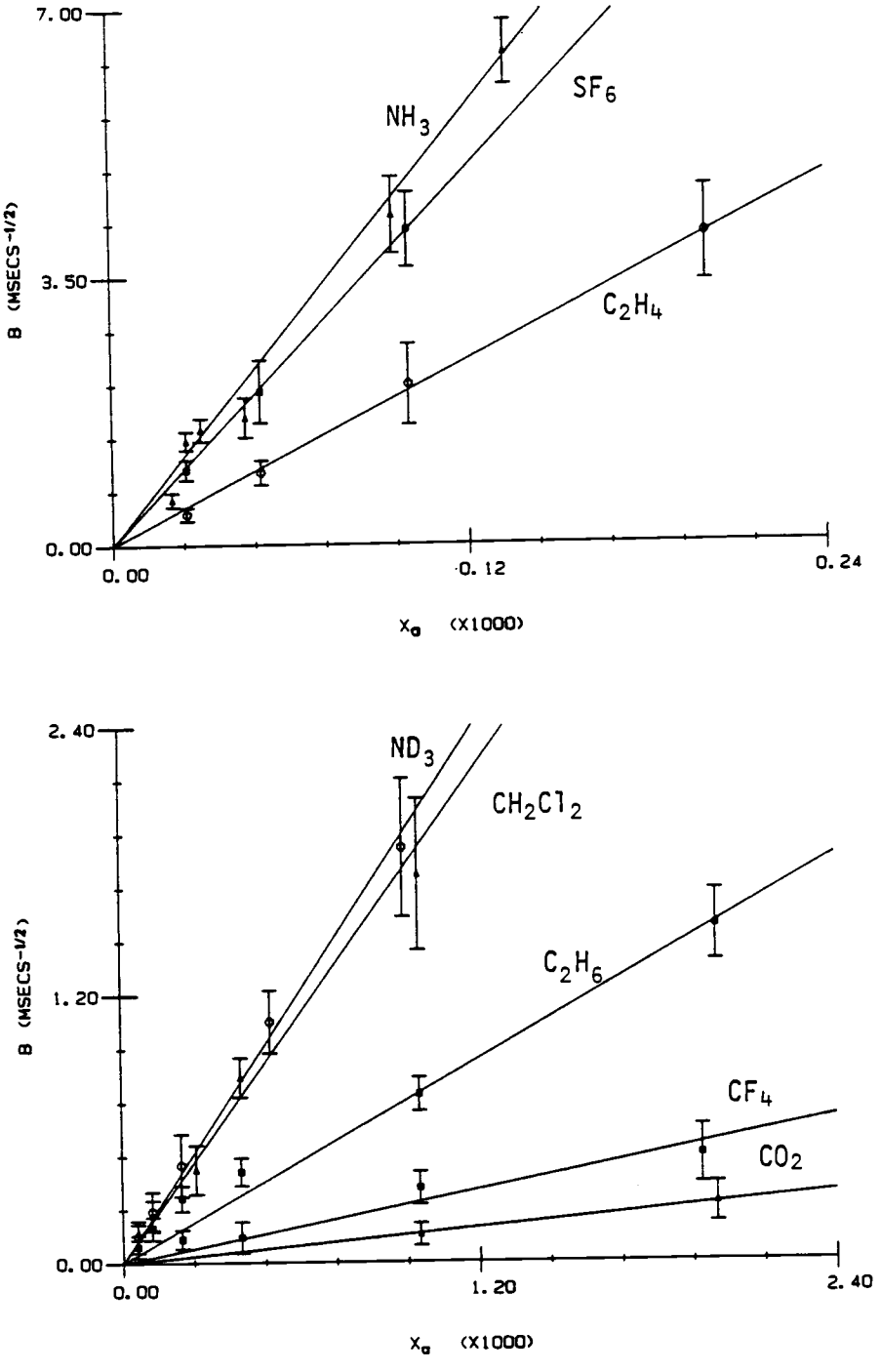

Figure 23: Fitted B parameters from equation (36) vs. mole fraction of added acceptor.

Table 12: Calculated coefficients of V-V transfer from AlO to various polyatomic acceptors.

Acceptor	Slopes $(msecs)^{-\frac{1}{2}}$	ΔE^* (cm^{-1})	C_{da} $(msecs)^{-1}$	$\log_{10} C_{da}$	$\log_{10} C_{da}$ (normalized)
NH_3	47.7 (2.3)	0	41.3 (2.8)	1.62	1.62
SF_6	41.07 (0.44)	35	30.60 (0.46)	1.49	0.293
C_2H_4	20.32 (0.46)	28	7.42 (0.24)	0.870	0.378
ND_3	1.949 (0.074)	206	6.89×10^{-2} (0.0037)	-1.16	-0.881
CH_2Cl_2	1.867 (0.082)	81	6.32×10^{-2} (6.0039)	-1.20	-0.0828
C_2H_6	0.759 (0.031)	154	1.045×10^{-2} (6.0×10^{-4})	-1.98	-1.53
CF_4	0.265 (0.021)	345	1.27×10^{-3} (1.4×10^{-4})	-2.90	-2.67
CO_2	0.0931 (0.0052)	313	1.57×10^{-4} (1.2×10^{-5})	-3.80	-3.93

* Difference in energy of first fundamental mode of the acceptor and AlO at 975 cm^{-1}.

DISCUSSION

The Energy Gap Law

The transfer of vibrational energy from AlO to all of the acceptors in Figure 20 is expected to be dominated by a dipole-dipole V-V transfer. In Figure 24, the measured values of C_{da} are plotted versus the difference in vibrational energy of AlO at 975 cm^{-1} and the first infrared active fundamental of each impurity species. There is clearly a pronounced decrease in the value of C_{da} with energy mismatch. This is displayed in a five order of magnitude decrease in C_{da} for the transfer from AlO to NH_3 and to CO_2. However, there are several anomalies in these observed values of C_{da} which cannot be understood by a simple energy gap law:

1. The transfer coefficient for SF_6 is larger than for transfer to C_2H_4, yet the energy gap is larger for SF_6.
2. The transfer from AlO to ND_3 is 10 times faster than transfer to C_2H_6. However, the difference in energy is 50 cm^{-1} larger for ND_3.
3. The difference in energy from AlO to CF_4 is 344 cm^{-1}, yet the transfer to CO_2, ΔE = 312 cm^{-1}, is 10 times slower.

In the original theory by Forster,[23] the probability of microscopic V-V transfer between donor and acceptor is given by equation (4). This equation expresses the transfer rate as proportional to the overlap integral of donor and acceptor lineshapes. The lineshape function of the acceptor is essentially the integrated

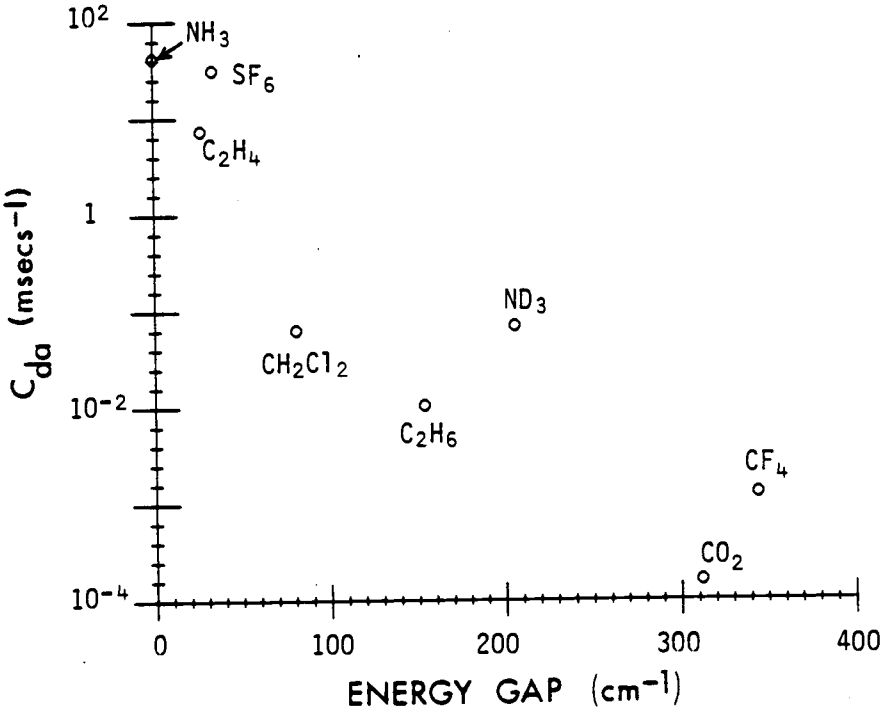

Figure 24: Plot of measured transfer coefficient C_{da} vs. energy gap of the acceptor.

absorbance of the accepting vibrational mode. In the subsequent work by Lin et al.[26] and Blumen et al,[28] the transfer rate is proportional to the square of an acceptor dipole derivative integral. The square of this integral is again proportional to the integrated absorbance of the accepting mode in the infrared spectrum.

These lineshape functions are an integration over the absorption bands of both donor and acceptor in the infrared spectrum. In the best case, the lineshape function of the AlO stretch could be measured along with lineshapes of the various acceptors of Figure 20. The lineshape integral could then be evaluated and eliminated as a variable in the microscopic theories. However, obtaining accurate lineshapes from those recorded by a spectrometer is difficult.

Alternatively, one can easily measure the relative absorbances of each acceptor mode. The values of C_{da} in Table 12 can then be divided by the appropriate relative absorbances in order to examine the relative changes in this ratio. This would leave only the energy gap dependence in the resulting values of C_{da}. The relative absorbances of the infrared active modes for each dopant species used in this experiment are shown in Table 10. The ν_3 mode of SF_6 is much stronger than any other mode and is given a relative absorbance of 1.0. The values of C_{da} were then divided by the relative absorbances and the results are shown in Table 12. These relative C_{da}' values have been multiplied by a constant factor such that the transfer to NH_3 ($\Delta E=0$) is unchanged by the procedure. The resulting values of C_{da}', which will be referred to as "normalized" coefficients, are plotted in Figure 25.

The most dramatic aspect of the plot in Figure 25 is that the "normalized" rate of transfer to SF_6 is now less than the transfer rate to C_2H_4. This is in accord with the expected energy gap law, since the SF_6 accepting mode is 7 cm^{-1} lower in energy than the accepting mode in C_2H_4. However, there are several features of this plot that still cannot be explained by an energy gap law alone.

The rate of transfer to ND_3 is about two orders of magnitude faster than expected, when compared to the rates of transfer to C_2H_6 and CO_2. For ND_3, there is only one vibrational mode below 1000 cm^{-1}, so the transfer has to be to this mode. Although great care was taken to minimize proton exchange of ND_3 in the preparation of the samples, some exchange is expected to take place. If this exchange did occur, it would decrease the amount of ND_3 thought to exist in the samples and would produce ND_2H and NH_2D impurities. The ND_3 was purchased from Merck, Inc., and had nominal 99.5% D purity. The 0.5% H impurity, nominally in the sample, indicates that approximately 2% NHD_2 exists in the sample prior to proton exchange. The proton exchange process, increases the concentrations of the NH_2D and ND_2H impurities in the matrix sample after deposition.

In the gas phase, the ν_2 modes of these molecules consist of doublets at 894 cm^{-1} and 874 cm^{-1} for NH_2D and at 818 cm^{-1} and 808 cm^{-1} for NHD_2. In the V-V transfer process, small concentrations of either of these species would increase the observed rate of transfer above that characteristic of the transfer to pure ND_3. Since 2% of the sample is known to be these impurities, the measured rate is probably far too high, and not representative of the transfer to pure ND_3. The possibility that such small amounts of these impurities

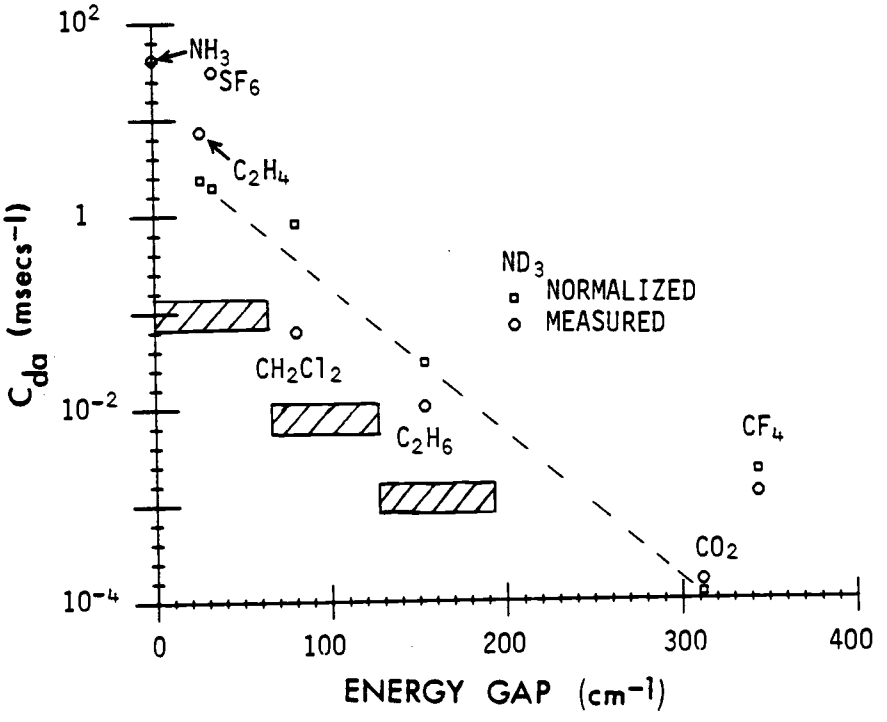

Figure 25: Comparison of measured transfer coefficients with normalized transfer coefficients. Shaded areas represent theoretical calculations from equation (39).

have such a pronounced effect on the rate, indicates the inefficiency of the V-V transfer to a molecule such as ND_3.

There are other aspects of Figure 25 which cannot be explained on the basis of a simple energy gap law. The normalized transfer coefficient from AlO to CF_4 is far larger than that to CO_2. The CO_2 molecule has only one mode lower in energy than the AlO stretch at 975 cm^{-1}, observed at 662 cm^{-1} in the argon matrix. However, CF_4 has three vibrational modes below the AlO stretch. For CF_4, there are two infrared active modes: The strong ν_4 mode at 630 cm^{-1} and a much weaker ν_2 mode at 430 cm^{-1}. The fact that the ν_2 mode is much weaker in the infrared spectrum and is also 200 cm^{-1} lower in energy than the ν_4 mode, suggests that it is not accepting vibrational energy. The first overtone of this ν_2 mode, at approximately 860 cm^{-1}, is not infrared active and, therefore, not a viable path for relaxation.

Consequently, the only alternative path for relaxation is a V-V transfer to the Raman active ν_1 mode, which is observed at 904 cm^{-1} in the liquid.[96] Although the transfer to this mode has a much lower energy mismatch, ΔE = 75 cm^{-1} (versus 344 cm^{-1} for ν_4), a dipole to induced dipole transfer is expected to be much less efficient. However, the fact that the transfer to the ν_4 mode is such an inefficient process (involving 344 cm^{-1}/64 cm^{-1} = 5 phonons of the Debye frequency of 64 cm^{-1}), this dipole to induced dipole transfer is occurring at the same time and is a competitive path for relaxation.

The rate of transfer to CH_2Cl_2 may also be effected by transfer to several modes which are infrared active. For this molecule, there are three infrared active modes which were attributed to fundamental

vibrations in the CH_2Cl_2 molecule. The first fundamental was observed at 894 cm^{-1}, 81 cm^{-1} from the A1O stretch and was very weak in the spectrum. The two other modes were more than 50 times stronger in intensity than this mode and occurred at 750 cm^{-1} and 711 cm^{-1}. The magnitudes of the dipole derivative in these modes may be large enough to overcome the differences in energy between these modes and the ν_7 band at 894 cm^{-1}, these modes may be accepting some of the vibrational energy. However, transfer to these modes may be less important than the transfer to the $(\nu_3 + \nu_4)$ combination band observed at 945 cm^{-1} in the gas phase.[96] Although this mode was too weak to observe in this work, the small energy mismatch between A1O and this combination band, ΔE = 30 cm^{-1}, may make transfer to this mode a competitive path for relaxation. With all the possible channels of relaxation in CH_2Cl_2, one would expect the measured value of C_{da} to represent the sum of the transfer rates to all the possible modes. Therefore, the measured value of C_{da} would be higher than expected for a transfer to any one of the accepting modes.

This difficulty of having several possible channels of V-V relaxation is not expected to be a problem with SF_6 even though there are several infrared active modes in SF_6. The strongest mode is the fundamental $\nu_3(f_{1u})$ stretch at 940 cm^{-1} with all other modes occurring well below this value. The fact that this mode is so strong in the spectrum and occurs only 35 cm^{-1} below the A1O stretch (1 phonon) suggests that relaxation will be through this mode and other channels will have a negligible rate.

The transfer rates to the molecules in Figure 20, which have not been discussed so far, are particularly interesting. These

molecules, NH_3, C_2H_4, C_2H_6, and CO_2, have only one mode which can accept vibrational energy from AlO in a V-V transfer. Therefore, the observed rate of AlO relaxation to these molecules is not complicated by any other channel for relaxation. Therefore, these molecules including SF_6, provide the basis for the following discussion of the energy gap law.

As shown in Figure 25, the normalized C'_{da} values measured for the transfer from AlO to CO_2, C_2H_4, C_2H_6, and SF_6 fall on a reasonably straight line. A decrease of five orders of magnitude between AlO transfer to C_2H_4 (ΔE = 28 cm^{-1}) and to CO_2 (ΔE = 312 cm^{-1}) is observed. The resonant transfer to NH_3 (ΔE = 0) does not fall on this line, but is an order of magnitude too high. The normalized rates for all of these molecules obey an expected energy gap law as rates for all of these molecules obey an expected energy gap law as rates of transfer decrease dramatically with vibrational energy mismatch.

Most theories for such off-resonant transfer assume that the phonons accept the difference in vibrational energy. In argon, the phonon density of states has a maximum near 35 cm^{-1} and 55 cm^{-1} below that of the Debye cutoff, (w_D = 63.9 cm^{-1} in argon). In these theories, the accepting phonons are considered to be on the order of the Debye cutoff frequency, and the energy gap expression is given in units of this "bulk" phonon. From Figure 25, the rate of transfer decreases over four orders of magnitude in about 300 cm^{-1}, implying a rough energy gap law of one order of magnitude for each "bulk" phonon.

Prior to comparison of the observed form of the energy gap expression with current theoretical work, it would be useful to reiterate what has been learned so far about the form of the energy gap law:

1. The magnitude of the square of the dipole derivative determines the magnitude of the coupling between donor and acceptor. If the observed rate is divided by the relative absorbances (α $(u')^2$) of several acceptors, the observed rates fit a reasonable energy gap expression.
2. The energy gap expression for phonon assisted V-V transfer is of the form: Rate α $10^{\Delta E/w_D}$.
3. The resonant V-V process, $\Delta E=0$, does not fit the energy gap form of (2). The difference of the rate in a resonant process and that requiring one bulk phonon is larger than one order of magnitude.
4. Acceptor molecules which have several vibrational modes below the donor vibrational level provide alternative paths for vibrational relaxation.
5. The dipole-induced dipole V-V transfer mechanism is several orders of magnitude less efficient than dipole-dipole V-V transfer. This mechanism provides another path for vibrational relaxation when the dipole-dipole transfer is extremely inefficient.

Theoretical Forms of the Energy Gap Function

The physics of dipole-dipole transfer was originally considered by Forster in 1949.[23] The coefficient of the microscopic transfer rate in this theory is of the form given by equation (4). This equation expresses the transfer probability as proportional to the overlap integral of the emission band of the donor and the absorption band of the acceptor. If these bands do not overlap, no transfer is possible. For most V-V transfer processes observed in this work, the widths of the vibrational bands, are at most, ten wavenumbers. However, in the case of V-V transfer from AlO to CO_2, the separation is on the order of 300 cm^{-1}. Although transfer is inefficient in this case, it still occurs in contrast to the predictions of this theory.

The possibility that the phonons of the lattice host may assist in the transfer process was first considered by Orbach[25] for electronic transfer, and by Lin et al.[26] for V-V transfer. Lin and coworkers have theoretically related the non-resonant energy transfer rates to the rates of multiphonon relaxation in the isolated donor and acceptor. In this theory, the interaction Hamiltonians between the molecules and lattice are the same for both vibrational relaxation and non-resonant transfer and the resulting microscopic rate equation is given by equation (5). In this theory, the energy gap law is incorporated into the value of $k_d(\Delta E)$ and $k_a(\Delta E)$, which are the rates at which the donor and acceptor dissipate the energy $\Delta E = \omega_d - \omega_a$ directly into the lattice host.

Consider the dipole-dipole V-V transfer from AlO to CO_2, C_2H_4, SF_6, and C_2H_6. In all of these cases, the accepting vibrational

quantum number, v_a, is zero and the donor vibrational quantum number is one. More importantly, the permanent dipole moment of all of these acceptors is zero. Therefore, the transfer rate to these molecules, based on equation (5), then takes a much simpler form shown below:

$$k_{1-0}^{0-1} = \left[\frac{1}{3\epsilon} \cdot \frac{(\mu_d^0)^2(\mu_a')^2}{2\bar{h}w_a^3} k_a(\Delta E)\right] R^{-6} \qquad (37)$$

In this work, the experimental rate coefficients are a measure of the quantity in large parentheses in equation (37). Under the conditions where the permanent dipole moment of the acceptor is zero, as in the molecules above, all of the energy mismatch is then passed into the lattice through the donor-lattice interaction. The energy gap law is then specified by the magnitude of $k_d(\Delta E)$.

The relative absorbances shown in Table 10 are proportional to the relative magnitudes of the $(\mu')^2$ values. Therefore, the normalized coefficients of transfer to the molecules above do not depend on any acceptor parameters other than w_a. The energy gap law, as predicted by the theory of Lin, may then be examined in a relative sense by calculating the ratio of k_d (ΔE) terms at different ΔE values. These results are shown below:

$$\frac{k_d(28\ cm^{-1})}{k_d(35\ cm^{-1})} = 1.3$$

$$\frac{k_d(28\ cm^{-1})}{k_d(154\ cm^{-1})} = 120 \qquad (38)$$

$$\frac{k_d(154\ cm^{-1})}{k_d(312\ cm^{-1})} = 480$$

$$\frac{k_d(28\ cm^{-1})}{k_d(312\ cm^{-1})} = 6 \times 10^4$$

Qualitatively, the relative values shown in equation (38) are in line with the measured rates observed in this work. There is a steady decrease of about two orders of magnitude for every two bulk phonons. The relative rate of transfer from AlO to C_2H_4 to that of AlO to CO_2 is 6×10^4 compared to the measured value of 2×10^4. Also, the normalized rate of transfer to SF_6 is slower than to C_2H_4 in accord with the expected energy gap behavior.

The values of k_d (ΔE) calculated above are measures of the rate at which the donor dissipates the energy ΔE into the lattice. The donor may couple this energy into the lattice phonons either directly or via local rotational modes. If the energy is dissipated directly into phonons then a plot of the logarithm of the rate of transfer versus ΔE should be linear. As was shown for the normalized rate coefficients in Figure 25, this is indeed the case.

However, if the excess energy is coupled via local rotational modes, then a plot of the logarithm of the rates versus J_m should be linear. As before, J_m is defined as the minimum number of rotational

quanta of the donor which is necessary to fill the energy mismatch. Using the gas phase rotational constant for AlO, B_e = 0.6413 cm^{-1},[62] the values of the donor J_m necessary for phonon-assisted transfer to SF_6, CO_2, C_2H_4, C_2H, and CF_4, are shown in Table 13. The calculated values of k_d (ΔE) from equation (38) are plotted versus these J_m values in Figure 26. Also shown in Figure 26 are the normalized transfer coefficients, C'_{da} plotted versus the calculated J_m values.

It is clear from this figure that the normalized rate coefficients and the calculated transfer rates from equation (38) are not linear in J_m. This suggests that the local rotational modes of the AlO are not participating in the V-V transfer process. The choice of the rotational constant as equal to the gas phase constant assumes complete, unhindered, rotation in the matrix. If, however, the rotation is hindered or even restricted to only a librational type of motion, then the calculated J_m values would be different.

The theoretical expression for the V-V transfer rate in equation (37) assumes that because the permanent dipole moment of the acceptors is zero, the donor is dissipating all of the energy mismatch. Equation (37) was obtained from equation (5) which depends on both k_d (ΔE) and k_a (ΔE). If the energy mismatch is accepted into the lattice through acceptor rotational modes, then the normalized coefficients should be linear in the acceptor J_m values. Shown in Table 13 are the calculated J_m values using the gas phase rotational constants (A or B) of the various acceptors.

It is clear from Table 13 that the acceptor rotational modes do not participate in the V-V process. The calculated J_m values for SF_6 and C_2H_4 differ dramatically, yet the normalized rate coefficients are

Table 13: Calculated rotational quanta for V-V transfer.

Molecule	ΔE (cm^{-1})	Jm* (donor)	log C_{da} (normalized)	log C_{da} (from Lin)**	Rotational Constant (acceptor)	Jm (acceptor)
NH_3	1		1.62		9.94 (B)	0
C_2H_4	28	7	0.378	-0.69	4.83 (A)	2
SF_6	35	7	0.293	-0.79	0.0907	20
CH_2Cl_2	81		1.20		1.07 (A)	9
C_2H_6	155	16	-1.53	-2.7	2.68 (A)	8
CO_2	313	22	-3.93	-5.5	0.390	28
CF_4	344	23	-2.66	-4.3	0.195 (B)	42

* Assuming B = 0.6413 cm^{-1} for AlO.

** See reference (26).

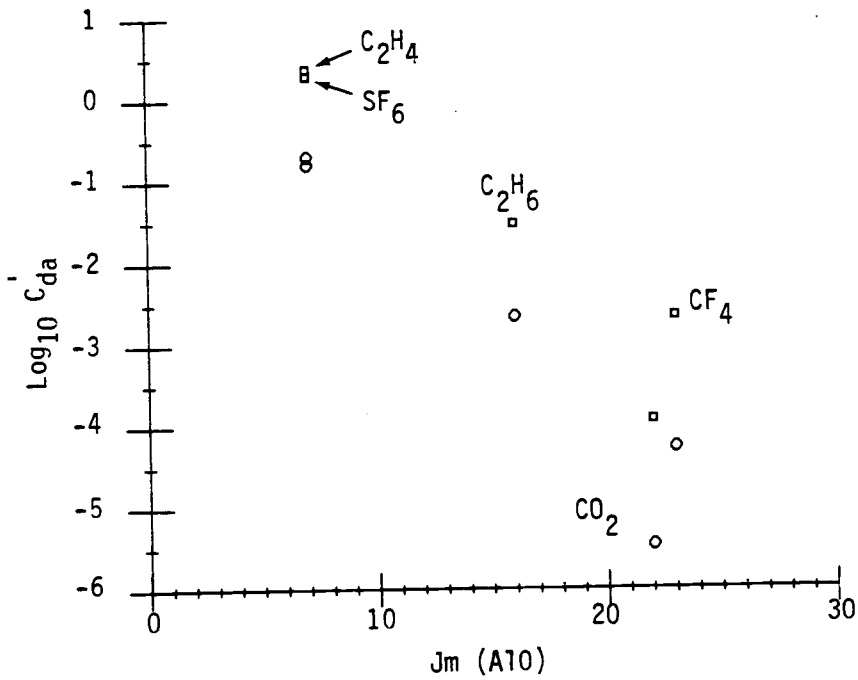

Figure 26: Comparison of normalized rate coefficients and calculated rate coefficients with donor rotation model.

▫ -- Normalized rate coefficients

○ -- Calculated rate coefficients

very close. Also, the J_m values for CH_2Cl_2 and C_2H_6 are similar (8 versus 9), yet the normalized rates differ by two orders of magnitude. The gas phase rotational constants of the various acceptors which were used do not reflect the possibility that the acceptors may only librate in the argon lattice. However, a pronounced dependence on the acceptor motion does not exist.

Recently, Blumen et al.[28] have developed a more comprehensive theory for the rate of V-V transfer between polar diatomic molecules in matrices. This model assumes that the V-V transfer takes place directly through the interaction between donor and acceptor and the energy mismatch, ΔE, between the two harmonic oscillators, relaxes directly into the matrix bath. This assumption is in contrast to that of Lin where the donor-lattice and acceptor-lattice interactions are considered to be the dominant interactions.

In the theory of Blumen,[28] the phonon assisted transfer from a donor to acceptor is expressed as a product of a Forster type overlap integral and an energy gap expression. The overlap integral in this theory is considered over the bandshapes of two, assumed identical, donor oscillators times a factor which measures the interaction of the donor with the lattice. This interaction is measured by the gas-to-matrix shift of the 0 - 1 vibrational band. For AlO, the 0-1 vibrational energy is 975 cm^{-1} in the argon lattice, 9.7 cm^{-1} larger than in the gas phase.[62]

The ratio of the non-resonant rate constant to the resonant rate constant, given by these authors, contains only the information on the energy gap law. For transfer from an excited donor (v=1) to an unexcited acceptor (v=0), the energy gap expression is given to be:

$$\frac{k\ (\text{phonon assisted})}{k\ (\text{resonant})} = \frac{\delta E}{w_D} \cdot \left[\frac{\Delta\omega_{vib}}{w_D}\right]^{N_{min}} {}_{w_D}{}^{N_{min}+1} F_{N_{min}}(w_D,\Delta E) \quad (39)$$

where δE is the bandwidth of the donor infrared absorption in cm^{-1}, w_D is the Debye cutoff frequency (w_D = 63.9 cm^{-1} for argon), and N_{min} is the minimum number of bulk phonons required to match the difference in vibrational energy of donor and acceptor, ΔE. $F_{N_{min}}(w_D,\Delta E)$ is the spectral density of phonons which needs to be evaluated for each one, two, three ... phonon process. The reader is referred to reference 28 for the actual derivation of these functions. Note that when this function is averaged over all phonon assisted processes and then substituted into equation (39), the function shown in equation (5) is obtained.

The expression in equation (39) is a step function in units of N_{min}. The predicted rates of phonon assisted transfer decrease in unit jumps as more bulk phonons are required to fill the energy gap between the donor and acceptor vibrations. This function has been plotted in Figure 25, with $\Delta\omega_{vib}$ = 9.7 cm^{-1}. The shaded areas in this plot represent the calculated values of the ratio given in equation (39). These ratios are of constant value over the entire range of each required bulk phonon. The calculated values from this function have been normalized in this plot such that the resonant case, i.e., equation (39) equal to unity, has the same value as the measured transfer rate from AlO to NH_3.

The shaded areas in Figure 25 clearly establish a similar pattern, as was observed in this work. That is, a one order of magnitude decrease in the rate for each bulk phonon. The most striking

difference between the shaded areas in Figure 23 and the normalized rate coefficients occurs between the resonant case of transfer to NH_3 and the case of transfer to C_2H_4. The transfer to C_2H_4 requires one bulk phonon. The predicted ratio of these two rates is just over two orders of magnitude, whereas, only a factor of about 20 was observed. This difference probably reflects the fact that the resonant transfer in the theoretical description is between two identical diatomic molecules. This is only approximated in the transfer from AlO to NH_3 since these molecules only overlap vibrationally, but are electronically very different.

Unfortunately, we do not have enough experimental data to verify the insensitivity of the energy gap function over a non-phonon range. Only in the case of the AlO transfer to SF_6 and to C_2H_4 has such a ΔE range been examined. Qualitatively, a decrease is observed for this 7 cm^{-1} range, but more work could be done to elucidate the validity of this prediction.

BIBLIOGRAPHY

1. "Picosecond Investigations of Dynamic Processes in Polyatomic Molecules in Liquids," A. Lauberau and W. Kaiser, In: Chemical and Biological Applications of Lasers, Vol. II, Academic Press, New York (1977).

2. R. L. Fulton, J. Chem. Phys., 61, 4141 (1974).

3. J. Marcoux, Can. J. Phys., 48, 1948 (1970).

4. H. Y. Sun and S. A. Rice, J. Chem. Phys., 42, 3826 (1965).

5. A. Nitzan, S. Mukamel, and J. Jortner, J. Chem. Phys., 60, 3929 (1974).

6. A. Nitzan, S. Mukamel, and J. Jortner, J. Chem. Phys., 63, 200 (1975).

7. A. Nitzan and R. J. Silbey, J. Chem. Phys., 60, 4070 (1974).

8. S. H. Lin, J. Chem. Phys., 61, 3810 (1974); S. H. Lin, H. P. Lin, and D. Knittel, J. Chem. Phys., 64, 441 (1976).

9. S. H. Lin, J. Chem. Phys., 65, 1053 (1976).

10. J. Jortner, Mol. Phys., 32, 379 (1976).

11. J. M. Weisenfeld and C. B. Moore, J. Chem. Phys., 70, 930 (1979).

12. L. E. Brus and V. E. Bondybey, J. Chem. Phys., 63, 786 (1975).

13. V. E. Bondybey and L. E. Brus, J. Chem. Phys., 63, 794 (1975); V. E. Bondybey, J. Chem. Phys., 65, 5138 (1976).

14. K. F. Freed and H. Metiu, Chem. Phys. Lett., 48, 262 (1977).

15. K. F. Freed, D. L. Yeager, and H. Metiu, Chem. Phys. Lett., 49, 19 (1977).

16. D. J. Diestler, E. W. Knapp, and H. D. Ludouceur, J. Chem. Phys., 68, 4056 (1978).

17. D. Knittel and S. H. Lin, Mol. Phys., 36, 893 (1978).

18. R. B. Gerber and M. Berkowitz, Phys. Lett., 39, 1000 (1977).

19. M. Berkowitz and R. B. Gerber, Chem. Phys. Lett., 49, 260 (1977).

20. M. Berkowitz and R. B. Gerber, Chem. Phys., 37, 369 (1979).

21. H. Kono and S. H. Lin, J. Chem. Phys., 78, 2607 (1983).

22. H. Kono and S. H. Lin, J. Chem. Phys. (in press).

23. Th. Forster, Ann. Physik., 2, 55 (1948).

24. D. L. Dexter, J. Chem. Phys., 21, 836 (1953).

25. R. Orbach, In: Optical Properties of Ions in Crystals, (H. M. Crosswhite and H. W. Moos, Eds.), p. 445, Wiley and Sons, (New York), 1967.

26. S. H. Lin, H. P. Lin, and D. Knittel, J. Chem. Phys., 64, 441 (1976).

27. J. Goodman and L. E. Brus, J. Chem. Phys., 65, 1156 (1976).

28. A. Blumen, S. H. Lin, and D. Knittel, J. Chem. Phys., 69, 881 (1978).

29. H. Dubost and R. Charneau, Chem. Phys., 12, 407 (1976).

30. M. J. Weber, Phys. Rev., B4, 2932 (1971).

31. M. Yokota and O. Tanimoto, J. Phys. Soc., Japan, 22, 779 (1967).

32. D. S. Tinti and G. W. Robinson, J. Chem. Phys., 49, 3229 (1968).

33. J. S. Shirk and A. M. Bass, J. Chem. Phys., 52, 1894 (1970).

34. V. E. Bondybey and J. W. Nibler, J. Chem. Phys., 56, 4719 (1972).

35. V. E. Bondybey and L. E. Brus, J. Chem. Phys., 63, 794 (1975).

36. V. E. Bondybey, J. Chem. Phys., 66, 995 (1977).

37. J. Goodman and L. E. Brus, J. Chem. Phys., 69, 1853 (1978).

38. V. E. Bondybey and J. H. English, J. Chem. Phys., 72, 3113 (1980).

39. V. E. Bondybey, J. Mol. Spectrosc., 63, 164 (1976).

40. J. L. Wilkerson and W. A. Guillory, J. Mol. Spectrosc., 66, 188 (1977).

41. V. E. Bondybey and J. H. English, J. Chem. Phys., 67, 664 (1977).

42. V. E. Bondybey, J. Chem. Phys., 66, 4237 (1977).

43. V. E. Bondybey and J. H. English, J. Chem. Phys., 68, 4641 (1977).

44. H. Dubost, L. Abouaf-Marquin, and F. Legay, Phys. Rev. Lett., 22, 603 (1973).

45. L. Abouaf-Marquin, B. Gauthier-Roy, and F. Legay, Chem. Phys., 23, 443 (1977).

46. L. Young and C. B. Moore, J. Chem. Phys., 76, 5869 (1982).

47. L. J. Allamandola, A. M. Rohjantalab, J. W. Nibler, and T. Chappell, J. Chem. Phys., 67, 99 (1977).

48. V. E. Bondybey, J. Chem. Phys., 65, 5138 (1976).

49. F. Legay, In: Chemical and Biological Applications of Lasers, Vol. II, Academic Press, New York (1977), see ref. 1.

50. L. J. Allamandola and J. W. Nibler, Chem. Phys. Lett., 28, 335 (1974).

51. P. J. Dagdigian, H. W. Cruse, A. Shultz, and N. Zare, J. Chem. Phys., 61, 4450 (1974).

52. J. J. Reuther and H. B. Palmer, J. Chem. Phys., 77, 83 (1982).

53. R. A. Gottscho, J. Chem. Phys., 70, 3554 (1979).

54. B. S. Ault and L. Andrews, J. Chem. Phys., 62, 2312 (1975).

55. H. M. Rojhantalab, L. Allamandola, and J. W. Nibler, Ber. Bunsenges Phys. Chem., 82, 107 (1978).

56. M. L. Lesiecki, Ph.D. Thesis, Oregon State University (1975).

57. Franck-Condon Factors were calculated by a FORTRAN program written by J. W. Nibler (1980).

58. C. K. N. Patel and A. C. Tam, Rev. Mod. Phys., 53, 517 (1981).

59. B. Meyer, J. J. Smith, and K. Spitzer, J. Chem. Phys., 53, 3616 (1970).

60. W. Weltner, D. McLeod, and P. L. T. Kasai, J. Chem. Phys., 46, 3172 (1967).

61. J. Pomeroy, Physical Review, 29, 59 (1927).

62. K. P. Huber and B. Herzberg, "Constants of Diatomic Molecules," Van Nostrand Reinhold, 1978.

63. J. K. McDonald and K. K. Innes, J. Mol. Spectry, 32, 501 (1969).

64. J. K. McDonald, K. K. Innes, V. W. Goodlett, and T. W. Tolbert, J. Mol. Spectry., 32, 511 (1969), and ref. 63.

65. L. B. Knight and W. Weltner, J. Chem. Phys., 55, 5066 (1971).

66. H. Rosenwaks, R. Steele, and H. P. Broida, J. Chem. Phys., 63, 1963 (1975).

67. D. Davis, Astrophys. J., 106, 28 (1947).

68. B. Authier, Ann. Geophys., 20, 353 (1964).

69. L. Pasternack and P. J. Dagdigian, J. Chem. Phys., 67, 3854 (1977).

70. P. J. Dagdigian, H. W. Cruse, and R. N. Zare, J. Chem. Phys., 62, 1824 (1975).

71. S. E. Johnson, G. Capelle, and H. P. Broida, J. Chem. Phys., 56, 663 (1972).

72. R. F. Porter, P. Schissel, and M. G. Ingram, J. Chem. Phys., 23, 399 (1955).

73. A. V. Yarkov, V. F. Shevel'kov, and A. A. Mal'tsev, Zh. Neo. Khim., 25, 1685 (1980).

74. A. Fontijn, W. Felder, and J. J. Houghton, Chem. Phys. Lett., 27, 365 (1974).

75. H. Abe and D. M. Kolb, Ber. Bunsenges Phys. Chem., 87, 523 (1983).

76. P. A. Finn, D. M. Gruen, and D. L. Page, "Radiation Effects on Solid Surfaces," R. F. Gould, ACS (1976).

77. A. Lagerquist, Ark. Fys., 12, 543 (1957).

78. B. H. Lengsfield and B. Liu, J. Chem. Phys., 77, 6083 (1982).

79. M. J. Linevski, D. White, and D. Mann, J. Chem. Phys., 41, 542 (1964).

80. A. Snelson, J. Phys. Chem., 74, 2574 (1970).

81. D. M. Makowiecki, D. Lynch, and K. Carlson, J. Phys. Chem., 75, 1963 (1971).

82. C. P. Marino and D. White, J. Phys. Chem., 77, 2929 (1973).

83. D. Lynch, M. Zehe, K. Carlson, J. Phys. Chem., 78, 206 (1974).

84. J. S. Anderson, J. S. Ogden, Chem. Phys., 51, 4189 (1969).

85. L. Andrews, J. Chem. Phys., 50, 428 (1969).

86. J. S. Ogden, M. J. Ricks, J. Chem. Phys., 53, 896 (1970).

87. L. Andrews, J. Chem. Phys., 54, 4935 (1971).

88. H. Huber, W. Kotzbuctner, and W. Ozin, Can. J. Chem., 51, 2722 (1973).

89. M. Farber, R. Srivastava, and O. Uy, J. Chem. Soc. Faraday Trans., 68, 249 (1972).

90. E. Wilson, J. Decius, and P. Cross, "Molecular Vibrations," Dover Press, 1965.

91. B. Meyer, "Low Temperature Spectroscopy," American Elsevier Publishing, 1971.

92. H. H. Michels, J. Chem. Phys., 56, 665 (1972).

93. P. Steinfeld, "Introduction to Molecular Spectroscopy," Academic Press, New York, 1974.

94. P. R. Bevington, "Data Reduction and Error Analysis for the Physical Sciences," McGraw-Hill, 1969.

95. H. Dubost and R. Charneau, Chem. Phys., 41, 329 (1979).

96. G. Herzberg, "Infrared and Raman Spectra," Van Nostrand Reinhold (1945).

97. D. E. Milligan and R. M. Hexter, J. Chem. Phys., 34, 1009 (1961).

98. M. Sienko and R. Plane, "Chemical Principles and Properties," McGraw-Hill, 1974.

99. J. R. Durig, In: Matrix Isolation Spectroscopy, (A. J. Barnes and D. Reidel, Eds.), 1981.

100. W. Weltner, D. McLeod, and P. H. Kasai, J. Chem. Phys., 46, 3172 (1967).

101. K. Dressler, O. Oehler, and D. A. Smith, Phys. Rev. Lett., 28, 335 (1974).

102. D. Richards and R. F. Barrow, Nature, 217, 842 (1968).

103. M. Knudsen, Ann Physik, 29, 179 (1909).

104. A. R. Miller, "Fraction of Effusing Molecules Striking a Collector Plate Over a Circular Capillary," Task # 3.2.2, U.S. Army Eng. React. Group (1965).

105. "Handbook of Chemistry and Physics," CRC, 55th Ed, 1975.

APPENDICES

Appendix 1

Calculations of Effusion Rates of Barium and Aluminum Vapor

Knudsen[103] developed a method for determining the vapor pressure of a substance by measuring its rate of vaporization through a small orifice into a vacuum. The pressure (in Atm) is calculated from the formula:

$$P = \frac{m\ (2\pi RT/M)^{1/2}}{1013250.\ t\ A} \qquad (A1)$$

where m is the mass of the vapor (grams) of molecular weight M which vaporizes through an orifice of cross sectional area A (cm^2) in time t when heated to a temperature T (K). The vapor pressure is assumed to be low enough (< 1 torr) such that molecules in the vapor collide mainly with the vessel walls rather than with each other.

Ideally, the orifice is infinitesimal in length. In practice, however, the shape is chosen to be a right circular cylinder with a finite length to radius ratio (L/r). Finite values of L/R reduce the number of molecules which exit the orifice by a constant factor f. This correction accounts for the fraction of molecules that enter the orifice at such an angle that when they strike the orifice walls are re-emitted back into the sample container. The correction factor has been evaluated by Miller[104] as a function of the effusion angle Θ and L/R several ratios. The number of moles per hour which effuse into the matrix sample can be obtained by rearranging equation (A1) into the following form.

$$\frac{\text{\# moles}}{\text{hour}} = \frac{3600\ 1013250.\ P\ f\ A}{M\ (2\pi RT/M)^{1/2}} \qquad \text{(A2)}$$

The Knudsen type oven used in this present study has been described elsewhere.[56] Only those molecules which effuse through an 18 degree cone can reach the cold sample tip. With this information and the experimental L/R ratio of 2, the fraction f is given as 0.08269.[104] Using the known vapor pressure data of barium and aluminum,[105] the effusion rates of these metals at various temperatures are shown in Table 14. Assuming that all of the metal atoms that strike the matrix tip distribute randomly throughout the sample, the calculated metal to argon ratios are shown in Table 14.

Table 14: Effusion rates of barium and aluminum from equation (A2).

T_{kn} (C)	#moles/hr (Al)	#moles/hr (Ba)	Ar/Ba*	Ar/Al*
700	---	1.6×10^{-7}	3.7×10^{4}	---
750	---	4.1×10^{-7}	1.5×10^{4}	---
800	2.8×10^{-9}	9.4×10^{-7}	6.4×10^{3}	2.2×10^{6}
850	1.0×10^{-8}	2.0×10^{-6}	3.0×10^{3}	5.8×10^{5}
900	3.4×10^{-8}	4.1×10^{-6}	1.5×10^{3}	1.7×10^{5}
950	1.0×10^{-7}	7.7×10^{-6}	7.8×10^{2}	5.8×10^{4}
1000	2.9×10^{-7}	1.4×10^{-5}	4.3×10^{2}	2.1×10^{4}
1050	7.4×10^{-7}	2.4×10^{-5}	2.5×10^{2}	8.1×10^{3}
1100	1.8×10^{-6}	4.0×10^{-5}	1.5×10^{2}	3.4×10^{3}
1150	4.0×10^{-6}	---	---	1.5×10^{3}
1200	8.4×10^{-6}	---	---	7.1×10^{2}
1250	1.7×10^{-5}	---	---	3.5×10^{2}
1300	3.3×10^{-5}	---	---	1.8×10^{2}

* Assuming flowrate = 6 mmol/hr for argon.

Appendix 2

Computer Controlled Vibrational Lifetime Measurements

The FORTRAN and assembly language programs used in the vibrational lifetime measurements of Chapter 3, 4, and 5 are listed in the following pages. This program requires a t=0 sync out-pulse from the CO_2 laser to start execution. An AR-11 timing clock on the PDP-11 was used for all Δt measurements with an estimated time jitter of < 10 usecs. All intensity measurements were made with 10 bit analogue to digital converters on the DR-11K board of the PDP-11. The required electrical connections are described in the following program under "Setup Instructions." The sub-routine "A10" was used for all graphics on the Tektronics 4012 screen. All library graphics were written by Tom Lundeen (OSU).

```
      PROGRAM VIBTM
      DIMENSION IFILE(10),FS1(50),XRAY(500),YRAY(500),YDEV(500)
      DOUBLE PRECISION NAME(4)
C*****************************************************************
C                                                                *
C     PROGRAM VIBTM.   THIS PROGRAM MEASURES THE VIBRATIONAL     *
C     LIFETIME OF ALUMINUM OXIDE USING THE CO2 LASER AND THE     *
C     CMX-4 DYE LASER. SEE BELOW FOR SET UP. THE PROGRAM         *
C     REQUIRES TCLT.MAC AND HPTLIB.OBJ . THE TEK TERMINAL IS     *
C     ALSO REQUIRED.                                             *
C                                                                *
C                                                                *
C     VARIABLES REQUIRED FOR INPUT                               *
C                                                                *
C     1.   MAXIMUM TIME DELAY IN MSECS.                          *
C          CHOOSE BETWEEN 2,10,20,100 MSECS                      *
C          WITH A DEFAULT VALUE OF 2 MSECS.                      *
C     2.   NUMBER OF SHOTS TO AVERAGE WHICH                      *
C          MUST BE LESS THAN 50.                                 *
C     3.   FILENAME AND EXTENSION FOR COLLECTED                  *
C          DATA.                                                 *
C     4.   DELAY TIME FOR MAXIMUM FLUORESCENCE                   *
C          INTENSITY IN UNITS OF 10 USECS.                       *
C                                                                *
C            HARDWARE REQUIREMENTS                               *
C                                                                *
C     1.   TEKTRONICS  4012 GRAPHICS TERMINAL                    *
C     2.   10 BIT A/D CONVERTER (3).                             *
C          CH00, CH01, CH02 OF DR-11K BOARD                      *
C     3.   AR-11 PROGRAMABLE TIME CLOCK                          *
C                                                                *
C                     NOTES                                      *
C                                                                *
C     1.   SETUP ROUTINE WILL CONTINUE UNTIL A                   *
C          KEY IS STRUCK.                                        *
C                                                                *
C     STEVEN J. BARES                                            *
C                                        12-DEC-1983             *
C                                                                *
C*****************************************************************
      LOGICAL*1 IANS,JANS,KANS
      TYPE 101
 101  FORMAT(' SETUP INSTRUCTIONS
     1,/,/,'    THE CO2 SYNC OUT GOES TO ERASE RETURN. THIS '
     2,/,' TRIGGER STARTS A CLOCK WHICH WHEN FINISHED,SENDS A TTL'
     3,/,' PULSE, TO FIRE THE CMX-4 OUT *DISP. CH. 2 *.'
     4,/,' THIS PULSE MUST ALSO BE DELAYED IN ORDER TO INITIATE THE'
     5,/,' A/D CONVERSION OF THE PMT SIGNAL.THE PMT SIGNAL GOES '
     6,/,' THROUGH THE SCOPE PREAMP, INTO THE SCOPE , AND INTO CH 00.
     7,/,' THE CMX-4 POWER GOES THRU THE ITHACO,TO CH02.'
     8,/,' THE CO2 POWER COMES OUT OF THE SAMPLE AND HOLD (SHA5).'
     9,/,' THE TRIGGER FOR THE SHA5 IS THE FALLING EDGE OF THE CO2 '
     1,/,' SYNC OUT OR THE FALLING EDGE OF ANOTHER PULSE.',/,/)
```

```
C
C
C
 10     NPNTS=100
        TYPE 110
 110    FORMAT(' ENTER THE MAXIMUM DELAY TIME IN MILLISECONDS ',$)
        ACCEPT *,ITMAX
        IF(ITMAX.EQ.100) GO TO 123
        ICLK=0
        IDELTA=2
        JDELTA=20
        IF(ITMAX.EQ.2) GO TO 121
        ICLK=1
        IDELTA=1
        JDELTA=100
        IF(ITMAX.EQ.10) GO TO 121
        JDELTA=200
        IDELTA=2
 121    TYPE 122,JDELTA
 122    FORMAT(' THERE ARE ',I6,' MICROSECONDS BETWEEN POINTS')
        GO TO 125
 123    ICLK=-1
        IDELTA=1
        JDELTA=1
        TYPE 124
 124    FORMAT(' THERE IS 1  MILLISECOND BETWEEN EACH POINT',/)
C
C
 125    TYPE 129
 129    FORMAT(' ENTER THE NUMBER OF POINTS TO BE AVERAGED ',$)
        ACCEPT *,IAV
        NTOT=IAV*NPNTS
        TOTTM=FLOAT(NTOT)/600
        TYPE 126,NTOT
        TYPE 130,TOTTM
 126    FORMAT(' THE TOTAL NUMBER OF DATA POINTS IS THEN  ',I6)
 130    FORMAT(' IT WILL TAKE ABOUT ',F7.3,' MINUTES FOR THIS RUN',/)
C
C
C
  40    TYPE 135
 135    FORMAT(' ENTER THE FILE NAME AND EXTENSION.')
        ACCEPT 103,IFILE
 103    FORMAT (10A2)
        OPEN (UNIT=3,NAME=IFILE,TYPE='NEW',INITIALSIZE=40,ERR=50)
        GO TO 60
  50    TYPE *,' ****ERROR IN OPENING THE FILE NITWIT ! ****  '
        GO TO 40
 60     CONTINUE
        CALL SETUP
        JTIME=JDELTA
        ITIME = IDELTA
T?'     TYPE *,' DO YOU WANT TO RATIO THE CMX-4 POWER TO THE PMT OUTPU
        ACCEPT 161,JANS
```

```
      PAUSE' (CR) TO START COLLECTION '
C
C     REMOVAL OF BASELINE OFFSET (CMX-4 ONLY)
C
      BASE=0.
      DO 3999 J=1,10
      CALL TCLT(1,0,IBPMT,IBPWR,ICO2)
      BASE=BASE+FLOAT(IBPMT)
 3999 CONTINUE
      BASE=BASE/10.
      IBASE=BASE
C
C
C
      DO 4000 J=1,NPNTS
   59 DO 3000 I=1,IAV
   61 CALL TCLT(ITIME,ICLK,IBPMT,IBPWR,ICO2)
      IF(IBPWR.EQ.0) GO TO 61
      IBPMT=IBPMT-IBASE
      IF(JANS.EQ.'N') IBPWR=1000
 3000 FS1(I)=1000.*(FLOAT(IBPMT)/(FLOAT(IBPWR)))
      CALL SDEV(IAV,FS1,STDEV,SMEAN)
      TYPE *,JTIME,SMEAN,STDEV
      IF(J.EQ.1.OR.J.EQ.30.OR.J.EQ.60.OR.J.EQ.90) CALL ERR
      IF(J.EQ.120.OR.J.EQ.150.OR.J.EQ.180.OR.J.EQ.210) CALL ERR
      XRAY(J)=FLOAT(JTIME)
      IF(ICLK.EQ.-1) XRAY(J)=XRAY(J)*1000.
      YRAY(J)=SMEAN
      YDEV(J)=STDEV
      JTIME=JTIME+JDELTA
 4000 ITIME=ITIME+IDELTA
      CALL ALO(XRAY,YRAY,YDEV,NPNTS,IFILE)
      DO 5000 I=1,NPNTS
 5000 WRITE(3,*) XRAY(I),YRAY(I),YDEV(I)
      CLOSE (UNIT=3)
      CALL PLOTEN
      CALL ALPHAS
      TYPE 801
  801 FORMAT(' DO YOU WANT TO RECORD THE SAME THING AGAIN ? ',$)
      ACCEPT 161,IANS
  161 FORMAT(A1)
      IF(IANS.EQ.'Y') GO TO 10
      STOP
      END

      SUBROUTINE ERR
      LOGICAL *1 ER(2)
      ER(1)='033
      ER(2)='014
      TYPE 9999,ER
 9999 FORMAT(1X,2A1)
      RETURN
      END
```

```
      SUBROUTINE SETUP
      DIMENSION FS2(30),SIG1(30)
      LOGICAL*1 IANS
      ICLK=0
      N=30
10    TYPE *,'  ENTER THE TIME FOR A MAXIMUM SIGNAL IN 10 USECS'
      ACCEPT *,ITMAX
      CALL ERR
20    DO 1000 I=1,N
30    CALL TCLT(ITMAX,ICLK,IBPMT,IBPWR,ICO2)
      FS2(I)=FLOAT(IBPMT)
      IF(IBPWR.EQ.0) IBPWR=1
      SIG1(I)=FLOAT(IBPMT)/FLOAT(IBPWR)
      TYPE *,ITMAX,IBPMT,IBPWR,ICO2,SIG1(I)
      CALL IPOKE(%44,%10000.OR.IPEEK(%44))
      ICHAR=ITTINR()
      IF(ICHAR.LT.0) GO TO 35
      GO TO 40
35    CALL IPOKE(%44,%10000.XOR.IPEEK(%44))
1000  CONTINUE
      CALL SDEV(N,FS2,SD,AV)
      CALL SDEV(N,SIG1,SD1,AV1)
      SAV=AV*AV1
      IF(SAV.EQ.0) GO TO 50
      PCNT1=SD1*100/AV1
      PCNT=SD*100/AV
50    CALL ERR
      TYPE *,AV,AV1
      TYPE *,SD,SD1
      TYPE *,PCNT,PCNT1
      GO TO 20
40    CALL IPOKE(%44,%10000.XOR.IPEEK(%44))
      CALL ERR
      TYPE *,'   IS THE DELAY CORRECT ? '
      ACCEPT 61,IANS
61    FORMAT(A1)
      IF(IANS.EQ.'N') GO TO 10
      RETURN
      END
```

```
      SUBROUTINE SDEV(N,FILE,STDDEV,SMEAN)
      DIMENSION FILE(1)
      SUM=0.0
      DO 10 I=1,N
10    SUM=SUM+FILE(I)
      SMEAN=SUM/N
      SUM=0.0
```

```
      DO 20 I=1,N
20    SUM=SUM+(FILE(I)-SMEAN)**2
      STDDEV=SQRT(SUM/(N-1))
      RETURN
      END


      SUBROUTINE ALO(XRAY,YRAY,YDEV,ICNT,NAME)
      DIMENSION XRAY(1),YRAY(1),YDEV(1)
      DIMENSION YFIT(100),YDFIT(100)
      DOUBLE PRECISION NAME(4)
      XMAX=0.0
      YMAX=0.0
      DO 25 I=1,ICNT
      IF(XRAY(I).GT.XMAX) XMAX=XRAY(I)
      IF(YRAY(I).GT.YMAX) YMAX=YRAY(I)
25    CONTINUE
      DO 30 I=1,ICNT
      YFIT(I)=YRAY(I)*1.75/YMAX
      XRAY(I)=XRAY(I)/1000.
      YDFIT(I)=YDEV(I)*1.75/YMAX
30    CONTINUE
      CALL ERR
      XMAX=XMAX/1000.
99    YMAX=2.
      XMIN=0.
      YMIN=0.
      CALL PLOTYP(2)
      XFACT=6.5/(XMAX-XMIN)
      YFACT=5.3/(YMAX-YMIN)
      CALL SCALE(XFACT,YFACT,1.5,.9,XMIN,YMIN)
      NLTX=3
      NLTY=3
      NSTX=9
      NSTY=9
      LFX=1
      LFY=1
      SLB=.10
      XSIZE=1.
      YSIZE=1.
      CALL AXISL(XMIN,XMAX,XMIN,YMIN,YMAX,YMIN,NLTX,NLTY
      1,NSTX,NSTY,LFX,LFY,XSIZE,YSIZE,SLB)
      MARK=9
      CALL POINTS
      CALL LINE(XRAY,YFIT,MARK,ICNT)
      DO 40 I=1,ICNT
      Y=YFIT(I)+YDFIT(I)
      Y2=YFIT(I)-YDFIT(I)
      CALL VECTOR
      CALL PLOT(XRAY(I),Y,0,0)
      CALL PLOT(XRAY(I),Y,1,9)
      CALL PLOT(XRAY(I),Y,0,0)
      CALL PLOT(XRAY(I),Y2,1,0)
      CALL PLOT(XRAY(I),Y2,1,9)
```

```
40      CONTINUE
        SLB=.11
        YPOS=1.60+.5/YFACT
        XPOS=XMAX/2.
        CALL SYMBOL(XPOS,YPOS,0.0,SLB,16,NAME)
        NAME(1)='DELAY (M'
        NAME(2)='SECS)   '
        NAME(3)='        '
        NAME(4)='        '
        XPOS=.75
        YPOS=-1*(.6/YFACT)
        CALL SYMBOL(XPOS,YPOS,0.00,SLB,16,NAME)
        NAME(1)='PMT SIGN'
        NAME(2)='AL/PUMP '
        NAME(3)='POWER   '
        YPOS=.5
        XPOS=-1*(.7/XFACT)
        CALL SYMBOL(XPOS,YPOS,90.0,SLB,32,NAME)
60      RETURN
        END
```

```
;*********************************************************
;*                                                       *
;* NAME     = TCLT                                       *
;* PURPOSE  = TO COLLECT FLUORESCENCE SIGNALS AS A       *
;*            FUNCTION OF DELAY FROM A PUMP BEAM.        *
;* USAGE    = CALL TCLT (DELTAT,ICLK,SIG0,SIG2,SIG1)     *
;*               DELTAT= THE TIME DELAY BEFORE SENDING   *
;*                       A PULSE OUT TO FIRE THE CMX4    *
;*                       IN 10 USEC UNITS ,CLK=0         *
;*                       IN 100 USEC UNITS ,CLK=1        *
;*               ICLK  = COUNTING FREQUENCY OF CLOCK     *
;*                       CLK=0 , CLOCK AT 100 KHZ        *
;*                       MAXIMUM DELAY = 2550 USECS      *
;*                       OR 2.5 MSECS                    *
;*                       CLK=1 , CLOCK AT 10 KHZ         *
;*                       MAXIMUM DELAY = 25500 USECS     *
;*                       OR 25.5 MSECS                   *
;*                       CLK=-1 , CLOCK AT 1KHZ          *
;*                       MAXIMUM DELAY = 255000 USECS    *
;*                       OR 255 MSECS                    *
;*               SIG0  = IS THE PMT SIGNAL GOING IN CH.0 *
;*                       OF THE A/D CONVERTER.(INTEGER)  *
;*               SIG2  = IS THE SIGNAL GOING IN CH. 02   *
;*                       OF THE A/D CONVERTER.(INTEGER)  *
;*               SIG1  = IS THE CO2 POWER GOING FROM     *
;*                       THE SAMPLE AND HOLD TO CH01.    *
;*                                                       *
;*********************************************************
        .TITLE  TCLT.MAC
        .GLOBL  TCLT
;
;       DEFINE   REGISTERS
;
CLKCSR  =170404
CLKBUF  =170406
;
DSR     =170410
CSR     =170400
DBR     =170402
CH00EX  =020020
CH01    =020401
CH02    =021001
;
;
;
TCLT:   TST     (R5)+           ;THROW AWAY NUMBER OF
                                ;ARGUMENTS
        MOV     @(R5)+,R3       ;STORE THE TIME BETWEEN
                                ;CONVERSION
        NEG     R3              ;CONVERT IT TO A NEGATIVE
                                ;NUMBER
        MOVB    R3,CLKBUF       ;LOAD THE DELAY TIME
                                ;IN THE CLK BUFFER
        MOV     @(R5)+,R3       ;ICLK INTO R3
```

```
        TST     R3              ;CHECK ICLK
        BEQ     1$              ;ICLK=0
        BPL     2$              ;ICLK=+1
        BR      3$              ;ICLK=-1
1$:     MOV     #24,@#CLKCSR    ;INITIALIZE THE CLOCK
                                ;TO 100 KHZ
        BR      4$
2$:     MOV     #26,@#CLKCSR    ;INITIALIZE THE CLOCK
                                ;TO 10 KHZ
        BR      4$
3$:     MOV     #30,@#CLKCSR    ;INITIALIZE THE CLOCK
                                ;TO 1 KHZ
4$:     BIS     #011000,@#DSR   ;ALLOW EXT PULSE IN
        BIC     #2000,@#DSR     ;ON ERASE RETURN
5$:     TSTB    @#DSR           ;WAIT FOR TRIGGER
        BPL     5$
        INC     @#CLKCSR        ;START THE CLOCK
6$:     TSTB    @#CLKCSR        ;WAIT FOR THE CLOCK
        BPL     6$              ;BEFORE FIRING CMX4
        BIS     #1000,@#DSR     ;PULSE OUT TO FIRE
        NOP                     ;THE CMX4
        BIC     #1000,@#DSR
        MOV     #CH00EX,@#CSR   ;SAMPLE PMT ON CH 00 A/D EXT START
7$:     TSTB    @#CSR           ;A/D DONE?
        BPL     7$
        MOV     @#DBR,R0
        MOV     #CH02,@#CSR     ;SAMPLE CH02
8$:     TSTB    @#CSR           ;WAIT FOR DONE BIT
        BPL     8$
        MOV     @#DBR,R2        ;MOVE TO REGISTER
        MOV     #CH01,@#CSR     ;SAMPLE CH01
9$:     TSTB    @#CSR           ;WAIT FOR DONE BIT
        BPL     9$
        MOV     @#DBR,R1        ;MOV TO REGISTER
        MOV     R0,@(R5)+       ;STORE SIG0
        MOV     R2,@(R5)+       ;STORE SIG2
        MOV     R1,@(R5)+       ;STORE SIG1
        RETURN
        .END
```